CHAPTER ONE
INTRODUCTION

1.1 Background to the Study

The understanding of the Earth has been man's desire from the moment he started to exist. Looking at the entire body of knowledge, it was discovered that it is impossible to discuss the Tectonic Plates, without the Continental Drift theory. One name that was found to reoccur each time the continental drift theory is mentioned is Alfred Wegener, a German Meteorologist, who was strongly opposed mostly by the German geologists (Brown, 2016). Although Wegener was not the originator of the Continental Drift Theory, he re-proposed, championed the theory and even died in November, 1930, on the Greenland Inland Ice, in the process of defending the theory (Ingolfsson, 2008).

His argument was that the entire landmass of the earth was in one piece and that the continents gradually drifted apart. This idea, despite the opposition and controversies that followed it, does not negate what the Bible recorded in Genesis 1 vs 9 and 10:

> *"and God said, let the waters under the heaven be gathered together unto one place, and let the dry land appear: and it was so. And God called the dry land Earth; and the gathering together of the waters He called, Seas: and God saw that it was good".*

According to Jadhav (Undated), Wegener called the landmass Pangaea and called the universal ocean, Panthalassa. It is then inferred that it was this land mass that God called Earth in Genesis chapter one that Wegener referred to as Pangaea and God's Sea, he called Panthalassa. The only deficiency in Wegener's proposal was that he failed to provide explanations to the force that is driving the continents apart.

Where as in Wegener's work he thought that the force of Earth's spin was sufficient to cause continents to move, a wrong idea of the propelling force as it were, Scottish Scientist, Arthur Holmes was the one that provided the explanation that what propels the continental drift were the Earth's Convection Currents, which heat up the fluids trapped beneath earth's crust, cause

it to rise, cool close to the crust and drop back down (Ingolfsson, 2008). Further discoveries such as the Mid Ocean Ridges as well as the Sea Floor Spreading gave credence to Holmes' convection theory and gave insight to the Great Global Rift, which is the breaking up of the earth crust into chunks, outlined by the rifts, called Tectonic Plates.

Interestingly, the name Plates was first used by a Canadian, J. Tuzo Wilson, in 1965 to describe the divisions and pattern of relative movement between different regions of the Earth's surface (i.e. plate tectonics) (Gatt, 2016). He further proposed a tectonic cycle to describe the lifespan of ocean basin. The Tectonic Plate is the combination of the earth crust and the upper cooler mantle referred to as the Lithosphere. The Lower Mantle made of fluid metal heat up, and because of the fact that solid metal is less dense than fluid, the fluid metals well up towards the crust, cools and solidifies and then wells down at subduction zones. Subduction zones occur at convergent plate boundaries, where one tectonic plate is forced to go below another plate. Usually, the Oceanic plate is the one that goes below the continental plate. At the continental-to-continental convergent boundary, like the Himalayas where the Indian Plate is pushing into the Eurasian Plate, we see very high mountains that continue to grow.

At Divergent boundaries, also known as constructive boundaries, new plates are created when magma come to the surface through the volcanoes. And because new plates are created, and destroyed at the convergent boundaries, there is a cycle that is natural and self-sustaining. Unfortunately, the activities at these boundaries, as much as they are one of the awesomeness of the earth just like eclipse and other natural activities that are thrilling, are not very friendly as the volcanoes, earthquakes, avalanche and landslides that occur as a result of these tectonic motions, are detrimental to human lives and usually come with economic losses.

Because these activities that arise as a result of the natural interactions at plate boundaries are dangerous and result to loss of lives and properties, an early warning system that redicts accurately the occurrence of these activities is one of the greatest concerns of the field of Geodesy and Geodynamics in particular. The different technologies that the field of geodesy provides for the geodynamic monitoring of plate motions include Very Long Baseline Interferometry (VLBI), Satellite Laser Ranging (SLR), Doppler Orbitography and Radiopositioning Integrated by Satellite (DORIS) and Global Navigation Satellite System (GNSS) (Bastos, Bos and Fernandes, 2010 and Hentone*t al*, 2006).

According to Hentone*t. al*, (2006) the most commonly used space-geodetic technique for geodynamic studies is still Global Positioning System (GPS). El-Rabbany(2002) indicated that the GPS provides continuous positioning and timing information, anywhere in the world under any weather conditions because it serves an unlimited number of users as well as being used for security reasons. The GPS has developed so much in recent years that it can now be continuously tracking as an unmanned system and continue to provide data needed for different solutions. The type of GPS with this capability is known as Continuously Operating Reference System (CORS). This one-way-ranging (passive) system, i.e. users can only receive the satellite signals, provides day to day data which can be processed with the use of some specialized software packages such as GAMIT/GLOBK (GNSS Analysis at Massachusetts Institute of Technology / Global Kalman filter), and the Bernese to investigate the crustal motion of different plates. The processed GPS observation has the capability of revealing both the horizontal and vertical motions of a place over a given time. These motions could be inter-plate motions or intra-plate motions.

At Plate boundaries, either divergent, convergent or transform motions may be experienced, alsothe three types of motion but mostly divergent motions are experienced within the plates, typical examples are different faults and especially, the East African Rift, where a new plate known as the Somali plate is forming and pulling away from the Nubian plate. The understanding of plate motions that the GPS, as well as other methods of space geodesy, provide, increases the predictability of some of these natural hazards. Improved predictability of the hazards provides data and information for early warning about the hazard and most importantly, save lives and property.

All along, Nigerians and West Africans in general have believed that there are no possibilities of earthquakes and other disasters within the region. Nigerian seismologists are all agreed that Nigeria is no longer an earthquake-free zone (aseismic) as previously believed following the series of earth tremors in different parts of the country in recent timesAfegbua in Orakpo (2017). Historically however, the assertion that the region is aseismic is a fallacy given the records of earthquakes and pockets of tremors within the last thirty years. Earthquake Track (2018) has a list of documented earthquakes in West Africa which includes (this list does not include the tremors experienced in the region):

i. 2012 Mw4.2 magnitude, 10 km depth Gaoual, Boke, Guinea,
ii. 2010 Mw4.5 magnitude, 10 km depth MermozBoabab, Dakar, Senegal,
iii. 2009 Mw4.4 magnitude, 10 km depth Abomey-Calavi, Atlantique, Benin,
iv. 2007 Mw7.2 magnitude, 280 km depth Sassandra, Bas-Sassandra, Ivory Coast,
v. 2007 Mw5.0 magnitude, 41 km depth Sassandra, Bas-Sassandra, Ivory Coast,
vi. 2007 Mw7.1 magnitude, 18 km depth Odienné, Denguélé, Ivory Coast,
vii. 2002 Mw4.4 magnitude, 10 km depth Nouakchott, Nouakchott, Mauritania,
viii. 2000 Mw4.5 magnitude, 10 km depth Siluko, Edo, Nigeria,

ix. 1999Mw4.4 magnitude, 10 km depth Saint-Louis, Saint-Louis, Senegal,

x. 1998 Mw4.2 magnitude, 33 km depth Kolokani, Koulikoro, Mali,

xi. 1987 Mw4.2 magnitude, 10 km depth Gaoual, Boke, Guinea,

xii. 1983 Mw6.3 magnitude, 11 km depth Gaoual, Boke, Guinea,

xiii. 1939 Mw6.4 magnitude, 15 km depth Swedru, Central, Ghana

According to Akpan and Yakubu (2010), although Nigeria is not located within the major seismic zones of the world; over the years, several minor earthquakes have been experienced in some parts of the country.

1.2 Statement of Problem

Earthquakes, volcanoes, tsunamis, landslides and tremors are natural hazards that take place because of earth movements referred to as tectonic movements. Because these uncontrollable motions cannot be influenced by any man-made system, yet the implications remain devastating, it would be necessary to predict these implications. According to Hackl, Malservisi and Wdowinski(2009), the 1994, Mw=6.7 Northridge and the 1995, Mw=6.8 Kobe earthquakes caused unprecedented damage of more than US $40 billion and US $100 billion, respectively. These two events demonstrated in a dramatic way the shortcomings of traditional seismic hazard assessment, mainly based on probabilistic models derived from catalogs of regional seismicity and supplemented by additional geologic information only for known active faults. They explained that in the case of Northridge, the rupturing fault was previously unknown without any surface expression and, hence, termed blind thrust fault. In Kobe the fault was assumed to be related to low seismic hazard.Many efforts are being made all over the world to achieve this predictability. Every region of the world mostly the Eurasian and Indian plates' inhabitants are gearing efforts towards creating early warning

systems that would help them evacuate lives and property when earthquakes are about to take place.

The African Tectonic Plate is the Nubian Plate. This plate, as shown in McGregor (2018)'s Map of the World with Tectonic Information (fig 2.8), has lots of tectonic hotspots and volcanic locations. It is also a popular knowledge that the divergent relationship in the East African Rift is increasing and that the Somali plate is separating continuously from the Nubian plate(Stamps, Saria and Kreemer, 2016). A closer look at West Africa on the figure 2.8 indicates volcanic locations in the Cameroon and tectonic hotspots in Nigeria and Cameroon.

Nigeria lies on the eastern flank of the Atlantic Ocean, and since Jurassic times, the Atlantic Ocean margins have been opening consistently. Unlike the Pacific Ocean margins which are characterized by subduction tectonics and occurrence of devastating earthquakes, the Atlantic margins are generally thought to be quiet and as a result, there was little consciousness and preparedness for earthquake occurrences and mitigation in Nigeria. However, earthquakes have been reported in some countries in the west coast of Africa that border the Atlantic Ocean (Akpan and Yakubu, 2010).The records from Earthquake Track (2018) indicate that the West African region is no longer "aseismic" as previously believed.Afegbua in Orakpo (2017) documented that the recent trend of earthquakes/tremors in Nigeria is an indication that seismic activities within the country are increasing and urgent measures need to be adopted to avert devastating consequences of big earthquakes in the country.

Researchers like Afegbua in Orakpo (2017); Eze *et al*. (2012); Tsalha*et al*. (2015);Afegbua*et al*. (2011) and Akpan and Yakubu (2010) have made several efforts to look at Earthquakes and Tremors that happened in Nigeria from 1933 to date, and have recorded over 35. They all

affirm to the presence of fault lines in the country, but unfortunately, none of them has made an attempt at the geographic definition of the fault lines.

There is need, therefore, to assess the motions, especially with the availability of few GPS CORS network in the region today and also to define the fault lines, with a view to channeling attention to areas along the fault which are susceptible to such activities.

1.3 Aim and Objectives

The aim of this study is toInvestigate the Crustal Motions of the Nigerian Region of the Nubian Plate using GPS CORs Technology between 2012 and 2014 with a view of determining the stability or otherwise of the region. This aim would be achieved through the following objectives:

1. To acquire and analyze the daily GPS CORs data of the NIGNET from 2012 to 2014, using GAMIT Software,
2. To evaluate the velocities and positions of the tectonic motions of Nigeria within the period using GLOBK Software,
3. To evaluate the quality of data from the different stations asan assessment of the health of the Network,

1.4 Research Questions

In order to achieve the above stated objectives, the following questions would be answered:

i. At what magnitude and direction is the Nigerian Region of the Nubian plate moving between 2012 and 2014?

ii. What is the Health of the Nigerian CORs Network in the period under review?

1.5 Hypothesis

1. H_o The Nigerian Region of the Nubia Plate did not experience any movement between 2012 and 2014.

2. H_o The Nigerian CORs Network is not healthywithin the period under review.

1.6 Study Area

1.6.1 Nigeria

Nigeria is located within longitudes $2^o30'E$ and $14^o30'E$; and latitude 4^oN and 14^oN(Uzodinma and Ezenwere, 1993). Fig 1.1 shows that Nigeriais located in West Africa, and bordered by Niger in the north, Chad in the northeast, Cameroon in the east, and Benin in the west. Its coast in the south is located on the Gulf of Guinea in the Atlantic Ocean.Owing to its large population and economy, Nigeria is referred to as the Giant of Africa (Holmes, 1987). Nigeria is the most populous country in Africa and the seventh most populous country in the world with a population of 186 million inhabitants. She has the third-largest youth population in the world, after India and China, with more than 90 million of its population under age 18.

1.6.1.1 Ethnicity and Languages

According to Ibezim(2014), Nigeria is viewed as a multinational state as it is inhabited by 250 ethnic groups, of which the three largest are the Hausa, Igbo and Yoruba; these ethnic groups speak over 500 different native languages and are identified with a wide variety of cultures. The most populous and politically influential include: Hausa/Fulani 29%, Yoruba 21%, Igbo (Ibo) 18%, Ijaw 10%, Kanuri 4%, Ibibio 3.5%, Tiv 2.5%. Eberhard, Simonsand Fennig(2019) indicated that the number of individual languages listed for Nigeria is 525. Of

these, 517 are living and 8 are extinct. Of the living languages, 507 are indigenous and 10 are non-indigenous. Furthermore,Eberhard *et al* (2019) opined that 19 languages are institutional, 76 are developing, 299 are vigorous, 81 are in trouble, and 42 are dying. The official or principal language in Nigeria is English Language.

1.6.1.2 Climate and Vegetation.

Different areas in Nigeria have different climates. The climate of Southern Part of Nigeria is tropical monsoon climate designated "Am" by theKöppen climate classification. Monsoon which influences the climate originates from the South Atlantic Ocean and is transported to Nigeria by the Maritime Tropical (MT) airmass, a warm moist sea to land seasonal wind. Its warmth and high humidity gives it a strong tendency to ascend and produce copious rainfall, which is a result of the condensation of water vapour in the rapidly rising air(Krishnamurti, 2019).The tropical savanna climate or tropical wet and dry climate is extensive in area and covers most of western Nigeria to central Nigeria beginning from the tropical rainforest climate boundary in southern Nigeria to the central part of Nigeria, where it exerts enormous influence on the region. The Sahel climate or tropical dry climate is the predominant climate type in the northern part of Nigeria. Annual rainfall totals are lower compared to the southern and central part of Nigeria.

Alpine climate or highland climate or mountain climate are found on highlands regions in Nigeria. Highlands with the alpine climate in Nigeria, are well over 1,520 meters(4,987 ft) above sea level. Due to their location in the tropics, this elevation is high enough to reach the temperate climate line in the tropics thereby giving the highlands, mountains and the plateau regions standing above this height, a cool mountain climate.

Generally, Nigeria has a tropical climate with variable rainy and dry seasons, depending on location. It is hot and wet most of the year, in the southeast, but dry in the southwest and farther inland. A savanna climate, with marked wet and dry seasons, prevails in the north and west, while a steppe climate with little precipitation is found in the far north. In general, the length of the rainy season decreases from south to north (Encyclopedia Britannica, 2019).

1.6.1.3 Rainfall and Temperature

According to Adedeji (2011), the Tropical monsoon climate in the south has a very small temperature range. The temperature ranges are almost constant throughout the year, for example, Warri town in the southern part of Nigeria, records a maximum of 28 °C (82.4 °F) for its hottest month while its lowest temperature is 26 °C (78.8 °F) in its coldest month. The temperature difference of Warri town is not more than 2 °C (35 °F). The southern part of Nigeria experiences heavy and abundant rainfall. These storms are usually convectional in nature due to the regions proximity, to the equatorial belt. The annual rainfall received in this region is very high, usually above the 2,000 mm (78.7 in) rainfall totals giving for tropical rainforest climates worldwide. Over 4,000 mm (157.5 in) of rainfall is received in the coastal region of Nigeria around the Niger delta area. Bonny town found in the coastal region of the Niger delta area in southern Nigeria receives well over 4,000 mm (157.5 in) of rainfall annually. The rest of the southeast receives between 2,000 and 3,000 mm (118.1 in) of rain per year.

The southern region of Nigeria experiences a double rainfall maxima characterized by two high rainfall peaks, with a short dry season and a longer dry season falling between and after each peaks. The first rainy season begins around March and last to the end of July with a peak in June, this rainy season is followed by a short dry break in August known as the August break which is a short dry season lasting for two to three weeks in August. This break

is broken by the short rainy season starting around early September and lasting to mid October with a peak period at the end of September. The ending of the short rainy season in October is followed by long dry season. This period starts from late October and lasts until early March with peak dry conditions between early December and late February(Adedeji, 2011).

The rainy season in the northern part of Nigeria last for only three to four months (June–September). The rest of the year is hot and dry with temperatures climbing as high as 40 °C (104.0 °F). The tropical savanna climate exhibits a well marked rainy season and a dry season with a single peak known as the summer maximum due to its distance from the equator. Temperatures are above 18 °C (64 °F) throughout the year. Abuja, Nigeria's capital city found in central Nigeria, has a temperature range of 18.45 °C (65.21 °F) to 36.9 °C (98.4 °F), and an annual rainfall of about 1,500 mm (59.1 in) with a single rainfall maxima in September. The single dry season experienced in this climate, the tropical savanna climate in central Nigeria beginning from December to March, is hot and dry with the Harmattan wind, a continental tropical (CT) airmass laden with dust from the Sahara Desert prevailing throughout this period.


Legend
Water-Bodies
Nigeria
Nigeria_Rivers
Nigeria
West Africa
Deg

Fig. 1.1 Map of Nigeria (Maps of Africa and West Africa Showing Nigeria)

1.6.2 The Nubian Plate

The Nubian Plate also known as the African Plate is a major tectonic plate straddling the equator as well as the prime meridian. It includes much of the continent of Africa, as well as oceanic crust which lies between the continent and various surrounding ocean ridges(Sawitsky, 2010).According to Bird (2003), the Nubian Plate encompasses almost the entire African continent, save for the eastern most portion. Between 60 million years ago and 10 million years ago, the Somali Plate began drifting from the African Plate along the East AfricanRift(EAR).Because of the myriad of interactions between the Nubian Plate and adjacent plates, and its gross geographical size a very detailed analysis of the plate remains a necessity.

On Nubia's western flank (fig 1.2), extension is occurring at the Middle Atlantic Ridge(MAR) and Terceira ridges, which then transitions via a triple junction at the Azores(fig 1.2) (Africa, Eurasia, and North America), to the Gloria transform fault (Serpelloni et al., 2007)(McClusky, Reilinger, Mahmoud, Ben Sari, andTealeb, 2003). This fault extends to the Mediterranean, where continental lithosphere comes into play, and the tectonic interactions become complex due to the collision of Africa and Eurasia (Vernant et al., 2010).

The portion of the Nubian plate under the Atlantic Ocean contains some of the oldest oceanic lithosphere (~180 Ma) on the Earth (except for a region in the South Pacific)(Wang, Lin,

Tucholke, and Chen, 2011). At the Mid-Atlantic Ridge (MAR), active upwelling of basaltic magma creates new oceanic crust in an extensional setting (a spreading centre). It is characterized by a slow-spreading regime at the MAR and is therefore thought to be a magma-limited environment. Whereas, at regions where there is enhanced upwelling of magma (due to a hot spot), such as at the Azores, the region is characterized by elevated topography, a pronounced negative Bouguer anomaly, and enriched mantle chemical compositions (Wang et al., 2011).

The South Eastern Nubian Plate is bounded to the North-East by the Sinai sub-plate and associated divergent plate boundary; the Suez Rift, the Arabian plate and the Red Sea divergent boundary (Joffe and Garfunkel, 1987). Further south is the Afar Triangle (fig 1.2) the triple junction between the Nubian Plate, Arabian Plate, and Somalian Plate. The Danakil micro-plate is found within the Afar Triangle (Eagles, Gloaguen, and Ebinger, 2002). The contact between the Nubian plate and the Somalian plate continues further south along the East branch of the East African Rift system (Joffe and Garfunkel 1987).

The divergent boundary between the Nubian plate and Somalian plate has three recognized micro-plates in-between; Victoria, Rovuma, and Lwandle plate (Corti, 2009). The boundaries of the first two are well defined; however the Lwandle plate has only been detected via space geodesy (Corti, 2009). The Nubian and Somalian plates never contact again, as the Lwandle plate and the Nubian plate make a final triple junction in this rifting system with the Antarctic plate (Corti, Van Wijk, Cloetingh and Morley, 2007).

Bellahsen, Faccenna, Funiciello, Daniel, and Jolivet. (2003) argued on the basis of analogue experiments that variations in the subduction pull along strike of the Nubia–Arabia/Eurasia subduction boundary, and weakening of the Nubia/Arabia Plate (prior to separation) by the Afar plume provide a plausible explanation for Nubia and Somalia separation from Arabia.

Le Pichon andKreemer(2010) emphasize the role of toroidal asthenospheric flow around the eastern edge of the Nubian oceanic lithosphere subducting along the Hellenic Arc, in addition to slab rollback in driving counter-clockwise rotation of Arabia and Anatolia

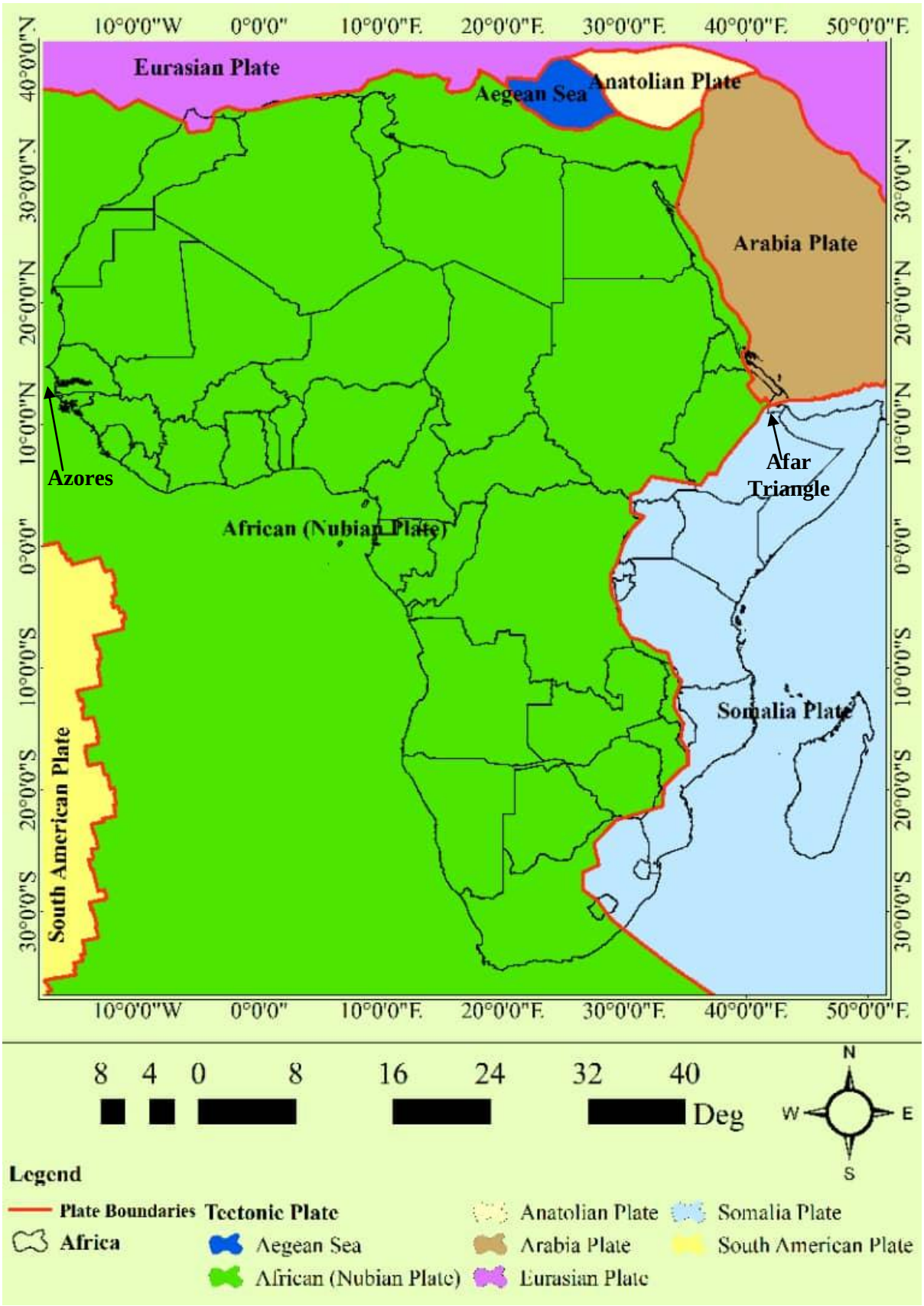

Fig 1.2: Nubian Plate and Its Interactions.
Source: Modified from Eagles, Gloaguen, and Ebinger (2002)

The Nubian-Antarctic boundary extends into the Southern Atlantic Ocean to the Mid Atlantic Ridge, which is composed of a series of divergent and transform boundaries in small succession and these boundaries continue across a final triple junction with the South American Plate and then Northward up the Atlantic Ocean into the North-Western Region of the Nubian Plate interactions.

1.7 Scope of Study

The Scope of this work is majorly towards the geodetic aspect of geodynamics, which implies the use of geodetic, especially space geodetic, techniques to take measurements of the tectonic movements within the country for period 2012 to 2014. The study would make use of the NIGNET CORS data in the country within the region for a consistent period of three years. It would investigate the displacements, and create an insight into the performance of the stations with respect to data logging.

1.8 Justification of the Study

This work will throw a lot of light on the tectonic activities in Nigeria, which has been neglected in the past, not just because our region was wrongly adjudged aseismic, but also because of the expensive nature of the proprietary software packages that possess the ability to manage such big data to detect the very little motions. It will also validate the global and regional models or predictions of the motions of the Nubia Plate.

1.8 Significance of the Study

There is a strong conviction that this study would be beneficial to the general body of knowledge, the International Union of Geodesy (IGU), the Federal Republic of Nigeria, the Nigeria Association of Geodesy and the National Union of Planetary and Radio Sciences.

This work would make strong contributions towards the understanding of the tectonic activities and relationships within the region and would also be beneficial to the students of geodesy and geodynamics in general. This study would mostly be beneficial to the Nigerian government as it would advise on the health status and efficiency of the Nigerian CORs Network.

Works like this over time are collated to help define the presence or otherwise of fault lines, compute strain rates and predict tectonic occurrences.

CHAPTER TWO
LITERATURE REVIEW

2.1 THEORETICAL FRAMEWORK

2.1.1 The Earth Layers

In order to fully understand the concept of plate tectonics and even the different concepts and theories about it, it is important to get a picture of what the earth's layers looks like and how the activities between different layers affect the plate. According to Nace, (2016), the earth's layers provide us the clues to the earth's formation, the layers of other planetary bodies, the sources of some earth resources and much more. Oregon State University (OSU, 2018) indicated that it is the view of many geologists that as the Earth cooled the heavier and denser materials sank to the center and the lighter materials rose to the top. This explains why the crust is made up of the lightest materials (rock- basalts and granites) and the core consists of heavy metals (nickel and iron). In fact, Nace(2016) further indicated that geologists, in differentiating the layers of the earth, lump subdivisions into two categories, either rheologically or chemically.

Rheological classification of the earth's layers looks at the liquid state of rocks under tremendous temperature and pressure. It is a known fact that rocks do not have the same responses when strained under normal atmospheric temperatures and pressures. With respect to rheology, the Earth layers are the lithosphere, asthenosphere, mesosphere, outer core, and inner core (Nace, 2016). The chemical variations of the earth however look at the layers as crust, mantle, outer core, and inner core (fig 2.1). As would be seen in later, the two classifications do not negate each other, but only compare and classify differently.

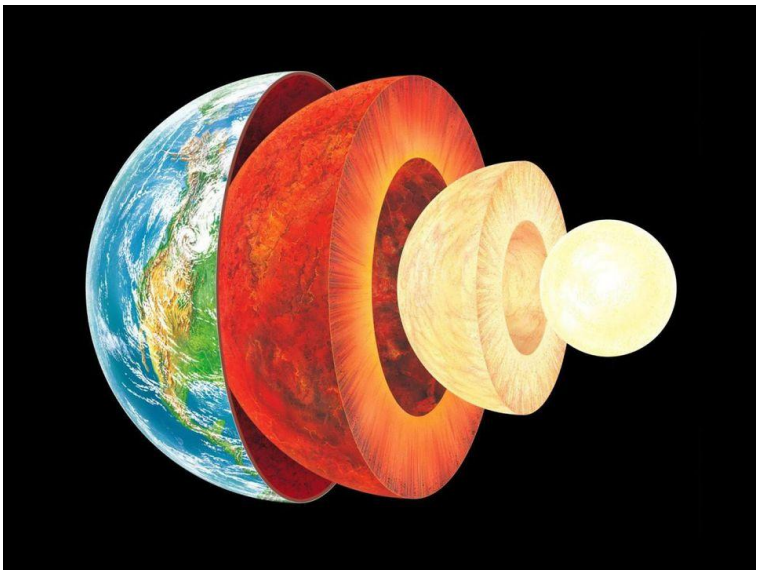

Fig 2.1 Layers of the Earth
Source: Nace(2016)

2.1.1.1 Earth Crust

OSU (2018) introduced the Crust simply as the layer we live on. They referred to it as the most widely studied and understood layer of the earth. Alden (2018) stated that the crust is an extremely thin layer of rock that makes up the outermost solid shell of our planet. He compared the thickness of the crust to the skin of an apple, stating that it amounts to less than half of 1 percent of the planet's total mass but that it plays a vital role in most of Earth's natural cycles. OSU (2018) agrees with this comparison and stated categorically that the crust is the thinnest, compared to the other layers.

The crust, according to Alden (2018) can be thicker than 80 kilometers in some spots and less than one kilometer thick in others. The thickness varies depending on where you are on the earth, with oceanic crust being 5-10 km and continental mountain ranges being up to 30-45 km thick. Thin oceanic crust is denser than the thicker continental crust and therefore 'floats' lower in the mantle as compared to continental crust. You will find some of the thinnest oceanic crust along mid ocean ridges where new crust is actively being formed. In comparison, when two continents collide as in the case of the India Plate and Eurasia Plate,

you get some of the thickest sections of crust as it is crumpled together (Nace, 2016). In agreement, OSU has it that the crust is only about 3-5 miles (8 kilometers) thick under the oceans (*oceanic crust*) and about 25 miles (32 kilometers) thick under the continents (*continental crust*). More so, the temperature of the crust varies from air temperature at the surface to about 870^{o}C in deeper sections, closer to the mantle (Nace, 2016; OSU, 2018).

According to Alden (2018), the composition of the crust is basically many different types of rocks that fall into three main categories: igneous, metamorphic and sedimentary. However, most of those rocks originated as either granite or basalt. OSU (2018) more categorically stated that the crust is composed of granite and basalt. That the continental crust is mostly granitic and the oceanic crust consists of a volcanic lava rock called basalt. Basaltic rocks of the ocean plates are much denser and heavier than the granitic rock of the continental plates, therefore, the continents ride on the denser oceanic plates. The crust and the upper layer of the mantle, shown in fig 2.2, together make up a zone of rigid, brittle rock called the Lithosphere.

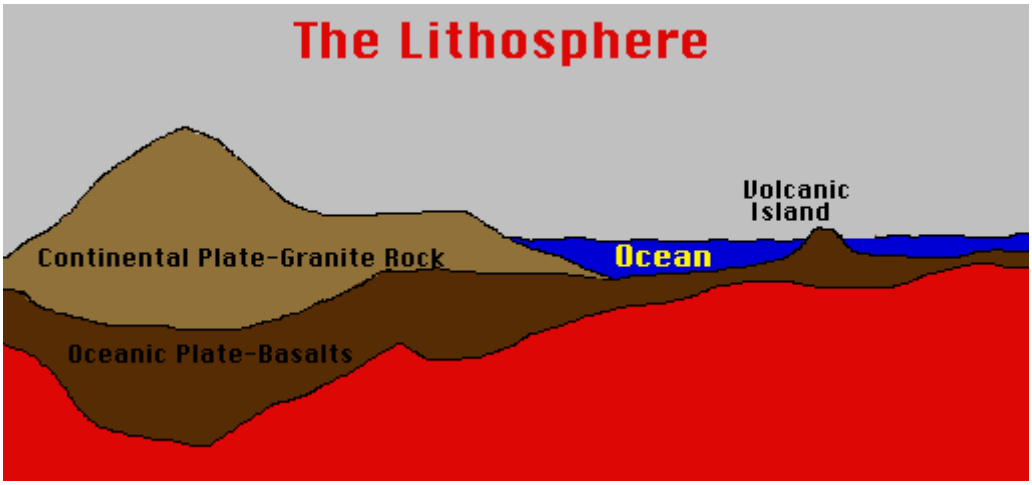

Fig 2.2: The Earth Crust (Lithosphere)
Source: OSU (2018)

Nace(2018), discussing the formation of new crust, stated that owing to the fact that Earth's surface is mostly constant in area, you cannot make crust without destroying a comparable

amount of crust. He argued that with convection of the underlying mantle, mantle magma is inserted along mid ocean ridges, constantly forming new oceanic crust. And in order to make room for this, oceanic crust must subduct (sink below) continental crust.

AndrijaMohorovicic in 1909 established a sudden change in seismic velocity, a discontinuity of some sort, about 50 kilometers deep in the Earth. Seismic velocity is the concept that measures the speed at which earthquake waves propagate through the different materials (i.e. rocks) below the surface. With a few important exceptions, it is believed that seismic velocity within the Earth tends to increase with depth. Mohorovicic's discovery indicated that seismic waves bounce off it (reflect) and bend (refract) as they go through the discontinuity, the same way that light behaves at the discontinuity between water and air. That discontinuity named the Mohorovicic discontinuity or "Moho" is the accepted boundary between the crust and mantle (Alden, 2018). Defining the Moho, Nace(2016) calls it the density contrast from less dense crust to denser mantle, where seismic wave velocities increase.

2.1.1.2 The Mantle

The mantle is the layer located directly under the earth crust; it is the largest layer of the Earth, about 1800 miles and thick making up 84% of Earth's volume. Earth's mantle is believed to be composed of bulk mineralogy similar to peridotite. It is composed of very hot, dense rock, acts similar to plastic and even flows like asphalt under a heavy weight. This flow is due to great temperature differences from the bottom to the top of the mantle (Nace, 2018; OSU, 2018).

The temperature of the Mantle ranges from 500 to 900 degrees Celsius in the upper portion to over 4,000 degrees Celsius near the core boundary. This temperature variation between the lower part of the mantle known rheologically as the mesosphere and the upper mantle known as the asthenosphere gives rise to a convectional current in the mantle. The convectional currents are caused by the very hot material at the deepest part of the mantle rising, then

cooling, sinking again and then heating, rising and repeating the cycle over and over; creating a large-scale upwelling and down-welling zones as shown in figure 2.3a. This is best explained by the way heat currents move materials in a liquid when heated. A quick example is the way soup or pudding moves in the pot when heated, shown in figure 2.3b. This convection current flow in the mantle moves the earth crust and by extension the plates the way a conveyor belt in a factory moves boxes (Nace, 2018; OSU, 2018).

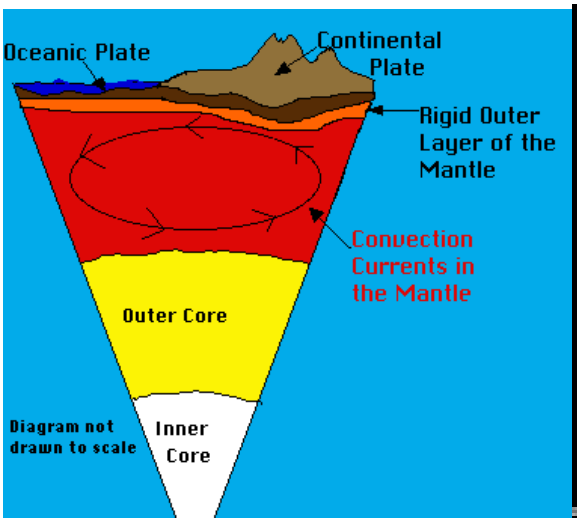

Fig 2.3a: The Convection Current in the Mantle
Source: OSU (2018)

Fig 2.3b: The Soup Pot Analogy
Source: Kudela(2016)

2.1.1.3 The Outer Core

Nace(2016) discussed the outer core as the liquid largely iron layer of the earth that lies below the mantle. He indicates that geologists have confirmed that the outer core is liquid due to seismic surveys of Earth's interior and that the outer core is 2,300 km thick, going down to approximately 3,400 km into the earth. Based on a couple of indicators, geologists have come to believe that the outer core is 80% iron, some nickel and a number of different lighter elements. Nace(2016) further implies that the lower you go in the layers of the Earth, the denser the materials because it is also believed that when the Earth was just beginning to cool billions of years ago, heavier elements sunk down into the center of the Earth, while less

dense elements rose to the surface. Therefore, we see a general increase in density, as you get closer to the center of the Earth.

The outer core is hot enough to be fluid, but not under as much pressure as to solidify the iron again, as seen in the inner core. The temperature of the outer core ranges from about 4,030 to 5,730 degrees Celsius. Amazingly, the outer core is fluid enough and low enough in viscosity that it may spins faster than the entire Earth. This differential velocity of spinning, along with convection and turbulent flow of the iron outer core, creates Earth's magnetic field.

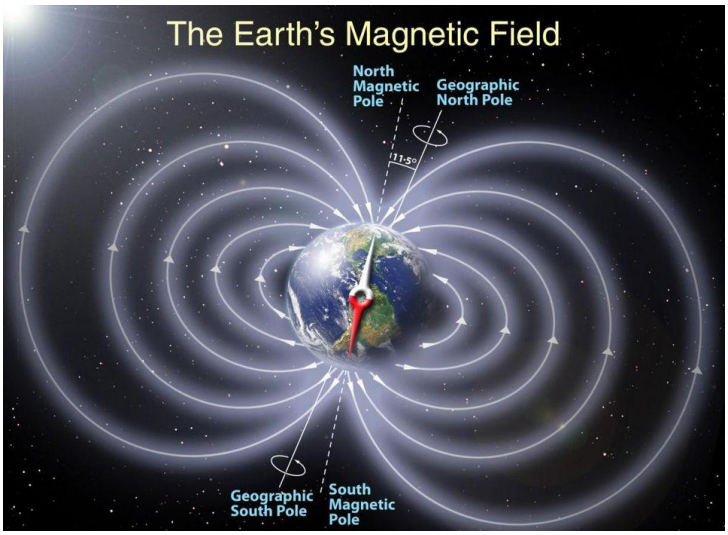

Fig 2.4: Earth's Magnetic Field created by the Outer Crust
Source: Nace(2016)

2.1.1.4 The Inner Core

The inner core is the layer at the center of the Earth and is in many ways similar to the outer core. It is also consists primarily of iron and nickel and has a radius of about 1,220 km. At the Inner Core, the pressures become high enough, up to 360 gigapascal, that despite very high temperatures of about 5,400 degree Celsius, the inner core is solid. OSU (2018) indicates that this is about three million (3,000,000) times the air pressure at sea level. It is also enriched in unusual heavy elements including gold, silver, platinum, palladium, and tungsten.

2.1.2 Continental Drift to Plate Tectonics.

There existed a misconception, which referred to the Earth crust as the tectonic plate. This was clearly debunked by scientists, indicating that the plate is the same as the lithosphere which is a combination of the crust and the upper layer of the mantle, a rigid zone that floats on the asthenosphere (Opara, 2015). Several authors (Brown, 2016; Ingolfsson, 2008; Jadhav, Undated; Kudela, 2016; Mcgregor, 2018; and many more) agree that the theory of tectonic plate is deeply rooted in the ancient theory of continental drift. Brown (2016) recorded that the theory of plate tectonics explains that the Earth's surface is divided into rigid plates of continental and oceanic lithosphere that, through time, move relative to each other, and which increase or decrease in area. The theory actually developed as an earlier idea of 'continental drift'.

2.1.2.1 Continental Drift.

According to Ingolfsson (2008), in 1596 a Dutch mapmaker Abraham Ortelius was the first to suggest that the Continents have not always been fixed in their present positions. Francis Bacon1620commented upon the 'conformable instances' along the mapped Atlantic coastlines and in 1858, Antonio Snider-Pellegrini suggested that continents were linked during the Carboniferous Period, because plant fossils in coal-bearing strata of that age were so similar in both Europe and North America (Brown, 2016). Ingolfsson (2008) agreeing with (Brown, 2016) recorded that in 1888, an Austrian geologist Eduard Suess gradually developed views on the connection between Africa and Europe and came to the conclusion that the Alps to the north were once at the bottom of an ocean, of which the Mediterranean was a remnant. He further discovered that the fossil glossopteris fern was found in South America, Africa, India and Antarctica. His explanation was that the three lands were once connected into a supercontinent, which he named Gondwana (after the indigenous homeland of the Gond

people of north-central India). Suess believed that the oceans flooded the spaces currently between those lands. He is credited with discovering the Tethys Ocean, which he named in 1893.

In Brown (2016)'s account, in 1910, American physicist and glaciologist Frank Bursley Taylor proposed the concept of 'continental drift' to explain the apparent geological continuity of the American Appalachian mountain belt (extending from Alabama to Newfoundland) with the Caledonian Mountains of NW Europe (Scotland and Scandinavia), which now occur on opposite sides of the Atlantic Ocean. This concept was re-proposed in 1912 by Alfred Wegener, a German Meteorologist. Wegener had initially been fascinated by the near-perfect fit between the coastlines of Africa and South America, and by the commonality among their geological features, fossils, and evidence of glaciations having affected these two separate continents. He compiled a considerable amount of data in a concerted exposition of his theory, and suggested that during the late Permian all the continents were once assembled into a supercontinent that he named Pangaea, meaning 'all Earth' and there was a universal ocean called Panthalassa. He drew maps showing how the continents have since moved to today's positions. He proposed that Pangaea began to break apart just after the beginning of the Mesozoic Era, about 200 Ma ago, and that the continents then slowly drifted into their current positions.

Between 1920 and 1960, a range of geophysical arguments was used to contest Wegener's theory. Most importantly, the lack of a mechanism strong enough to 'drive continents across the ocean basins' seriously undermined the credibility of his ideas. Most of the attacks were aimed at Wegener himself, an outsider who seemed to be attacking the very foundations of geology. This controversy made the theory of continental drift to remain a highly

controversial idea in those days (Brown, 2016 and Ingolfsson, 2008). Ingolfsson (2008) looking closely at the controversy highlighted that the most important reason Wegener's hypothesis was not accepted was because he suggested no mechanism for moving the continents. That Wegener thought that the force of Earth's spin was sufficient to cause continents to move, but geologists knew that rocks are too strong for this to be true. He also felt that the continents were moving through the earth's crust, like icebreakers plowing through sea-ice. However, geologists noted that plowing through oceanic crust would distort continents beyond recognition.

Both authors agree that in 1937South African geologist Alexander Du Toit, who became a staunch supporter of Wegener's theory after his visit to South America in 1923, provided support through the years of controversy by drawing maps illustrating a northern supercontinent called Laurasia (i.e. the assembled land mass of what was to become North America, Greenland, Europe and Asia). The idea of the Laurasian continent provided an explanation for the distribution of the remains of equatorial, coal-forming plants, and thus the widely scattered coal deposits in the Northern Hemisphere. He published his observations in Du Toit (1927), and later he developed his ideas in Du Toit (1937). There he argued for the separation of Wegener's Pangaea into the two super continents, Laurasia and Gondwana.

Despite the defamation of the Wegener's theory, it just wouldn't go away. Arthur Holmes, a British geologist and geo-morphologist championed the continental drift theory through the 1930s and 1940s. He performed the first uranium-lead radiometric dating to measure the age of a rock during his graduate studies, and furthered the newly created discipline of geochronology. His second famous work Holmes (1944) did not follow the traditional viewpoints and concluded with a chapter describing continental drift at a time when it was

deeply unfashionable with his more conservative peers (Wessel and Muller, 2007). In the duo's account, the problem with the continental drift theory was the mechanism of movement of the continents, which was solved by Holmes (1944) that proposed that the Earth's mantle contained convection cells that dissipated radioactive heat and moved the crust at the surface. He concluded that there were areas where fluids trapped beneath Earth's crust heat up, rise, spread laterally, then cool and drop back down as shown in his model in figure 2.5. Holmes (1944) ended with a chapter on continental drift, part of which formed the origin of the seafloor spreading concept.

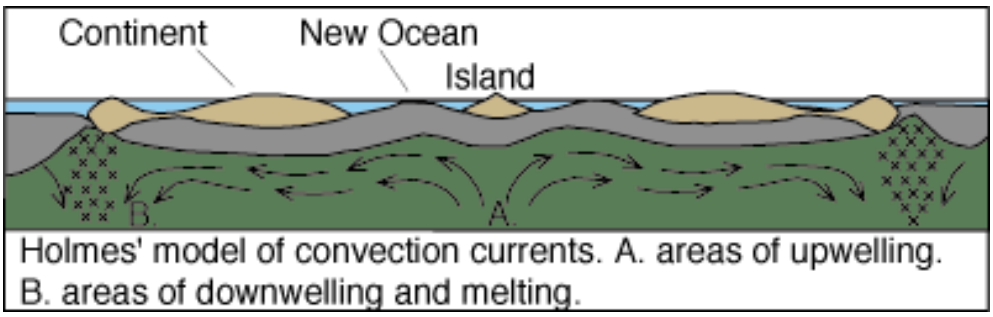

Fig. 2.5 Holmes' Model of Convection Currents
Source: Ingolfsson (2008).

2.1.2.2 Mid Ocean Ridges and Sea-Floor Spreading

With more people discussing and making discoveries with regards to the validity of the Continental Drift Theory, German geologists tried in the late 1930's to prove it, but the Second World War destroyed that effort. Prior to that, Ingolfsson (2008) recorded that Fritz Haber, a prominent German Chemist, started the discoveries of the Mid Ocean Ridges. Haber suggested that Germany could ease its debts after World War I by extracting gold from sea water (theoretically up to 56mg of gold could be extracted from $1m^3$ of sea water). In 1925, Germany outfitted a boat and set out for two years to systematically explore the Atlantic Ocean. At the end of the study, they returned with data that shows the existence of a major Mid-Atlantic Ocean Ridge.

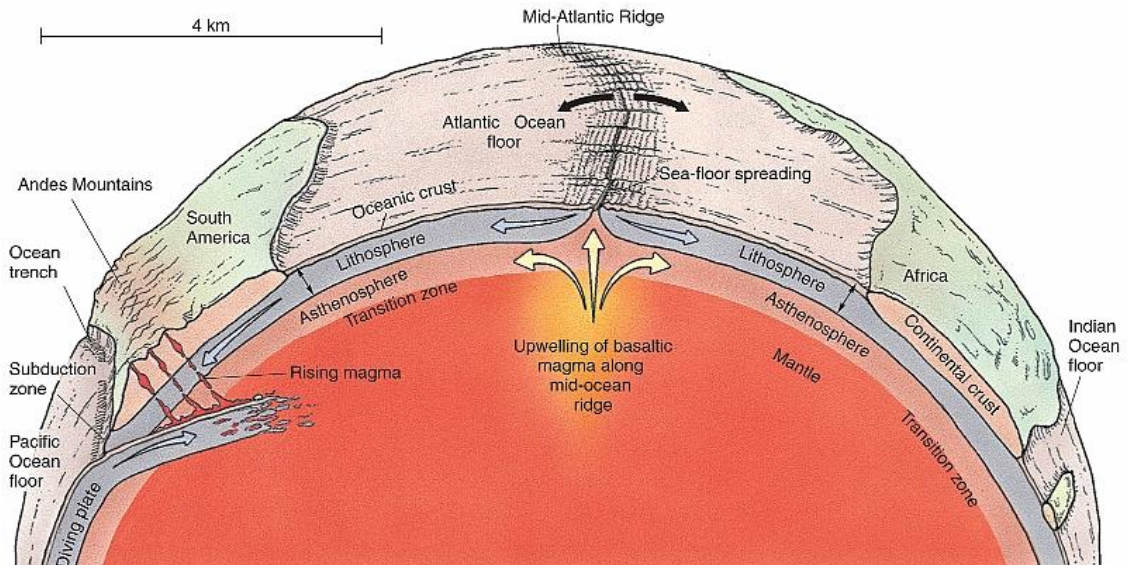

Fig. 2.6: Mid Atlantic Ridge
Source: McGregor (2018)

However, with the Second World War came the realization of the complexity of the ocean floor topography through the improvements on sonar equipment. Accordingly, Brown (2016) stated that there was a resurgence of interest in Wegener's theory by a new generation of geophysicists, such as Harry Hess (Captain in the US Navy and later professor at Princeton), through their investigations of the magnetic properties of the sea floor. In addition, an increasing body of data concerning the magnetism recorded in ancient continental rocks indicated that the magnetic poles appeared to have moved or 'wandered' over geological time. This Apparent Polar Wanderwas explained by the movement of the continents, and not the magnetic poles. Hess (1962) developed the idea of sea-floor spreading, which is a forerunner of plate tectonics.

He discovered hundreds of flat-topped mountains on the Pacific floor and named them Guyots, but found them very puzzling. They looked like their tops were eroded, but they were 2 kilometers under water.

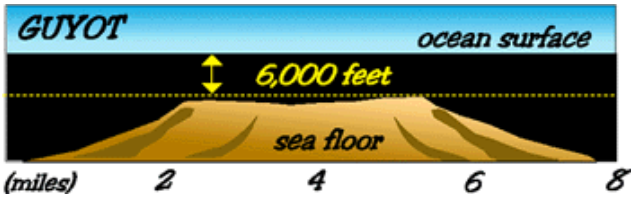

Fig 2.7a: Hess' Guyot (Section)
Source: Ingolfsson (2008)

Fig 2.7b: Hess' Guyot (Surface)
Source: Ingsolfsson(2008)

Furthermore, Ingolfsson (2008) has it that Hess had the following suggestions:

i. That distribution of flat-topped seamounts (guyots), or old volcanoes, rising from the seafloor, showed movements of the crust and subsequent subduction,

ii. That the continents had not plowed through oceanic crust (as posited by Wegener), but that the entire crust had moved,

iii. That the ocean basins were young and thus lacked thick sediments,

iv. That new crust was formed at the mid-ocean ridges and was destroyed in the deep trenches, and

v. That the crustal movements were driven by convective cells

By 1961the American geologists Robert Dietz, Bruce Heezen and Harry Hess proposed that linear volcanic chains (mid-ocean ridges) identified in the ocean basins are sites where new sea floor is erupted and once formed, this new sea floor moves toward the sides of the ridges and is replaced at the ridge axis by the eruption of even younger materials.

The foundations for modern plate tectonics were laid in 1963by two British Geoscientists, Fred Vine and Drummond Matthews, who linked Hess's Sea-floor spreading model with

their proposed hypothesis. They elegantly explained the concept of magnetic reversal stripes on the ocean floor, indicating that the new oceanic crust, formed by the solidification of basalt magma extruded at mid-ocean ridges, acquired its magnetization in the same orientation as the prevailing global magnetic field. These Palaeomagnetic, fossil magnetic properties frozen in rocks, stripes provide a chronological record of the opening of ocean basins. As magma cools and solidifies along the mid-ocean ridges, it becomes magnetized in the direction of the magnetic field at the time. Since paleomagnetic epochs on land can be dated, reversals recorded in the sea reveal the age of the ocean crust.

2.1.3 The Tectonic Plate

The Mid Atlantic Ocean Ridge was later, according to Ingolfsson (2008), discovered to extend to other great oceans in 1953. American physicists Maurice Ewing and Bruce Heezen discovered that through this underwater mountain range ran a deep canyon, which they called the Great Global Rift. The rift appeared to be breaks in the earth's crust. The rift outlined chunks of the earth's crust, which were named tectonic plates. In fact, the Canadian J. Tuzo Wilson in 1965offered a fundamental reinterpretation of Wegener's continental drift theory and became the first person to use the term 'plates' to describe the division and pattern of relative movement between different regions of the Earth's surface (i.e. plate tectonics). He also proposed a tectonic cycle (the Wilson cycle) to describe the lifespan of an ocean basin: from its initial opening, through its widening, shrinking and final closure through a continent-continent collision. Till date, there has been an increasingly wide acceptance of the theory of plate tectonics. A concerted research effort, such as the result shown in Figure 2.8, was made into gaining a better understanding of the boundaries and structure of Earth's major lithospheric plates, and the identification of numerous minor plates (Brown, 2016).

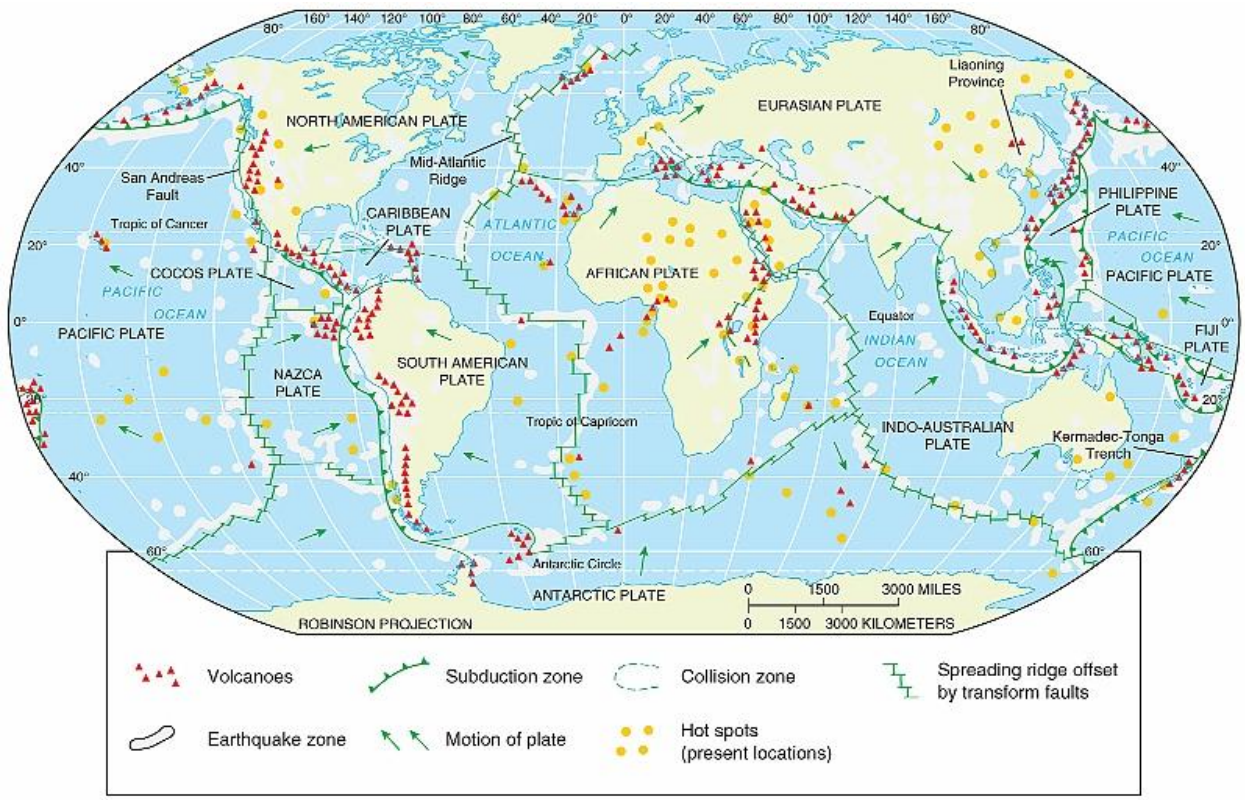

Fig 2.8: Map of the world, showing the Tectonic Plates and other Tectonic Information
Source: McGregor (2018)

2.1.4 Tectonic Plate Boundaries

The rigidity and fragmentation of the Earth's outer shell, at least of the continents, was implicit in the ideas of continental drift and in early works on seafloor spreading (Wegener, 1912 in Duarte and Schellart, 2016). Wilson (1965) introduced plates for the first time as "mobile belts, which may take the form of mountains, mid-ocean ridges and major faults with large horizontal movements, connected into a continuous network of mobile belts about the Earth which divide the surface into several large rigid plates." McKenzie and Parker, (1967) described how aseismic areas move as rigid plates on the surface of a sphere. Clear connection between the three types of plate boundaries and their associated three types of focal mechanisms, normal, thrust, and transform, were made in literature (Duarte and Schellart, 2016).

The modern conception of plate tectonics is that the surface of the Earth is composed of rigid lithospheric plates that incorporate the crust and the upper (strong) portion of the mantle and move coherently relative to one another over the asthenosphere through geological time, such that deformation, seismicity, and volcanism occur at their boundaries (Kreemer et al., 2003). On the average, plates are ~100 km thick, and move very slowly, at centimeters per year with respect to one another. The rigid plate model, propounded by Jason Morgan in 1967, immediately proved a powerful tool for computing present and past plate motions (Muller, Royer and Lawver, 1993) and, in particular, for constructing global plate kinematic models. Notwithstanding, it was soon recognized that in a number of regions, plate boundaries are broad regions of deformation several hundreds of kilometers wide rather than narrow regions that are at least an order of magnitude smaller. Isacksand Oliver (1968) was among the first to show that on a global scale earthquakes are distributed along "narrow seismic belts that outline aseismic blocks" and that focal mechanisms of more than 100 earthquakes remarkably correlate with the geometry and kinematics of the plates as proposed by Wilson, Le Pichon, Morgan, and McKenzie. Isacks noted that these belts are narrower in spreading zones (mid-Atlantic), broader in convergent regions (Andes), and diffuse within continents (Himalayas) (Duarte and Schellart, 2016).

According to Duarte and Schellart(2016), Gordon and Stein (1992) showed that such broad regions of seismic deformation occur not only in continents but also within the oceanic lithosphere (the Indian Ocean region of the Indo-Australian-Capricorn composite plate and at the eastern Azores-Gibraltar plate boundary). Plate boundaries cover 15% of the Earth's surface and cover a spatial range that spans from a single fault system to diffuse regions of deformation sometimes with stranded micro-plates (*Kreemer et al.*, 2014). To accommodate such diversity, Gordon and Stein (1992) in Duarte and Schellart(2016) used the term "plate

boundary zones," defined as a "zone of active deformation that takes up the motion between nearly rigid plate(s)." Such zones vary in width from a few hundreds of meters, such as the oceanic transforms, to thousands of kilometers, such as areas of continental collision like the Himalaya-Tibet mountain belt. According to the Incorporated Research Institutions for Seismology(IRIS, 2007), the three general types of plate boundaries are divergent, convergent, and transform boundaries.

2.1.4.1 Divergent Plate Boundaries

Discussing this type of boundary, Duarte and Schellart(2016) indicated that divergent plate boundaries are characterized by low to moderate seismicity and volcanism. At such boundaries, plates move away from each other such as at oceanic spreading ridges. IRIS (2007) stated that divergent boundaries can be spreading ocean ridges or continental rift zones, occurring inside the continents producing rift systems, such as the East African Rift, which are bounded by extensional normal faults. Divergent boundaries occur where plates are moving apart, basically because hot mantle rock rises and partial melting occurs. The new crust is then created and the magma pushes up from the mantle as shown in figure 2.9(a and b). This type of boundary is generally considered as regions of plate construction, where new tectonic plate material (lithosphere) is created.

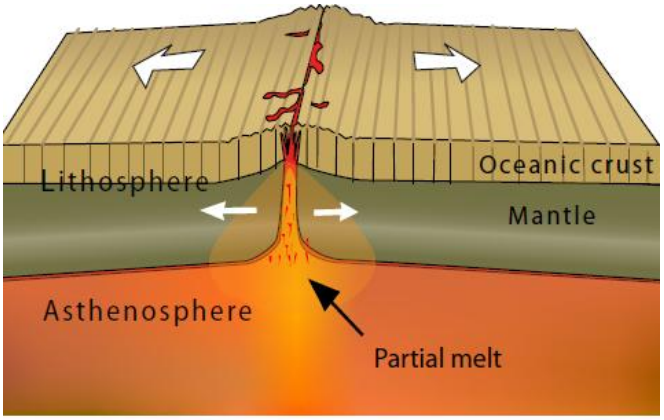

Fig 2.9a: Fast-spreading ridges—Mountain chain forms along the crest of the ridge. (Ex. East Pacific Rise) High heat and magma input making the ridge bouyant. New crust is added both as dikes and as erupted lava
Source: Brown (2016)

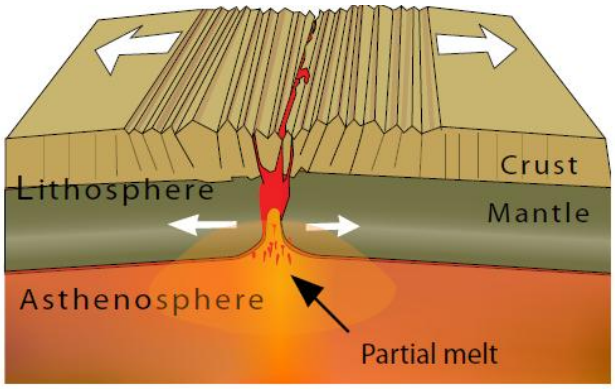

Fig 2.9b: Slow-spreading ridges form valleys on the ridge crests. Lower heat input (Ex. Mid-Atlantic Ridge). The early onset of extension forms a basin-and range province of parallel mountains and valleys dispersed across a broad uplifted area.
Source: Brown (2016)

Analyzing the lifethe evolution of a divergent plate boundary, Smart (2012), indicated that there exists three recognizable stages which include

i. **The birth of a divergent boundary:** this requires that an existing plate (whether oceanic or continental) begins to divide. This is the case of East Africa today, known as the East African Rift zone, the Somali Plate is being birthed. The African continent is slowly splitting in two and as the continental crust divides, magma from the asthenosphere fills in the gap. Several volcanoes are present in the rift zone.

ii. **The youth stage:**Eventually the gap will form a narrow oceanmuch like the Red Sea to the north of the East African Rift zone, separating Saudi Arabia from Africa, and similar narrow sea, the Gulf of California, which lies between much of Mexico and Baja California.

iii. **Mature Stage:** It takes millions of years to form a mature ocean, as rates of plate motions are slow (10-100 mm/yr). The oldest oceanic crust in the Atlantic and Pacific Oceans is the same age (~180 million years) but the Pacific is much wider than the Atlantic because it is spreading 2 to 3 times as fast

2.1.4.2 Convergent Plate Boundaries

Duarte and Schellart(2016) indicated that convergent plate boundaries are the loci of high to very high magnitude seismicity, thrust faulting and volcanism. According to IRIS (2007), Crust is destroyed as two plates move towards each other, the heavier plate dives (subducts) beneath the more-buoyant plate at a location known as a Subduction Zone. This type of boundaries is regarded as destructive plate boundaries, as plate material is destroyed and lost as it disappears into the mantle. gave the three varieties of convergent plate boundaries, depending upon the type of lithosphere that is juxtaposed across a subduction zone. They include:

i. Oceanic Plate vs. Oceanic Plate Convergence

The older and heavier of the two plates descends into the subduction zone when plates of oceanic lithosphere collide along a trench. The descending plate carries water-filled sediments from the ocean floor downward into the mantle. The presence of water alters the physical and chemical conditions necessary for melting and causes magma to form. The magma rises up through the overriding

oceanic plate, reaching the surface as a volcano, which may rise, as it grows, above sea level to form an island. Trenches often lie adjacent to chains of islands (island arcs) formed by magma from the subducted plate. Examples of the oceanic to oceanic plate convergence include the Aleutian Islands (Fig. 2.10) off the tip of Alaska were formed by magma generated when the Pacific Plate descended below some oceanic lithosphere on the margin of the North American Plate, 2004 Sumatra-Andaman earthquake and associated tsunami at the Sunda subduction zone, volcanic activity on the island of Montserrat in the Caribbean as a result of subduction of the South American Plate below an island arc that marks the edge of the Caribbean Plate, the 2011 Japan (Tohoku) earthquake and associated tsunami at the northwest Pacific subduction zone (IRIS (2007), Duarte and Schellart(2016).

ii. Oceanic Plate vs. Continental Plate Convergence

When an oceanic plate converges on a continental plate and the denser crust of the oceanic plate, which is consumed preferentially, sinks beneath the more-bouyant continental plate, which is almost never destroyed in subduction zones. In this type of convergence, trenches, strong, destructive earthquakes and the rapid uplift of mountain ranges are common. Water released from subducting slab facilitates melting, rise and builds volcanic arc. (*Examples*: Juan de Fuca plate subducting beneath the North American plate off shore in the Pacific Northwest, off the coast of South America along the Peru-Chile trench, the Nazca Plate dives below South America in a subduction zone that lies along the western margin of the continent. Convergence between these plates has resulted in the formation of the Andes Mountains (the second highest mountain range on Earth), extensive volcanism,

and widespread earthquake activity (Fig. 2.10). The largest earthquakes are concentrated along subduction zones.

iii. Continental Plate vs. Continental Plate Convergence

When two continents meet head-on, neither issubducted because the continental rocks are relatively light and, resist downward motion. Instead, the crust tends to buckle and be pushed upward or sideways. They usually are deformed adjacent to subduction zones rather than consumed. The tallest mountains in the world were formed (and continue to grow) as a result of continental collision. The Himalayan Mountain ranges, which dramatically demonstrates one of the most visible and spectacular consequences of plate tectonics, towering as high as 8,854 m above sea level, and form the highest continental mountains in the world, mark the boundary between the Indian and Eurasian plates (Fig. 2.10). The collision of the plates began over 40 million years ago when India smashed into the belly of Asia. The 2015 Nepal earthquake in the Himalayan collision zone is an example of activities in the Continental Convergent boundaries.

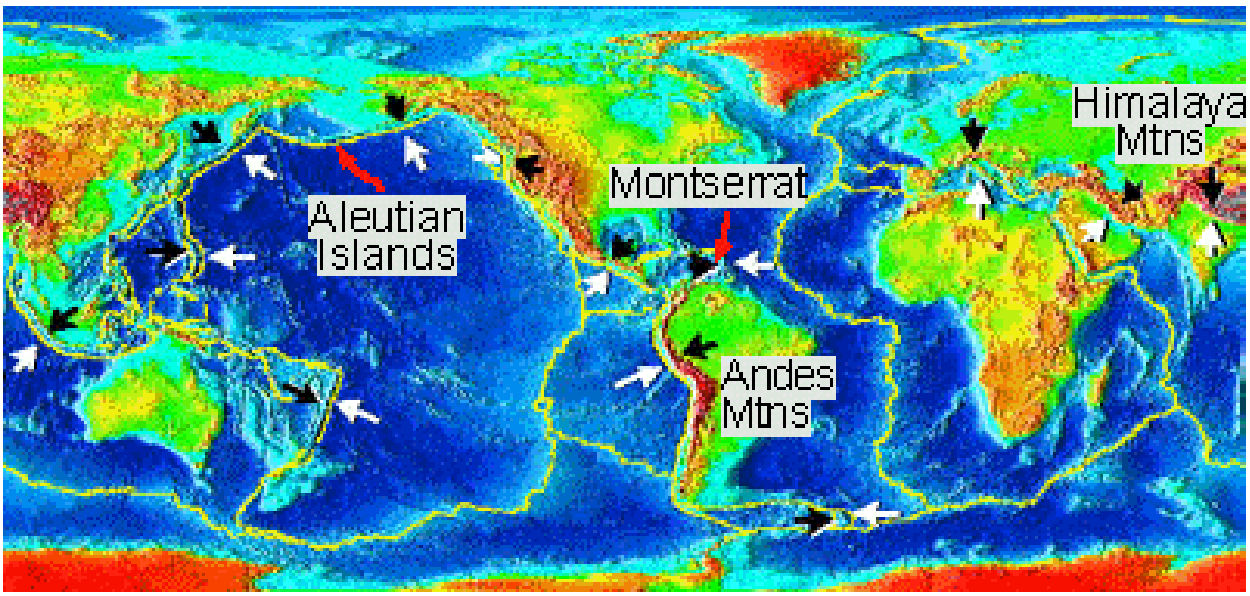

Fig. 2.10: Examples of convergent plate boundaries and Sense of plate motion indicated by arrows.
Source: Source: Brown (2016).

2.1.4.3 Transform Plate Boundaries

Transform plate boundaries are where two plates move past one another without significant convergence or divergence and where slip along the plate boundary fault predominantly has a horizontal movement. They basically involve plates sliding past each other and lithosphere is neither destroyed nor created; consequently, these boundaries are sometimes termed conservative plate boundaries. Analyzing its importance, ‘ ( )’likened transform boundaries to the nuts and bolts that hold massive structures together. They opined that transform plate boundaries are the underappreciated members of the plate tectonics machine. Seismicity in these regions is generally of moderate to high magnitude.

Transform boundaries join sections of convergent and/or divergent boundaries. Most transform boundaries occur in ocean basins where they offset oceanic ridges. Plates on either side of a transform boundary slide past each other without either plate being consumed and without a gap opening between the plates. Recent analysis of satellite altimeter data has allowed scientists to use slight variations in the elevation of the ocean surface to determine the topography of the seafloor. Examination of oceanic ridges along the East Pacific Rise or Mid-Atlantic Ridge show offsets along transform boundaries (Fig 2.11a).

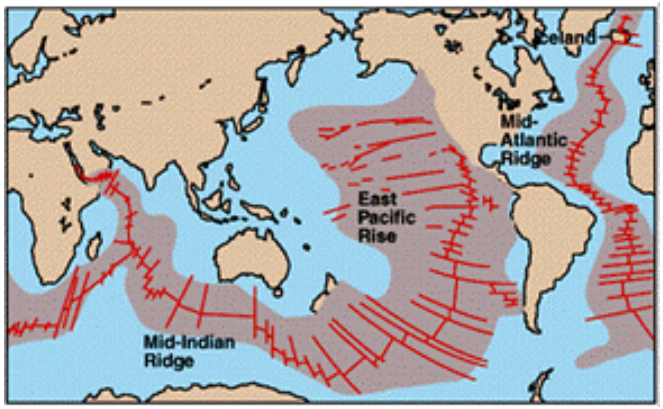

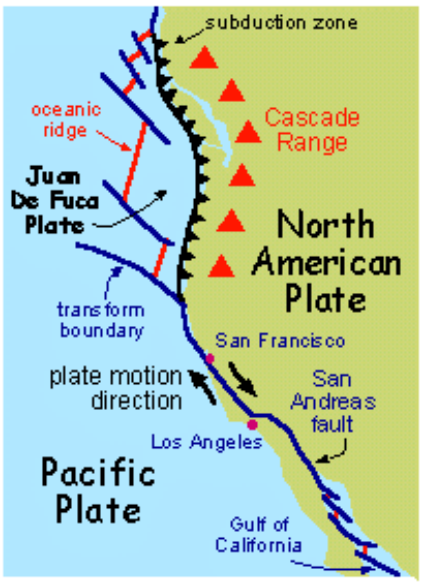

Fig 2.11a Transform Faults in the Oceanic Ridge *Fig 2.11b: The San Andreas Fault*
Source: Ingolfsson(2008)

Some transform boundaries such as the San Andreas Fault in California or the North Anatolian Fault in Turkey occur on land. The San Andreas Fault joins two oceanic ridges. The southern end of the fault begins in the Gulf of California at the north end of a young ocean (Fig 2.11b). The northern end of the fault becomes the Mendocino fracture zone offsetting a section of the oceanic ridge that defines one side of the small Juan de Fuca plate offshore from Washington and Oregon. Land on the west side of the San Andreas Fault, including Los Angeles and San Diego, is part of the Pacific Plate. San Francisco lies east of the fault and is on the North American Plate. This implies that Western California is being slowly displaced to the northwest relative to the rest of the state. It is not going to drop off into the ocean but it will eventually migrate along the western boundary of the North American Plate, eventually colliding with Alaska millions of years from now. Examples of very high magnitude events as a result of transform plate boundaries include the M8.4 earthquake of 25th November 1941 in the Gloria strike-slip fault in the Azores-Gibraltar plate boundary (Buforn, Udias, and Colombas, 1988) and the 11th April 2012 MW 8.6 and 8.2 events ocean-ward of the Sumatra subduction zone segment (Delescluse et al., 2012; McGuire and Beroza, 2012).

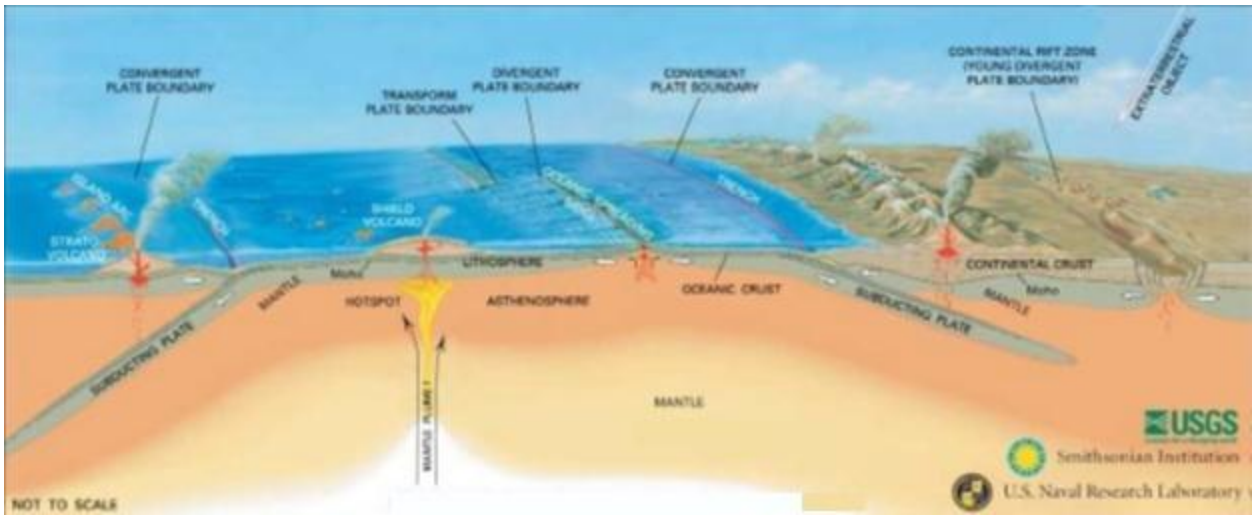

Fig. 2.12 Overview of Tectonic Activities
Source: McGregor (2018)

2.1.5 Crustal Deformation Monitoring

Deformation is the change in shape, size and/or figure of an object from its normal to an abnormal state as a result of forces acting on, under or near the object (Ono, Agbo, Ijioma&Chubado, 2009). According to Celik(1998), the Earth's lithosphere is deforming continuously due to plate tectonics. He further opined that the movement of the Earth's crust comprises both global (tectonic motion) and local (earthquakes) elements. Tectonic motion is described by the plate tectonic theory discussed in section 2.2. Plate tectonic motion which is generally governed by convection currents causes earthquakes, faults, plate boundaries and volcanoes. Shirzaei(2010) upholds this view that Monitoring of crustal deformation has contributed to our understanding of tectonics, earthquakes, volcanism and landslides. A continuous deformation monitoring and analysis scheme can provide a quick response system for natural disasters, such as volcanic unrest.

Discussing the importance of crustal deformation monitoring, Sagiya(2013) stated that it helps in the understanding of the size and mechanism of an earthquake and prediction of tsunamis. It even helps in the prediction of earthquakes. Surface deformation measurements are routinely used to constrain the subsurface geometry of magmatic sources, active faults and the spatial distribution of co-seismic slip. The data provided by this type of monitoring avail us a primary means for recording aseismic processes such as afterslips, viscoelastic and poroelastic adjustments and so-called silent earthquakes. Geodetic measurements provide invaluable constraints on the interseismic accumulation of strain that might be released in large and damaging earthquakes. Most volcanic eruptions are preceded by inflationary doming and stretching of the crust as large volumes of magma migrate from the mantle through the crust Shirzaei(2010). Although the rigidity of plates is still a useful concept used in many studies, modern space geodetic techniques can use intraplate stations to quantify

intraplate strain. Such approaches thus allow us not only to quantify directly the relative motion of the tectonic plates within and outside the plate boundary zones but also to compute their internal deformation (Stein and Sella, 2002).

According to Argus and Gordon, (1991), global motion models describe plate velocities based on the data from earthquakes, transform fault azimuths and spreading rates. The mechanism that creates earthquakes is still largely elusive, but it is believed to be associated with strain accumulation and one method of determining strain is to directly monitor the relative movements of the Earth's crust using geodetic methods. Agreeing with the duo, Shirzaei(2010) explained that the key to understanding earthquakes and the eruptive potential of a volcanic system is aided by the stress transfer concept. The ability to characterize the actual state of stress of a volcanic system and to understand how susceptible the system is to small parameter changes involves proper monitoring strategies including novel ground and space based observation methods.

2.3.1 Geodetic Methods of Crustal Monitoring

Hentone*t. al*(2006) stated that geodynamic monitoring is demanding in terms of observational accuracy and stability over a wide range of spatial and temporal scales. Classical and space geodesy play important roles in determining crustal deformation parameters, due to the fact that deformation, in general, means a change in geometric configuration. Celik(2008) explained that classical geodesy, unlike space geodesy, does not provide precise measurements over long distances. However, Davies(1997) indicated that since the 1960's space geodesy (VLBI, SLR and GPS) has been widely used for monitoring crustal movements, enabling precise vector measurements to be made between ground stations anywhere on the Earth. One of the most important aims of modem space geodesy is to monitor crustal movements (Celik, 1998).

The use of space-geodetic techniques to study geodynamic processes began with Very Long Baseline Interferometry (VLBI) in the early 1970s. By measuring the delay in arrival time of the signal from distant celestial objects, the distances between stations that are hundreds of kilometers apart can be derived with millimeter accuracy (Bastos*et. al,* 2010). Another technique that has been available since the early 1970s is Satellite Laser Ranging (SLR). SLR as a technique determines the distance to a satellite by measuring the round trip time of a light pulse that is sent to the satellite (Degnan1993in Bastos*et. al,* 2010). VLBI technique was, and still is, an important tool to support the realization of an accurate and stable celestial reference system. SLR has an important role in the determination of the Earth's geocentre and in calibrating geodetic microwave techniques. SLR and VLBI provided a fundamental contribution to clarify the kinematics of the tectonic plates on a global scale. During the 1980s, a quite extensive use of mobile VLBI and SLR systems was made in dedicated campaigns to monitor some specific regions of the world with more significant tectonic activity (Vermaat, Degnan, Dunn, Noomen and Sinclair1998). The limitations for a wider use of VLBI and SLR for geodynamic purposes are their relative lack of portability, high cost and operational complexity.

The advent of Global Navigation Satellite Systems (GNSS), such as GPS (Global Positioning System) and GLONASS (GLObalNAvigation Satellite System) in the 1980s made tremendous improvements in the methods of geodynamic monitoring. GPS rapidly started to be applied for geodynamic applications, whereas GLONASS, due to difficulties in achieving its full operational implementation, has not yet been used in many geodynamic studies. In the 1990s, radio satellite systems like DORIS (Doppler Orbitography and Radiopositioning Integrated by Satellite) started to give useful information for the study of regional and global geodynamics issues. Soudarin and Grétaux(2006) present a recent geodynamic study using 57

DORIS stations. Actually, the most commonly used space-geodetic technique for geodynamic studies is still GPS (Hentone*t. al*, 2006).

An appropriate reference frame is a requisite tool that enables better understanding of geodynamic systems that in turn provides better constraints to predicted impacts on society. However, the effects of geodynamic and geophysical crustal deformation processes can systematically bias the reference frames used for geodetic surveys (Hentone*t. al*, 2006). Kinematic processes affecting the Earth's surface, as explained by Hentone*t. al*, (2006), can systematically affect geodetic measurements and ultimately lead to inconsistencies between observations at different epochs. As measurement and processing accuracies and requirements have increased, the time-variability of geodetic outputs must be evaluated.

2.1.6 GAMIT/GLOBK

GAMIT is an acronym that means GNSS Analysis at Massachusetts Institute of Technology. It is a collection of programs to process phase data to estimate three-dimensional relative positions of ground stations and satellite orbits, atmospheric zenith delays, and Earth orientation parameters. The software is designed to run under any UNIX operating system. GLOBK, the acronym for Global Kalman filter, is a Kalman filter whose primary purpose is to combine various geodetic solutions such as GPS, VLBI, and SLR experiments. It accepts as data, or "quasi-observations", the estimates and covariance matrices for station coordinates, Earth orientation parameters, orbital parameters, and source positions generated from the analysis of the primary observations. The input solutions are generally performed with loose apriori uncertainties assigned to all global parameters, so that constraints can be uniformly applied in the combined solution (Floyd, 2018).

According to Herring *et al.*(2018c) although GLOBK has been developed as an interface with GAMIT(for GNSS) and CALC/SOLVE (for VLBI), there is little intrinsic to this pairing in its structure. We have used GLOBK successfully to combine solution files generated by other GNSS software (e.g. Bernese and GIPSY), as well as for terrestrial and SLR observations.

There are three common modes, or applications, in which GLOBK is used:

1. Combination of individual sessions (e.g., days) of observations to obtain an estimate of station coordinates averaged over a multi-day experiment. For GNSS analyses, orbital parameters can be treated as stochastic, allowing either short- or long-arc solutions.
2. Combination of experiment-averaged (from (1)) estimates of station coordinates obtained from several years of observations to estimate station velocities.
3. Independent estimation of coordinates from individual sessions to generate time series assessment of measurement precision over days or years.

Some things GLOBK cannot do.

1. GLOBK assumes a linear model. Therefore, any large adjustments to either station positions or orbital parameters (>10 m for stations and >100 m for satellite orbits) need to be iterated through the primary processing software to produce new quasi-observations.
2. GLOBK cannot correct deficiencies in the primary (phase) analysis due to missed cycle slips, "bad" data, and atmospheric delay modeling errors. You cannot eliminate the effect of a particular satellite or station at the GLOBK stage of processing, though GLOBK can be useful in isolating a session which is not consistent with the ensemble and in some cases the effect of a station on the GLOBK solution can be reduced.
3. GLOBK cannot resolve phase ambiguities: the primary GPS solution must be strong enough on its own to accomplish this. The need to combine sessions for ambiguity

resolution is the one reason you might want to perform a multi-session solution with primary observations.

According to Herring *et al.*(2018a) GAMIT/GLOBK is a comprehensive GNSS analysis package developed atMassachusetts Institute of Technology(MIT), the Harvard-Smithsonian Center for Astrophysics (CfA), Scripps Institution of Oceanography (SIO), and Australian National University(ANU) for estimating station coordinates and velocities, stochastic or functional representations of post-seismic deformation, atmospheric delays, satellite orbits, and Earth orientation parameters. Although the software is currently maintained by Herring T. A., King R. W., and FloydM. A.at MIT, many people have made substantial contributions. The orbital integration and modules used in computing the theoretical phase observable have their origins in the Planetary Ephemeris Program (PEP) written by Michael Ash, Irwin Shapiro, and Bill Smith at Lincoln Laboratory in the 1960's, with later contributions by Bob Reasenberg and John Chandler at MIT. The codes for processing GPS observations were developed at MIT in the 1980's by Chuck Counselman, Sergei Gourevitch, Yehuda Bock, Rick Abbot, and King. GAMIT attained its current form through the efforts of Bock, Danan Dong, Peng Fang (SIO), Kurt Feigl, Herring, King, McClusky (ANU), Mike Moore (ANU), Peter Morgan (Canberra University), Mark Murray (New Mexico Tech), Liz Petrie (University of Newcastle), BerkhardSchraffin(Ohio State University), Seiichi Shimada (NIED), Paul Tregoning(ANU), and Chris Watson (University of Hobart). GLOBK was developed by Herring and Jim Davis at CfA for combination of VLBI data and modified at MIT to incorporate GPS data. Funding for the early development of GAMIT was provided by the Air Force Geophysics Laboratory and for GLOBK by NASA. Current support for development and support of the scientific community comes primarily from the National Science Foundation.

Herring *et al.*(2018a) further explains that to control processing the software uses C-shell scripts (stored in /com and mostly named to begin with *sh_*) which invoke the Fortran or C programs compiled in the /libraries, /GAMIT, and /kf directories. The software is designed to ran under any UNIX operating system supporting X-Windows, including LINUX and MacOS. The parameter logic allows a maximum of 99 sites and the standard distribution is dimensioned for 80 sites, but since the run is proportional to the cube of the number of parameters, with networks larger than 50 sites greater efficiency is obtained by parallel processing using connected subnets.

2.2 Review of Related Literatures

Literary works related to deformation monitoring with the use of CORS technology were reviewed. Conscious efforts were geared towards identifying the methods and procedures the researchers used, benefit from their works, learn from their shortcomings and fill in the identified gaps in this research. The reviewed works include works done within and outside Africa.

Bawa, Ojigi and Dodo (2018)soughtto investigate the Velocity Time Series of the Nigerian CORs Network (NigNet) using the GAMIT/GLOBK GPS Processing Software. They used a five year data span between 2011 and 2015. A total of fourteen (14) station data were used which include: ABUZ, BKFP, GCCT, CLBR, FPNO, FUTA, FUTY, GEMB, HUKP, MDGR, OSGF, RUST, ULAG AND UNEC. The study adopted nine (9) IGS stations for the

stabilization of the NigNet stations which include: HARB (South Africa), SUTH (South Africa), RBAY (South Africa), NKLG (Gabon), RABT (Morocco), CAGZ (Italy), NOT1 (Italy), MAS1 (Spain) and SFER (Spain). The International Terrestrial Reference Frame 2008 was used for the solution constraint in the study. They used 3-sigma threshold for the outlier removal, which excludes all samples greater than 3-sigma from the final position and velocity estimate. The Weighted Root Mean Square (WRMS) on the average for 95% of the stations was found to be less than 1.9mm, 2.4mm and 8.1mm for the North, East and Up components respectively. The trio also recorded that the Normalized Root Mean Square (NRMS) on the average for 95% of the stations was found to be in agreement with Herring *et al*(2015 a&b) but failed to give the exact figures. The average velocity was found to be 19.24±0.14 mm/yr and 22.09±0.19mm/yr in the North and East directions respectively indicating a general North-East motion. These results are in agreement with the general motion of the Nubia Plate shown in Altamimi*et al* (2011).

Aung*et al*(2016) carried a study on Sagaing Fault Slip and Deformation in Myanmar using continuous GPS monitoring in order to analyze the Myanmar cGPS network observations and then measure the moving rate and direction of movement for each cGPS station using the GAMIT(GLOBK software packages). The trio defined Myanmar as the second-largest country in Southeast Asia which lies in the westernmost part of the Sundamegathrust. They explained that Myanmar is also affected by two more fault systems that behave according to the northward translation of Indian Plate on the Sunda block. The Sagaing Fault is one of the major active faults in Myanmar, more than 1200 km in length. The fault had experienced many earthquakes in her history, and because several major cities lie along this active fault, the seismic studies became critically important. They further investigated the co-seismic moving rate associated with the earthquake event using TRACK kinematic positioning

program. The data analysis covers a period of four years from 2011 to 2014. GAMIT, GLOBK, and TRACK software suite package was used for GPS data processing and analysis.

The analysis indicated that the west side of the Sagaing fault moves South-Eastward at the average rate of approximately 32-40mm/annum, whereas the east side of the fault moves northeastward at a rate of about 31-35mm/annum. For co-seismic analysis, two cGPS stations were analyzed in connection with the 2012 Mw6.8 ThaBeikkyin earthquake. The GPS data analysis showed clearly that the station at the eastside of the Sagaing fault immediately moved south by 15.0cm whereas the station at the Westside moved north by 3.0cm. In conclusion, the study demonstrated that the Sagaing fault's tectonic activities can be monitored by cGPS observations using geodetic processing techniques.

Stamps, Saria and Kreemer(2016), analyzingGeodetic Strain Rate Model for Sub Saharan Africa,described the Sub-Saharan Africa Geodetic Strain Model 1.0 with a view to contribute to the Global Earthquake Foundation (GEM) Strain Rate Project. The work targeted the improvement of the latest GEM geodetic strain model with an updated strain rate field of Sub-Saharan Africa. The study covered the East African Rift System (EARS), the active divergent plate boundary between the Nubian and Somalian plate which accommodates at least three micro-plates(Rovumba, Lwandle, and Victoria).

They developed an improved strain rate field for sub-Saharan Africa that incorporated an expanded geodetic velocity field within the Nubian-Somalian plate system and along the EARS, redefined regions of deforming zones guided by seismicity, distributions and updated constraints on block rotations from a recent publication by one of the authors. The area, they

studied on the work included part or all of the Somalia, Nubian, Rovumba, Lwandle, Victoria, Antarctica and Arabia plates/sub plates covering longitudes 22^{o} to 55.5^{o} and latitudes -52 to 20 with 0.59 (longitude) by 0.4^{o}(latitude) sprang because the values are compatible with GEM geodetic strain rate field. Stamps *et al*(2016) defined the regions of deformation by evaluating the locations of seismicity data from the international seismicity catalog, locations of APS Observations and previous studies that indicate rigidity. Even though it was evident from the seismicity catalog that the South western part of the EARS has profuse active seismicity, the zone was removed because there were no GPS data available to constrain possible deformation or rigidity of the region within observational error. To strengthen this reason, they noted that there was seismicity present in South Africa, but the available GPS observations indicated rigidity in Malservisi, Ugentobler, Wonnacott, and Hackl (2013). They employed a combination of CORS and episodic GPS observations. The CORS data required were to span a minimum of 2.5 years to minimize seasonal signals in the time series. While the episodic GPS sites were required to have three (3) or more occupations spanning 4 or more years. Areas with known or observed transient deformation were eliminated with the exception of one.

They used the publically accessible data for one solution and used episodic GPS data in Tanzania, Uganda and Madagascar for a second solution. They used the common sites ABPO, TANZ, EBBE, MBAR, SRTI, REUN and SEYI to compute the transformation parameters for the combination of the two solutions and rotation of the velocity solutions into a consistent Nubian-fixed reference frame. After the transformation, the RMS value for the 56 common sites in solution A and B was found to be 0.68mm/year.

Zhang, Lia, Liaob, and Wang(2016) carried out a study on the Source Rupture Process of the 2015 Gorkha, Nepal Mw7.9 Earthquake and its Tectonic Implications. They indicated that Nepal is located along the active Main Himalayan thrust arc, where the Indian plate under thrusts the Eurasian plate at a rate of 45mm/a towards the north-northeast providing one of the world's continental convergent plate boundaries. The region accommodates approximately a half of the tectonic convergence between these two plates. The locked part of the subduction interface has a low-dip angle (about 10^{o}) and is located at depths of 4-18 km, and has potential to generate Mw8+ earthquakes. Northward under thrusting of India beneath Eurasia generates numerous earthquakes and makes this area one of the most seismic activity regions.

In this study, inversion of teleseismic body-wave data was applied to activate the rupture process of the Nepal earthquake. Smoothing and non-negative constraints were introduced in order to obtain stable solutions. 48 teleseismic stations with good coverage were chosen. Finite fault model was established with length and width of 195km and 150km respectively. Similarly, initial seismic parameters were set, referring to Central Moment Tensor (CMT) solutions. The result indicates that the fault mechanism of the earthquake was thrust fault type, and the strike, dip and rake single are in accordance with CMT results. The seismic movement was 0.9195 x 10^{2}Nm (M_w 7.9) and source duration was 70s. Furthermore, the results show that the rupture nucleated near the hypocenter and then progressed along the dip direction to the southeast and that the maximum slip amounts to 5.2m. They recommended that the region should be paid more attention because the lack of shallow slip during the 2015 Gorkha earthquake implies future seismic hazards.

Reilinger and McClusky (2011)madeuse of geodetic and plate tectonic observations to constrain the Tectonic Evolution of the Nubia–Arabia–Eurasia plate system. They explained

the two phases of slowing of Nubia–Eurasia convergence, each of which resulted in an approximately 50 percent decrease in the rate of convergence which coincided with the initiation of Nubia–Arabia continental rifting along the Red Sea and Somalia–Arabia rifting along the Gulf of Aden at 24 ± 4 Ma, and the initiation of oceanic rifting along the full extent of the Gulf of Aden at 11 ± 2 Ma. In addition to that, they discovered that both the northern and southern Red Sea (Nubia–Arabia plate boundary) underwent changes in the configuration of extension at 11 ± 2 Ma, which included the transfer of extension from the Suez Rift to the Gulf of Aqaba/Dead Sea fault system in the north, and from the central Red Sea Basin to the Afar volcanic zone in the south. They further explained that while the Nubia–Eurasia convergence slowed, the rate of Arabia–Eurasia convergence remained constant within the resolution of their observations, and is indistinguishable from the present-day global positioning system rate and uncertainties estimation processed with the GAMIT/GLOBK software package. The timing of the initial slowing of Nubia–Eurasia convergence(24 ±4Ma)corresponds to the initiation ofextensional tectonics in the Mediterranean Basin, and the second phase of slowing to changes in the character of Mediterranean extension reported at approximately 11 Ma. The observations were found to be consistent with the hypothesis that changes in Nubia–Eurasia convergence, and associated Nubia–Arabia divergence, are the fundamental cause of both Mediterranean and Middle East post-Late Oligocene tectonics. We speculate about the implications of these kinematic relationships for the dynamics of Nubia–Arabia–Eurasia plate interactions, and favour the interpretation that slowing of Nubia–Eurasia convergence, and the resulting tectonic changes in the Mediterranean Basin and Middle East, resulted from a decrease in slab pull from the Arabia-subducted lithosphere across the Nubia–Arabia, evolving plate boundary.

LeGrand*et al*(2015) is a preliminary report of the International Association of Geodesy Working Group (IAG WG) Integration of Dense Velocity Fields in the ITRF (2011-2015)

which is a follow up of the IAG WG "Regional Dense Velocity Fields". Theirs was to provide a GNSS dense unified and reliable velocity field globally referenced on the ITRF (International Terrestrial Reference Frame which will be useful for geodynamical and geophysical interpretation). The WG combined the individual weekly solution SINEXs from the other sub-commissions with IAG Commission 1.3 including AFREF (Africa), APREF (Asia and Pacific), EUREF (Europe), NAREF (North America) SCAR (Antarctica) and SIRGAS (Latin America and Caribbeans). They stacked the weekly combined solutions in order to derive commutation – position and velocity solution as well as associated residual position time series.

The Data span was for 15 years between 1996-0 - 2011-3 which has a GPS week range of 834-1630. The number of GNSS stations providing both raw and data, selected after removal of outliers and those that are new after ITRF 2000 are shown in Table (2.1) below. They stopped the preliminary combinations of the individual solutions in GPS week 1630 when antenna models were charged from IGS05.atx to IGS08.atx notwithstanding, some solutions were using IGS08.atx while others were using IGS05.atx and EUREF solution was using additional individual calibration when available.

Table 2.1: List of the weekly solutions submitted to the WG

	AC	**Solution**	**Data span (year)**	**Antenna calibrations**	**# stations (raw)**	**# stations (selected)**	**# new stations wrt ITRF2008**
IGS	IGS	Global	1996.0-2012.9	igs05	1160	705	186
AFREF	AFR	Global	1996.0-2012.9	igs08	197	132	72
APREF	APR	Global	2004.0-2012.9	igs08	606	396	102
EUREF	EUR	Regional	1996.0-2012.9	igs05 + indiv	296	261	145
NAREF	GSB	Global	2000.0-2012.9	igs05	600	553	444
	NGS	Global	2000.0-2012.9	igs05	2830	1914	1519
SIRGAS	SIR	Regional	2000.0-2012.9	igs05	329	256	189
Total			**1996.0-2012.9**		**4077**	**2812**	**2251**

Source: LeGrandet al(2015)

The different sub-commissions submitted the following weekly solutions:

i. Weekly SINEXs (cleaned or with a list of the outliers to be removed)
ii. Cumulative solution and the associated residual position time series
iii. Position and velocity discontinuities that should be used for the commutative solution.
iv. Station site logs (if available)

The CATREF software package was used for the combination of the individual weekly SINEXs and the combination led to a typical 3D weekly RMS ranging from 2mm to 5mm.Outliers larger than 10cm were rejected even though at the time of the report, no refined outlier rejection had been performed.Outliers were removed based on individual cumulative solutions (position, velocity and associated residual position time series) based on individual SINEXs and (Residuals of the weekly combinations) detection of systematic bias in thenumber of common stations increased at 2000.0 (1042week) and large disagreements between the solutions gave rise to the large RMS increase for that GPS week. More so the incorrect antenna calibrations used during the analysis as well as different antenna calibration models resulted to large and small systematic biases. Furthermore, there were site log inconsistencies. All these notwithstanding, the WG agreed that the rough agreement between individual weekly solutions submitted to the WG is globally good and promising. They intended to solve the remaining problems by submitting all SINEXs generated with the IGS08.atc Model (individual calibration) by the end of 2013 for final combination on 2014. The inconsistencies arising from position differences could be theoretically mitigated by applying offsets coming from the Rebischung*et al*(2012) Model or Baire et al (2011) offsets for individual calibrations is just a patch and on the consistencies found on the SINEX headers contra-balance the utility of such an approach. Therefore reduction of RMS with the approach has to be confirmed.

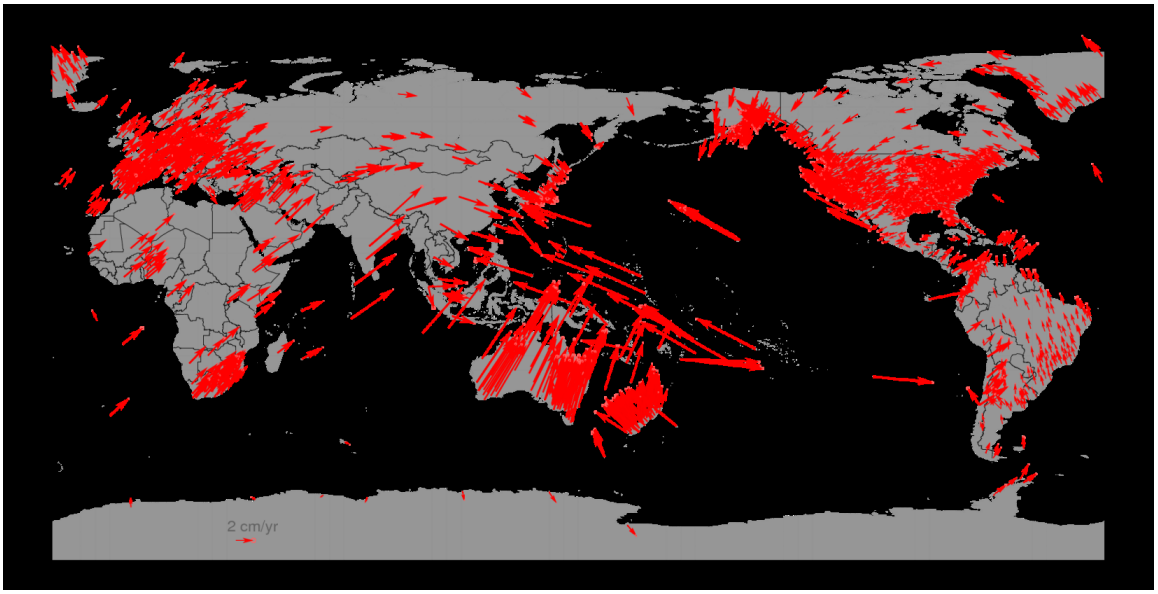

Fig 2.13: Preliminary horizontal velocity field
Source: Le Grandet al(2015)

Behr *et al*(1999) worked on the Continuous GPS Monitoring of Structural Deformation at Pacoima Dam, California. In this study, daily data from three continuous Pacoima Dam stations DAM 1, DAM 2, CMP9 plus three nearby SCIGN stations – CHIL, LEEP and ROCK were reprocessed by using precise orbits from the period Sept 1, 1995 to Nov9, 1997. The daily data were recorded at a 30s sampling interval but processed at 20s epochs. The GPS deformation analyzed in two step processes using GAMIT/ GLOBK software. In the GAMIT, bias fixing and least square adjustment were performed for the fixed stations network providing double differences of L1 and L2 phase observables recorded at the stations.

Satellite ephemeris and radiation pressure parameters provided by the IGS fixed precise orbit files were constrained to 0.01ppm and 0.01% respectively. Thirteen atmospheric delay parameters were estimated for each quarter day. Using GAMIT, biases were iteratively required using widen lane and then narrow-lane techniques. Loosely constrained GAMIT solution (with biases fixed) were performed to be passed as import to GLOBK

The result of analysis showed that the baseline time series to DAM2 indicated downstream (westward) motion of the dam centre during the fall and winter, followed by upstream deflection during the spring and summer. The reprocessed, refined and repaired time series indicated that DAM2 is undergoing periodic deflection of nearly 20mm peak-to-peak amplitude with approximately 1-year period. Station DAM1 often appears to be experiencing cyclic displacement of 1 year duration, though of a lower amplitude.

Wei, Jiang and Wu(2015) These researchers used the GPS data to analyze the earthquake preparation characteristics of the Kunlun Mountain Pass West (KMPW) Ms8.1 earthquake in 2001 and the Wenchuan Ms8.0 earthquake in 2008. In their work, they reviewed the main research developments of earthquake forecasting and the mechanisms of earthquake preparation using crustal deformation data from 1998 – 2006 for the KMPW, and 1999 – 2007 for the Wenchuan. They looked at the similarities and differences in the scientific approaches adopted by the Chinese and foreign scholars. They also analyzed the deformation characteristics of earthquake preparation, with respect to slip and dip-slip faults. Their results indicated that, in order to understand the relationship between crustal deformation and earthquake preparation, research focus should be expanded from fault-scale to larger scale regions and that the dynamic deformation characteristics associated with earthquake preparation must be considered as a multiscale, spatial-temporal process, in order to obtain the necessary criteria for strong earthquake forecasts.

They analyzed the use of Global Positioning System (GPS) to monitor large and midscale crustal deformations, and how it further enables us to study the development and occurrence processes of strong earthquakes from the large-scale, and to the meso-scale and fault scale of developing earthquakes. The Crustal Movement Observation Network of China (CMONOC)

established in 1998 with a regional network of 1000 stations, a basic network of 81 stations, and a fiducial network of 26 stations were used to evaluate the preparation processes of the two major earthquakes China mainland has suffered from; the Kunlun Mountain Pass West Ms8.1 earthquake in 2001 and the Wenchuan Ms8.0 earthquake in 2008.

The Kunlun Mountain Pass West Ms8.1 (KMPW 8.1) earthquake took place on November 14, 2001, due to the fact that the earthquake occurred in a depopulated zone in the middle of the Qinghai-Tibet Plate, it did not result in a severe human disaster, but remains the largest earthquake for a period of over 50 years in mainland China even though Sichuan was able to detect some outstanding abnormities prior to the earthquake. According to their result calculated using GPS data, the value of the principal stretching strain rate (i.e., the maximum principal strain rate) that occurred in the northwest area of the KMPW 8.1 earthquake was slightly larger than the strain rate of the principal pressing strain rate (i.e., the minimum principal strain rate) in the north and east in agreement with Jiang *et al* (2013) that the earthquake occurred in a region in which the surface strain rate was slightly stretching. This crustal deformation characteristic would have been beneficial for the full release of the strain close to the east and west, and it's revolving and rupture toward the left during the process of the violent earthquake. This contributed to a major understanding of the phenomenon that suggests that the rupture scale of that Ms8.1 earthquake was obviously too long (about 426 km) and the strength of the aftershock was relatively lower.

The processed GPS data was the basic network data (81 stations) of the CMONOC, and adopted changes in the 1998-2006 base line formed by all the simultaneous observation stations, based on whether or not a change was consistent with the associated influence of the revolving and rupture toward the left of the violent earthquake, after the 2001 Kunlun Mountain Pass West Ms8.1 earthquake. The trio analyzed the KMPW 8.1 earthquake and its scope of influence, which shows the large scope of the GPS station distribution of the

response to the influence of this violent earthquake process. Their analysis indicated that obvious changes influenced by the KMPW 8.1 earthquake occurred at many stations inside the borders of the Sichuan-Yunnan Plate, while its influence is not obvious at the JB34 station, situated at the eastern area of the Banyan Kara Ulla Plate close to the Longman Mountain fault zone (about 130 km).

The DLHA station was used as the base station in the crustal movement continuous observation network nearest to the fracture zone of the Kunlun Mountain Pass West earthquake. It is 300 km away from the eastern side of the fracture zone and the perpendicular distance between it and the fracture zone in which earthquake occurred is about 200 km. They used data from the DLHA and the LHAS stations, and the XIAA and the LUZH stations, which are relatively near to the fracture zone of the 2001 KMPW 8.1 earthquake, to calculate a time series of the second shearing strain parameter. The time series indicated a continuous decreasing tendency over the long term, which reflected a revolving wrench deformation towards the left in the east and the west, and towards the right in the south and the north. The wrench deformation in the several months prior to the KMPW 8.1 earthquake was in a state of stagnation or slight reverse. According to data accumulated over the period, the deviations from the typical relatively stable tendency proved obvious. However, when the data from the DLHA station, which is nearest to the earthquake fracture zone among all the calculation data, were extracted, there was no observable change. Such a change before an earthquake manifests as a pause or slowdown of the relative movement of crust from the accumulated strain over a long period of time.

They further used the DLHA station data, as well as the DXIN and XNIN CORs stations, which are relatively close to the DLHA station, to compute a time series of the strain parameter. Seen over the long term, the first shearing strain parameter, computed for the three GPS stations located in the northeast of the Kunlun Mountain Pass West earthquake fracture

zone, increases continuously, but was in a static state for nearly one year before the occurrence of the Kunlun Mountain Pass West earthquake. It implied that the DLHA station moved toward the west of the other two stations under normal circumstances, but the relative movement was once stagnant. The change of such abnormality and the change resulting from the rupture process of the earthquake occurrence are reversed in direction, which can be interpreted as a display of the frustration of the left-whirling twist deformation. This change prior to the earthquake also indicated that the relative movement of the Earth's crust accumulated either by long term strain pauses or by slowing down.

Wei*et al.*(2015) further analyzed the Wenchuan Ms8.0 earthquake occurred on May 12, 2008, in the Qinghai-Tibet Plate with strong tectonic deformation and in the Longmen Mountain fracture zone in a boundary strip of the stable South China Plate. The Wei *et al*'s department's monitoring ability of Longmen Mountain and the neighboring area was relatively low, and not enough to detect abnormal foreshadow activity, else it would have detected the Wenchuan Ms8.0 earthquake. Whereas the Kunlun Mountain Pass West Ms8.1 earthquake was detected because of some outstanding abnormities seen prior to the earthquake, no abnormities were detected prior to the Wenchuan earthquake. According to the GPS observation results, prior to the Wenchuan earthquake, it was reported that the GPS system did not detect any deformation of the Longmen Mountain fracture zone or of the Chengdu Plain situated at its east side (its size is smaller than the millimeter-sized observation error). However, the east part of the Bayan Kara Ulla Plate, located in the west of the Longmen Mountain fracture zone, reveals a large-scale slow deformation in which the crust cuts down, comparatively, the Longmen Mountain fracture zone, mainly revolving and wrenching it towards the right, while the compressional deformation is smaller. It was seen that the annual gross deformation from revolving and wrenching towards the right of the Longmen Mountain fracture zone and of the parallel fracture zone, on a spatial scale of 500

km from its northwest side between 1999 and 2007, is approximately 10.7 ± 0.8(mm/a). The relative deformation rate is 2.1 ± 0.2(10^{-8}/a), the average yearly deformation, in which the crust shortens the perpendicular fracture zone, is 3.5 ± 0.6 (mm/a), and the relative deformation rate is 0.7 ± 0.1(10^{-8}/a).

The trio stated that these deformations reflected large-scale strain accumulations. Compared with the magnitude of the revolving and wrenching towards the right of the Longmen Mountain fracture zone and of the parallel fracture zone, on a spatial scale of 500 km from its northwest side between 1999 and 2004 that during the period 2004-2007 increased by 1.6 ± 1.5 (mm/a). The deformation of revolving and wrenching towards the right in the area neighboring the Longmen Mountain fracture zone also increased (about 0.8 mm/a), but this observation is not indisputable with respect to observation accuracy (Jiang, 2009). The distribution of the Chinese Mainland strain rate field mainly reflected the crustal deformation of a relatively low frequency range, Among the various strain parameters, the distribution of the negative value of the east-west component strain rate and the first shearing strain rate have a relative relation at the site of the Wenchuan earthquake. Specifically, the east-west component strain rate has an extremely high negative value region in the east of the Bayan Kara Ulla Plate, which reflected the obvious east-west deformation in which the crust cut downward. Its distribution range was large and the quantity value was high, which was very similar to the large-scale negative value region in the middle of the Qinghai-Tibet Plate of the second shearing strain rate of the Chinese Mainland prior to the Kunlun Mountain Pass West earthquake. The Wenchuan earthquake took place in the east edge of the extreme value region of the negative east-west component strain rate, which shows that the construction power source of the Wenchuan earthquake is pushing the Bayan Kara Ulla Plate towards the east. If seen from the perspective of the strain rate field of the Sichuan-Yunnan area, it mainly reflected the increased compressive strain rate of the south section of Longmen Mountain

fracture zone in the 2004-2007 period. Jiang (2009) agreed that apart from its microscopic epicenter, most of the Wenchuan earthquake fracture zone was still in a zone characterized by a low strain rate.

It was evident that time series of the GPS base line, as it spreads towards the north and east and stretches across the North-South Seismic Belt several years before the Wenchuan earthquake, and especially in 2006, reflected the relative movement in which the crust cut down was relatively enhanced. The time series of the east-west base line also displays that relative movement of the east-west crust cut down being in an enhanced state. However, the time series of the east-west base lines between the Qinghai-Tibet Plate and the GPS station at its edge, and the TASH station and WUSH station in Xinjiang, showed a stretching exchange that was basically synchronous with the base line shortening of the North-South Seismic Belt. This indicates that the change in the enhanced shortening of the north-east and east-west base lines, as composed by the GPS base stations, was not caused by error influencing the scale factor in the GPS resolution, but may reflect a change in the relatively large-scale relative movement of the crust. This is because the enhancement of the relative movement of this crust shortening of the North-South Seismic Belt is fundamentally consistent with the relative crustal movement due to long-term strain accumulation in the North-South Seismic Belt.

Barzaghi*et. al.* (2018) opined strongly that one of the most important applications of GNSS is crustal deformation monitoring in seismogenic areas. They indicated that because of the new perspectives that GNSS opened, tectonic deformations can reliably be estimated either at regional or fault scale. The entire Seismic cycle can be studied whether it is the co-seismic, post-seismic and inter-seismic crustal deformation, they can be estimated using daily coordinates time series from GNSS CORS stations. They indicated that GNSS permanent

stations for deformation analysis are carefully monumented to detect crustal deformations. Deep-drilled brace are frequently used to fasten the GNSS antenna to the ground on a stable platform. In order to properly estimate the crustal movements, a detailed data analysis must be carried out. A detailed data analysis is then carried out in order to properly estimate the crustal movements.

The trio looked closely at the GNSS CORs network in Italy, stating that the *IstitutoNazionale di Geofisica e Vulcanologia*(INGV) had established the *Rete IntegrataNazionale GPS*(RING) with more than 180 stations and that the *IstitutoNazionale di Oceanografia e di GeofisicaSperimentale*(OGS) had implemented the Friuli Regional Deformation Network (FReDNet) in the North-East Alpine area. The data analysis adopted by the FReDNeT is Time Series and the most common parametric model that is used in analyzing the coordinate components $X = (x_1, x_2, x_3) = (N, E, Up)$ of the GNSS daily time series is

$$x_i = a + bt + \sum_{k=1}^{N}[A_k \cos(\varpi_k t) + B_k \sin(\varpi_k t)] + \sum_{j=1}^{M} c_j H(t - t_j) + \varepsilon_i(t)\ i = 1, 2, 3 \quad (3.1)$$

They explained that the linear term in the model accounts for the station velocity while harmonic components are included in order to model annual, seasonal and higher frequency time dependent phenomena. Possible discontinuities due to instrument/software and/or reference frame changes are modeled by the terms containing the Heaviside function $H(\cdot)$. Using least squares adjustment, the model parameters are estimated assuming different models for the colourednoise $\varepsilon_i(t)$.

Barzaghi*et. al.*(2018) further explained that $\varepsilon_i(t)$ is assumed to have a power spectrum that depends on the frequency *f* according to the formula.

$$P(f) \approx f^{k} \quad (3.2)$$

Based on the value of k, different stochastic process can be described with this model. When k is in the range $-1 \le k \le 1$, $\varepsilon_i(t)$ is a stationary stochastic process. For |k| > 1 $\varepsilon_i(t)$ is non-

stationary. Particular cases are for *k = 0, k = -1* and *k = -2* for which the $\varepsilon_i(t)$ process is, respectively, a white noise process, a Flicker Noise process or a Random Walk process.

However, Barzaghi*et. al.*(2018) employed a different time domain approach which was proposed by Barzaghi et al. (2004) where $\varepsilon_i(t)$ is assumed to be a second order stationary process, ergodic in the mean and in the covariance. Here the parameters estimation is done in a two steps procedure. The first least squares iteration is accomplished by considering that $\varepsilon_i(t)$ is White Noise. The $\varepsilon_i(t)$ least squares residuals are then computed and their stationarity is tested using the generalized KPSS-test. If stationarity condition is satisfied as is in the current case when removing the linear annual and semi-annual terms in equation (3.1), the empirical auto-covariance of $\varepsilon_i(t)$ is estimated and then modeled with a proper positive definite model function. Least squares adjustment is then repeated using the derived covariance structure. In order to detect and described possible high frequency effects that are present in the GNSS coordinates time series, collocation was applied for filtering the residuals $\varepsilon_i(t)$.

The filtering procedure of the GNSS coordinate time series as explained by the trio is done by first setting up outliers rejection and known discontinuities due to (instrumental changes) are removed. The parametric model (3.1) was then estimated assuming white noise behaviour of $\varepsilon_i(t)$. Least squares residual were then checked for stationarity by means of KPSS test ensuring stationarity of the residuals. The empirical auto covariance function is then estimated and fitted with a positive definite function. The final estimate of the model parameters is then accomplished in a further least square step that is performed using the proper covariance structure as defined by the model covariance function. Thus, the parametric model is optimally estimated taking into account the existing time correlations.

Barzaghi *et. al.* (2018) in analyzing the second step least squares residuals, applied a filtering procedure by assuming that the residuals can be modeled as the sum of a time correlated weakly stationary signal $s_1(t)$ and a white noise (uncorrelated) component $n_1(t)$, independent from $s_1(t)$.

$$\varepsilon_i(t) = s_1(t) + n_1(t) \quad i = 1,2,4 \tag{3.3}$$

Under these hypotheses, the empirical covariance function of $\varepsilon_i(t)$ was estimated and modeled. Collocation filtering method was applied to the residuals in order to estimate the signal component as

$$\hat{s}_i(t) = \sum_{j,k=1}^{N} C(|t - tk|)[C + \sigma_n^2 I]^{-1}_{kj} \varepsilon j(t_i)\, i = 1, 2, 3 \tag{3.4}$$

The filtered component allows defining some coherent behaviour of the residuals that could be related to some crustal deformations. Although this filtering procedure is quite effective, a further smoothing could be required to enhance the low frequency components of the filtered signal. It is in fact expected that possible inter-seismic crustal deformation have a smooth behaviour in time. In order to enhance the low frequency component in $\hat{s}_i(t)$ a moving average operator was applied. As it is well known this is equivalent to low pass filtering in the frequency domain.

This low pass filtering procedure was accomplished by kriging moving average. They considered an amplitude of the sliding time window equal to twice the correlation length of the covariance function $C(\cdot)$ of $\hat{s}_i(t)$(the correlation length is the distance at which the covariance function is half its value in the origin). The mean value of the signal over each sliding window was computed as

$$\hat{m}_s = \sum_{j=1}^{N} \varpi_j \hat{s}_i(t_j) \qquad i = 1, 2, 3 \tag{3.5}$$

Where N is the number of $\hat{s}_i(t)$ values in the window and the ω_k weights are given as the solution of the system

$$\left\{ \begin{array}{l} \sum_{j=1}^{N} \omega_j C(t_i - t_j) = \eta = 0 \\ \sum_{j=1}^{N} \omega_j - 1 = 0 \end{array} \right\} i = 1, \ldots, N \qquad (3.6)$$

The low pass filtered signal is thus smoother than the original values as it is shown in Fig. 3.1 (green line).

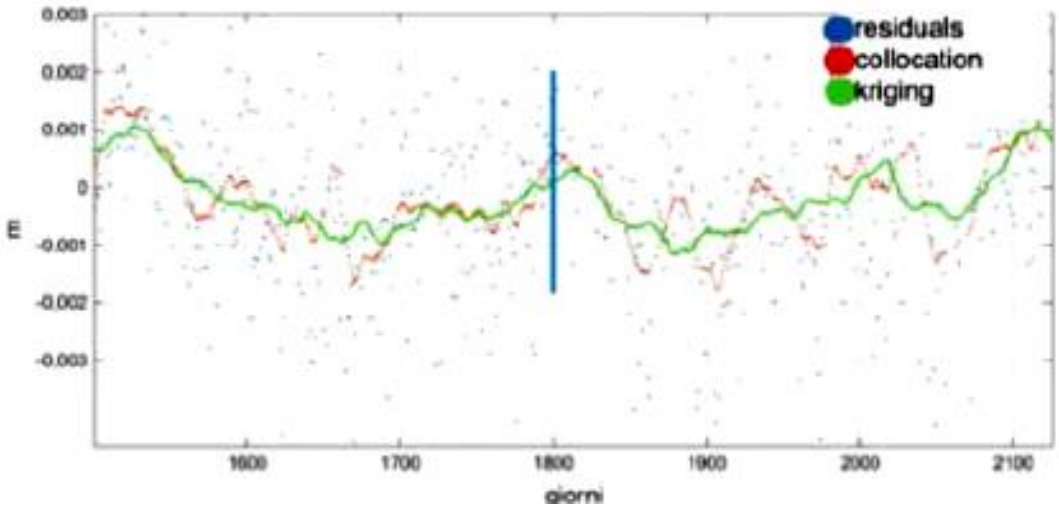

Fig 2.14: The Least Squares Residuals and the Filtered Signals
Source: Barzaghi et. al. (2018)

By using such regularized residuals, analyses on possible transient crustal deformation was performed effectively since most of the noise sources had been eliminated from the $\varepsilon_i(t)$ residuals.

Their analyses proved that the original signal and the filtered signal of only one station, namely the signal of the CANV station was found to be agreeing. In Fig. 3.2., they showed the CANV signal and its approximation obtained with the first singular value was represented and the agreement of the two signals was striking.

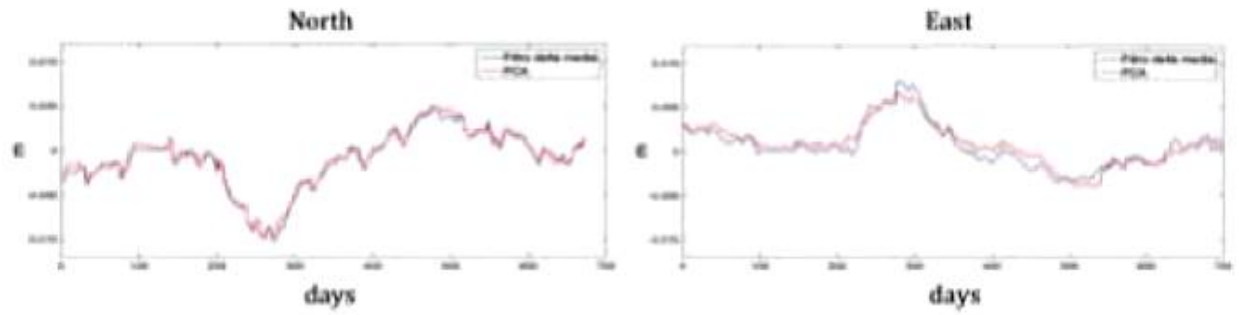

Fig 2.15: The analysis on the CANV Station Signals (blue original values; red filtered signal)
Source: Barzaghi et. al. (2018)

The same doesn't hold for the remaining stations. As an example, the signals of the NOVE station are displayed in Fig. 3.3

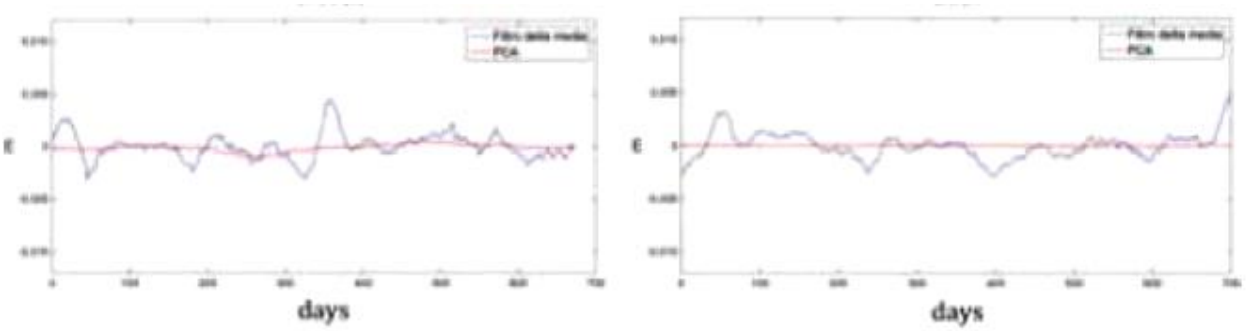

Fig 2.16: The filtered analysis on the NOVE Station Signal
(blue original values; red filtered signal)
Source: Barzaghi et. al. (2018)

They discovered from their work that the main variation in the covariance matrices was given by the CANV station. It implied that in the analyzed period, this station has highly varying coordinates. Barzaghi *et. al.* (2018) indicated that recent studies proved that this variability is given by a local effect related to groundwater storage in the Cansiglio plateau area (Devoti, Zuliani, Braitenberg, Fabris and Grillo, 2015), inferring that the proposed analysis proved effective since one physical phenomena was spatially related to a given station.

They reported that when they eliminated the CANV station and repeated the same analysis on the twelve remaining stations, they discovered no sharp differences among the singular values. The filtered signals based on the larger singular values didn't cluster in a specific

area. They reported, however, that some (weak) indications of a better fit between the original signals and the filtered ones (using only the two larger singular values in each component) in the SE area where an earthquake occurred on December 6th, 2011 (the gradiscad'Isonzo 0.8 magnitude seismic event). That studying the original signals of the stations clustered in PCA analysis closely, it would be seen that on that date, some coordinate variations are present. As an example, the East components of MDEA and TRIE (which are the closest stations to Gradiscad'Isonzo) are plotted in Fig. 3.4. On December 6th 2011 (blue line), they both display a common high signal variability.

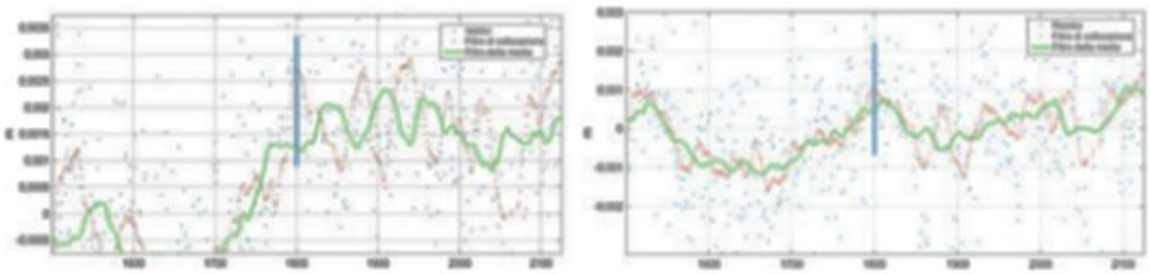

Fig 2.17: the TRIE and MDEA filtered East component residuals and the Gradisicad'Isonzo seismic event
Source: Barzaghi et. al (2018)

They concluded that the proposed filtering procedure proved to be effective and able to spatially cluster permanent stations having common behavior. In the FReDNet case study, the physical evidence depicted by the procedure include a groundwater storage effect in the Cansiglio area and a cluster of stations possibly related to a 0.8 magnitude seismic event in the Gradiscad'Isonzo area. The recommended that further investigations be carried out, to prove that this procedure can reveal other geophysical relevant phenomena related to the inter-seismic phase such as aseismic transient slip events.

Hu *et al*(2005) investigated the Feasibility of using Continuously Operating Reference System (CORS) in Victoria (GPSnet) for Deformation Monitoring and Analysis. The relative and absolute displacement of selected GPSnet stations were analyzed using chronological GPS CORS data and dedicated high precision scientific GPS data processing software

packages. In order to compute and analyze relative displacement of the GPSnet, relatively stable and precise IGS/ARGN reference stations close to the GPSnet were used. The significance of both absolute and relative displacements of the in-hole subnets was tested using F-test and the displacement significance of a single station was tested using T-test. The result of significance test showed that the absolute displacement of all the subnet points were significant. The average displacement velocity of the subnet points is 6.8cm/year.

Both the magnitude and direction of the whole subnet displacement agree well with the velocity of about 7cm/year and direction of current Australian continent derived independently. The significant test also shows that the relative horizontal displacements of all the subnet points are not significant. It was concluded that the relative horizontal positions of the subnet points were not affected by local geological features. Also the solution of Victorian regional CORs network is not precise enough and stable for high precise deformation monitoring and analysis if the amount of data used to generate the solution is less than 12hours. It was recommended for geological information to be taken into account when any new CORs stations are established.

Kalkan*et al*(2010) used multiple geodetic survey approaches such as GPS surveying, precise leveling and conventional surveying to monitor the deformation of Ataturk dam from May 2006 to November 2008. GPS surveying was performed in May 2007 in between days 125-130; that is, in 6 consecutive days, at 6 stages. The duration of measurement in each day was about 8 hours with an interval of about 5s. Each station was observed at least one day. Data sampling of 5s and elevation work of 10s were used throughout the campaign.

The GPS equipment and instrument used in the project included a 3Nos Ashtech Z-Xtreme, 3Nos Thales Z-max, 7 Topcon Higher GGD and PLUS, 12 single prisms, 8 Three prisms.

They however, failed to mention the accuracy level obtained after the processing and adjustment of the GPS surveying.

Static method of GPS surveying was observed in 55 different points of the dam embankment for testing whether or not GPS method can be used. GPS results between the 3rd period (May 2007) and 5th period (Nov 2008) were compared with each other for all points. Similarly, precise horizontal angle, vertical angle and distance measurement were performed to more than 200 object points using 9 pillars for relating the object and reference points. A few millimeter point position accuracy was obtained after the adjustment of each period measurement with appropriate stochastic model. Point position accuracy is less than 1cm for the deformation point on the dam embankment.

Measurement results of 6 periods performed by Istanbul Technical University (ITU) were compared. Stochastic model test was applied at first for double period comparing for the evaluation of the result, whether they be in the same set or not. Test value due to fisher distribution was calculated with 0.05 probability. An accuracy criterion of displacement vectors was calculated using double period analysis between the periods in the case of evaluation in the same set. Precision leveling measurement on dam crest was performed monthly for 6 months to determine the amount of settlement. Between May 2006 and November 2008, there were horizontal displacements of 63%, vertical displacements of 31% and radial displacement of 59% on the deformation points. The biggest displacement on horizontal direction is 9.9cm (radial direction is 9.8cm) and vertical direction is 11.6cm. The result also showed that the vertical displacement (settlement) is not dependent on the water level in the reservoir.

Liangqian, Wanju, Guohua, Juzhong and He(2011) analyzed the coastal movement and continental movement data observed repeatedly at GPS stations from 1999 to 2009 in order to study the effect of two earthquakes of Ms8.1 and Ms8.0 that occurred in 2001 and 2008 respectively in Qinghai-Tibet sub-plate and its eastern margin. Linear-elastic-block-motion model along with the results of GPS measurements were used to highlight the deformation of the blocks rather than smaller local changes. The block movement consists of two parts: an overall rotation and internal deformation. The overall movement field in the sub-plate during the 1999-2009 period was obtained by subtracting the overall rotation parameter from the observed side velocities in the global framework, using the calculated results of the GPS measurement during this period. The velocity was greater in the southwestern and the southern parts, and gradually decreased towards north and east to a minimum in Qai-dam Western Qunling region. The movement in the central and southern parts showed a clockwise rotation around the Asian tectonic node. They examined the horizontal deformation at different observation stages, the movement velocity changes were determined.

The result of the analysis showed that the average crustal shortening across the ruptured section is 1.04m, and an average right-lateral strike slip of -0.76m. The largest shortening was -1.38m, and right-lateral strike slip was 0.94m. The corresponding average principle comprehensive strain was -62.66 $x10^{-7}$, with principle axis in SE110.5° direction. The average principle tensile strain was 55.26 x 10^{-7} with axis in NE. The maximum shear strain was 117.62 x 10^{-7} and the plain strain was -7.39 $x10^{-7}$. Along the fault zone, the maximum earthquake-related principle compressive strain was -162.23 $x10^{-7}$, the maximum tensile strain was 59 $x10^{-7}$ and the normal strain was -57.00 $x10^{-7}$. The measurement movement changes in the blocks revealed some mid and long term anomalies before the large earthquake

Reilinger et al., (2006)carried out an extensive study that utilized over 17year data in their effort to investigate the GPS constraintson Continental Deformationin the Africa–Arabia EurasiaContinental Collision Zone and Implications for the Dynamics of Plate Interactions. They used GPS-derived velocity field(processed using GAMIT/GLOBK Software package)from 1988 to 2005 for the zone of interaction of the Arabian, African (Nubian and Somalian), and Eurasian plates which indicated a counterclockwise rotation of a broad area of the Earth's surface including the Arabian plate, adjacent parts of the Zagros and central Iran, Turkey, and the Aegean/Peloponnesus(Fig. 2.18) relative to Eurasia at rates in the range of 20–30 mm/yr. This motion was adjudged to be relatively rapid with respect to the framework of the slow-moving (approximately 5mm/yr relative motions) Eurasian, Nubian, and Somalian plates. They discovered that the circulatory pattern of motion increases in rate towards the Hellenic trench system. They also developed an Elastic Block Model to constrain Present-day Plate Motions (relative Euler vectors), regional deformation within the interplate zone, and slip rates for major faults. Substantial areas of continental lithosphere within the region of plate interaction show coherent motion with internal deformations below 1–2 mm/yr(approximately), including central and eastern Anatolia (Turkey), the southwestern Aegean/Peloponnesus,the Lesser Caucasus, and Central Iran. Geodetic slip rates for major block-bounding structures are mostly comparable to geologic rates estimated for the most recent geological period (approximately 3–5Myr). They concluded that the convergence of Arabia with Eurasia is accommodated in large part by lateral transport within the interior part of the collision zone and lithospheric shortening along the Caucasus and Zagros mountain belts around the periphery of the collision zone.

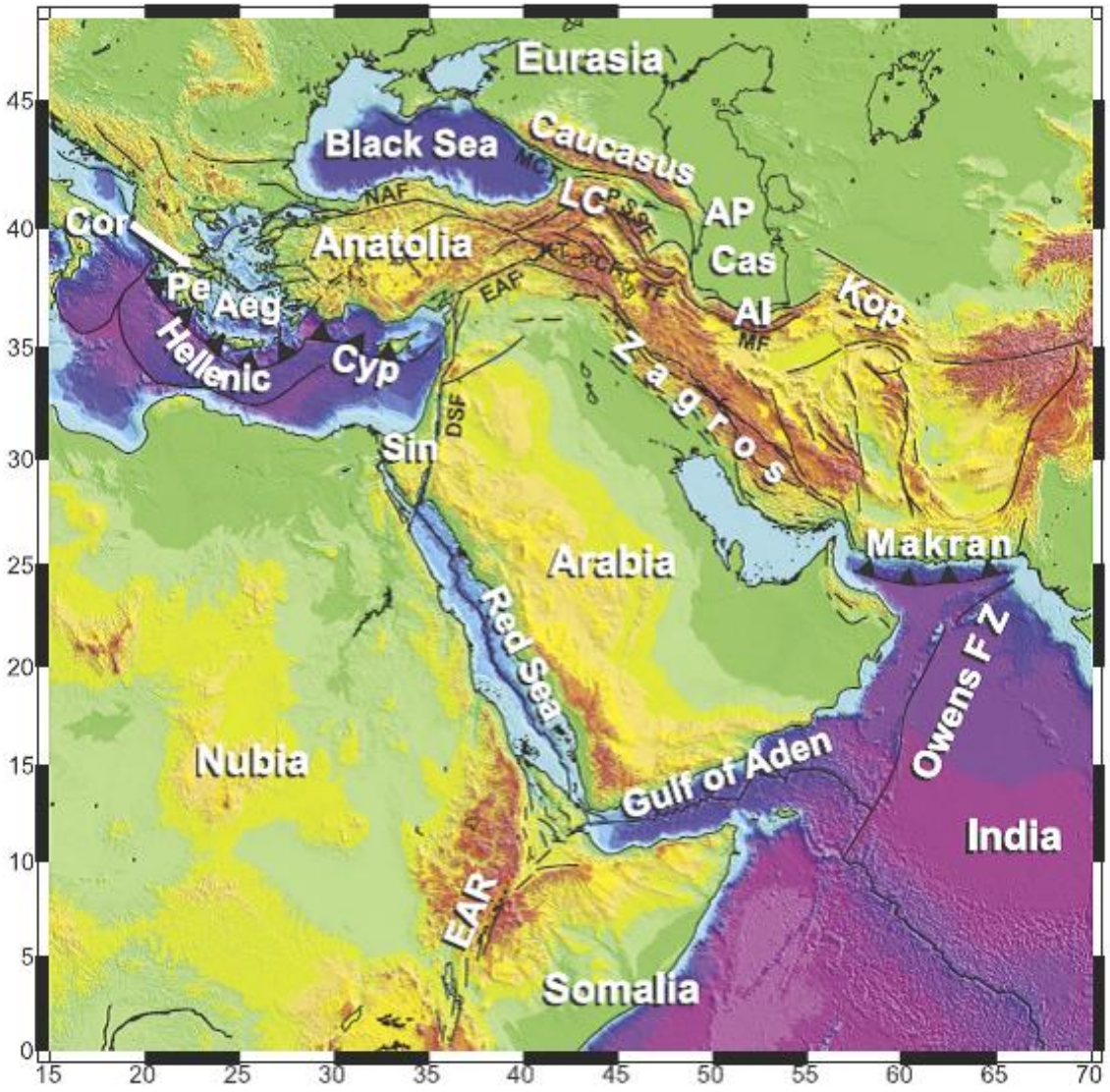

Fig 2.18: Map of the Zone of Interaction of the Nubian, Somalian, Arabian, and Eurasian plates. (North Anatolian fault (NAF), East Anatolian fault (EAF), Dead Sea fault (DSF), Mosha fault (MF), Pembak-Sevan-Sunik fault (PSSF), Tabriz fault (TF), Chalderan fault (CF), Gulf of Corinth (Cor), Peloponnesus (Pe), Aegean (Aeg), Lesser Caucasus (LC), Cyprus trench (Cyp), Karliova Triple junction (KT), Sinai (Sin), Caspian Sea (Cas), Main Caucasus Thrust (MCT), East African rift (EAR), Kopet Dag (Kop), Apsheron Peninsula (AP), Alborz Mountains (Al)).
Source: Reilinger et al., (2006)

They additionally discovered that the principal boundary between the westerly moving Anatolian plate and Arabia (East Anatolian fault) is presently characterized by pure left-lateral strike slip with no fault-normal convergence. This implies that ‘‘extrusion’’ is not presently inducing westward motion of Anatolia. On the basis of the observed kinematics, we hypothesize that deformation in the Africa- Arabia-Eurasia collision zone is driven in large

part by rollback of the subducting African lithosphere beneath the Hellenic and Cyprus trenches aided by slab pull on the southeastern side of the subducting Arabian plate along the Makran subduction zone. They finally recommended that the separation of Arabia from Africa is a response to plate motions induced by active subduction.

2.5 Gaps Identified

1. It was discovered from the literatures reviewed, that most of the literary works in geodynamics monitoring are in the Asian region, with only one work (Bawa*et al* (2018)) found to be done in Nigeria and West Africa in general. This was found to be insufficient and calls for attention.

2. Whereas Bawa*et al*(2018) indicated that the motion of the NigNet CORs were constrained with respect to the Arabian, Somali and Eurasian plates, they offered no explanation as to the methods, makes the investigation vague in that regards.

3. It was also discovered that most of the reviewed literature like Stamps, Saria and Kreemer(2016), Kalkan*et al*(2010),McClusky *et al* (2011)and so on failed to mention the processing software used for their studies. However, since the only software packages found in literature are the Bernese, Gipsy(both proprietary software packages) and GAMIT/GLOBK(an open sourced, but controlled, software package) this work will use the GAMIT/GLOBK.

4. Zhang et al (2016) used non-geodetic methods (inversion of teleseismic body-wave data), evidence in literature has shown that non-geodetic methods alone are not enough to study such hazards because they depend on probabilistic models(Hackl *et al*(2009).

5. Kalkan*et al* (2010) also failed to indicate the accuracy level obtained after the adjustment of his GPS observation. Stating that a few millimeters accuracy was achieved does not help in the assessment of such geodetic work.

CHAPTER THREE
METHODOLOGY

This chapter focuses on the methodology adopted in the execution of this research project.

Figure 3.1 represents the flow chart adopted in achieving the aim of this study.

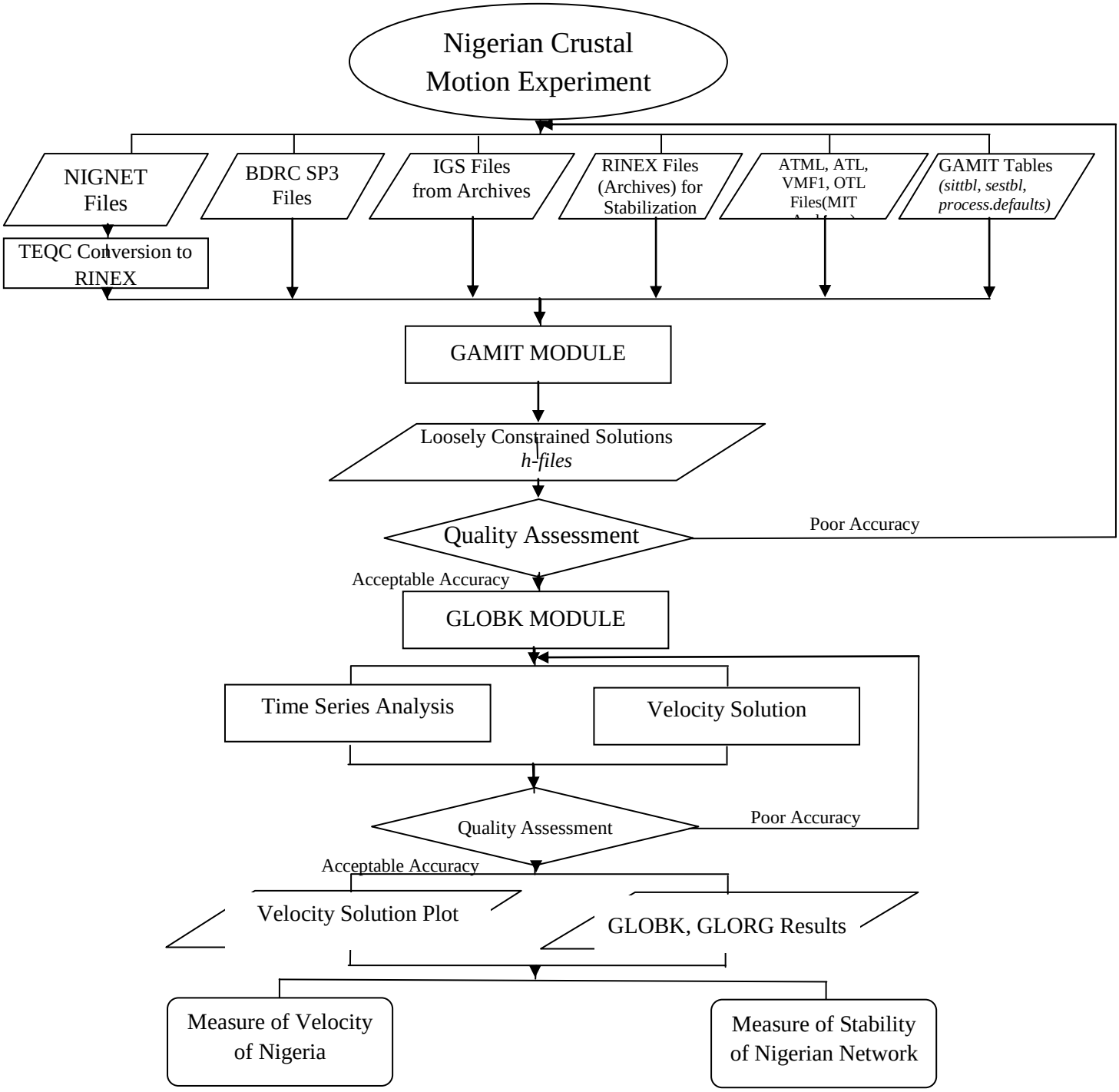

Figure 3.1: Flow chart of methodology adopted

3.1 Data Requirements

The data required for this experiment are all secondary data collected from the archives of different agencies. Thedata used for the geodetic evaluation of crustal movements are as follows:

i. GPS CORs data for 2012, 2013 and 2014for all the available NIGNET Stations.

ii. Daily RINEX (Receiver Independent Exchange Format) data from ten (10) IGS Stations for Stabilizing the Network for the three years from SOPAC and CDDIS Archives.

iii. Station Log files for the ten IGS Stations from IGS website

iv. Daily Broadcast Ephemeris (brdc) Navigation files for the three years from SOPAC Archives

v. Daily Precise IGS Orbit (sp3 ephemeris) files for the three years from SOPAC Archives

3.2 Hardware and Software Requirements

The following hardware and software were used:

3.2.1 Hardware

The hardware requirements include the following:

(i) A Linux (Ubuntu) based Laptop with minimum configuration of 8GB RAM, 500GB Hard disk, 3.00GHZ microprocessor speed.

(ii) HP Design jet AO Scanner.

(iii) HP 2050A Series A4 Printer

(iv) 32GB USB Flash disk.

3.2.2 Software

The following software would be used:

(i) Fortran 77 for Linux

(ii) C++ for Linux

(iii) GAMIT-GLOBK Software

(iv) Microsoft Excel 2007

(v) Microsoft Word 2007

(vi) Microsoft PowerPoint 2007

3.3 Data Sources

The GPS CORs data for Nigerian GPS Network (NIGNET) was acquired from the Office of the Surveyor General of the Federation (OSGoF), the Government Agency that is saddled with the responsibility of managing CORs data in Nigeria. The Broadcast and Orbit Ephemeris files were downloaded from Scripps Orbit and Permanent Array Center (SOPAC) Archives. The RINEX data for the ten IGS Stations chosen for Network Stabilization were downloaded from the SOPAC and Crustal Dynamics Data Information System(CDDIS) Archives.

3.4 Data Processing

The data processing involved the following stages:

i. Installation of the Prerequisites (Fortran 77 and C++),

ii. Installation of GAMIT-GLOBK,

iii. Download for GNSS Broadcast Ephemeris files (brdc),

iv. Download for GNSS Orbit Ephemeris files,

v. RINEX data for the IGS Stations for Network Stabilization,

vi. GAMIT Preprocessing Settingsfor the Corrections for Oceanic Loading Grid, Atmospheric Tidal Grid, Atmospheric Non-Tidal Grid and the Vienna Mapping Function.

vii. GAMIT processing of the GPS CORs data

viii. GLOBK processing to get Repeatabilities and a combined H-files for the data span

ix. Computation of the Velocities of the Motion

x. Plotting the Velocities to show the motion

3.4.1 Installation of the Prerequisites (Fortran 77, C++, X11, GMT, etc)

According Fadil(2019), the four fundamental requirements for installing GAMIT/GLOBK on any system, in addition to a basic UNIX- or Linux-based operating system OS, are

i. a Fortran compiler;

ii. a C++ compiler;

iii. X11 libraries (libX11.a, libX11.so, libX11.dylib, libX11.la or libX11.dll.a); and

iv. X11 headers an X11 header file (Xlib.h).

In order to install the compilers libraries and headers, the following shell scripts wereran in the Terminal of the Linux OS:

i. To install the gcc and g++ compilers, the build-essential package will be needed. This will also install GNU make. Build-essential contains a list of packages which are essential for building Ubuntu packages including gcc compiler, make and other required tools (Zilenas, 2012). In other to install the “build-essential”, the Ubuntu shell script ***apt-get install build-essential, gcc –v*** and ***make –v*** would beran in the home folder of the Terminal.

ii. To install the GNU FORTRAN 95 compiler - ***gfortran***, the following scripts wasran***apt-get install gfortran***and***gfortran –v***.

iii. To install the "gcc-multilib" and/or "gfortran-multilib" packages to ensure compatibility. Multilib is one of the solutions allowing users to ran applications built for various Application Binary Interfaces(ABIs) of the same architecture. The most common use of multilib is to ran 32-bit applications on amd64 (Gentoo, 2018). To install the multilibs, the shell: ***apt-get install gcc-multilibgfortran-multilib***was ran.

iv. To install X11 Libraries and Headers, which is a windowing system for bitmap displays, common on Unix-like operating systems, the shell ***apt-get install libx11-dev***was ran. This downloads and installs X11 libraries (libX11.a, libX11.so, libX11.dylib, libX11.la or libX11.dll.a); andX11 headers an X11 header file (Xlib.h).

v. To install "csh" and "tcsh", which are Unix C shell and shells based on and compatible with the C shell, respectively and are essentially the C shell with programmable command-line completion, command-line editing, and a few other features, ***apt-get install cshtcsh***.

vi. The File Transfer Protocol programs were set up byranning***apt-get install ncftp***.

vii. To install GMT (Generic Mapping Tools) required for any GAMIT/GLOBK Scripts for the production of Plots, ***apt-get install gmtgmt-dcwgmtgsh hg***was ran.

viii. Finally for prerequisites, the mail server to receive sh_GAMIT summary file was installed with local only configuration byranning***apt-get install mailutils***.

3.4.2 Installation of GAMIT/GLOBK

The GAMIT-GLOBKdirectory already created in the home directory and files downloaded from mit-geoweb, was slid into in the Terminal. The command ***chmod 755***

install_softwarewas ran. ***Chmod***(Change Mode) being the command and system call used to change the access permissions of file system objects (files and directories) and also used to change special mode flags (FreeBSD, 2019). Then the***install_software***command wasran to install the GAMIT/GLOBK. It also created the ***gg***(a shortcut folder) link in the home directory. After the installation, an experiment directory for this study was created in the home directory using the command ***mkdiruzoh*** creating the directory ***uzoh***. Inside this folder, the GPS CORS data for the NIGNET stations were saved with respect to their years. The ***vsoln*** which is the Velocity Solution folder was placed, and also the Station Log Files folder were also placed in the experiment folder. In the yearly folders, the following subdirectories were created:

i. brdc for the Broadcast Ephemeris files byranning***mkdirbrdc***.
ii. gfiles for the Orbit Ephemeris gfiles byranning***mkdirgfiles***.
iii. igs for the Orbit Ephemeris files byranning***mkdirigs***.
iv. rinex for the daily RINEX files for the ten IGS Stations chosen as Stabilization Points byranning***mkdirrinex***
v. The Table folder from GAMIT/GLOBK folder was also copied into the yearly file.

3.4.3 Download for GNSS Broadcast Ephemeris files (brdc),

Entering into the brdc subfolder inside the 2012 folder of the experiment folder,***uzoh***, in the Terminal, the GAMIT Script ***sh_get_nav -archive sopac -yr 2012 -doy 001 -ndays 366***was ran. According to Herring *et al*(2018b), these navigation files were used by ***makej***, ***makex***, and ***makek***operations to generate satellite and receiver clock files, and may be used by bctot to create an initial G-file and/or aT-file from the broadcast ephemeris.

This script means

sh_get_nav -archive sopac: Get Navigation files from SOPAC Archives

-yr 2012: for year 2012

-doy 001: Day of year to start from

-ndays 366: Number of days to download.

These operationswere repeated for the other two years 2013 and 2014.

3.4.4 Download for GNSS Orbit Ephemeris files.

Accessing igs subfolder in the 2012 folder, the GAMIT script ***sh_get_orbits -orbit igsf -yr 2012 -doy 001 -ndays 366 –makeg***was ran. The script implies:

sh_get_orbits-archive sopac: Get Orbit files from

-yr 2012 for year 2012

-doy 001 Day of year to start from

-ndays 366 Number of days to download

–makeg converts to G-file.

The G-file contains initial conditions and non-gravitational force parameters for each GNSS satellite at a particular UTC epoch. The G-file initial conditions serve as starting points for a numerical integration of the satellite orbits and the generation of a T-file (Herring *et.al.* 2018a).The G-files were moved to the gfile directory.

3.4.5 RINEX data for the IGS Stations for Network Stabilization

Ten IGS stations has been chosen as Stabilization points considering geometric spread in order to provide a truly stable network for the Reference Frame of the experiment. The ten stations, their locations and the host tectonic plates are as seen in Table 3.1 and Figure 3.2.

Table 3.1: Stabilization Stations

S/N	IGS Station	Country	Tectonic Plate
1	DEAR	South Africa	NUBIAN

2	ABPO	Madagascar	NUBIAN
3	RAMO	Israel	NUBIAN
4	DARK	Senegal	NUBIAN
5	MELI	Spain	NUBIAN
6	ASCG	Saint Helena, Ascension and Tristan Da Cunha	SOUTH AMERICAN
7	MOIU	Kenya	SOMALI
8	ZAMB	Zambia	NUBIAN
9	NOT1	Italy	EURASIAN
10	BHR4	Bahrain	ARABIAN

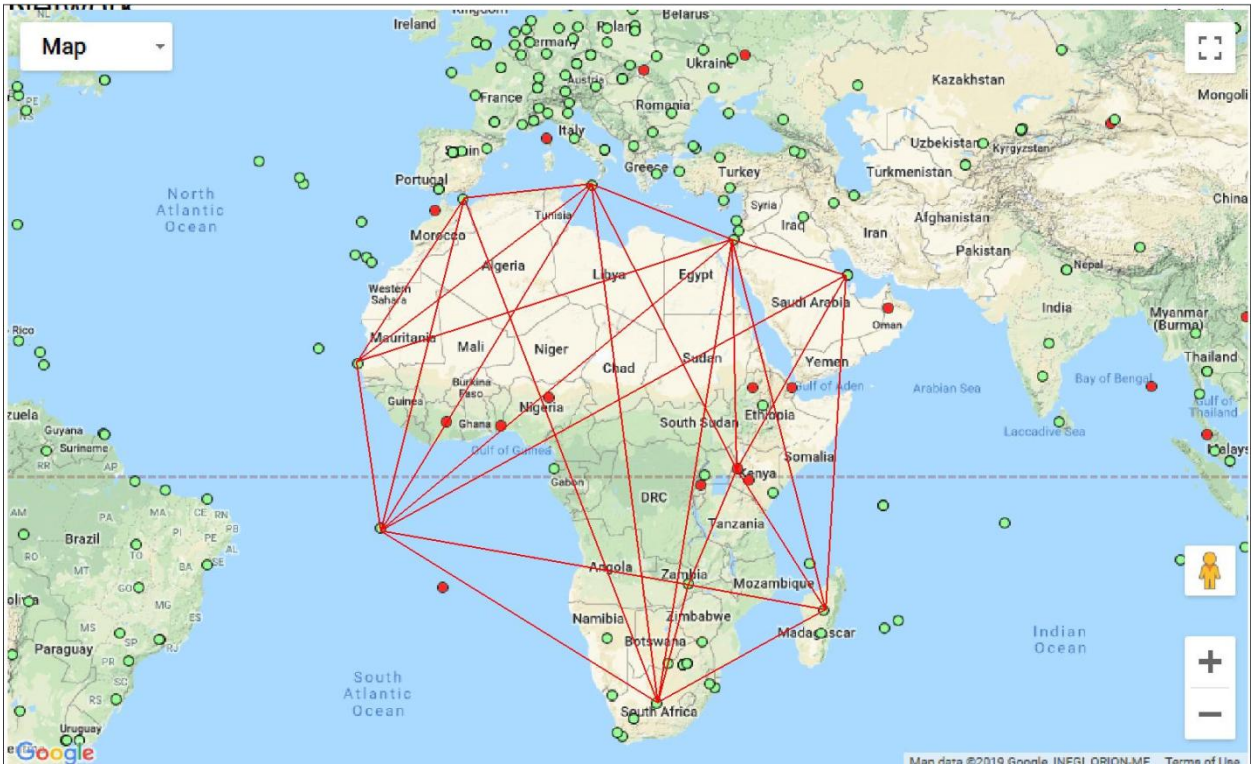

Fig. 3.1: IGS Stations for Stabilization Network
Source: Modified from IGS (2019)

To download the daily GNSS data for these stations, the GAMIT Script ***sh_get_rinex -archive sopaccddis -yr 2012 -doy 001 -ndays 366 -sites dear abporamo dark meliascgmoiuzamb not1 bhr4***was ran. This script means

sh_get_rinex -archive sopaccddis	Download RINEX files from SOPAC or CDDIS archives
-yr 2012	for year 2012
-doy 001	Day of year to start from
-ndays 366	Number of days to download

-sites dear abporamo dark meli for the listed sites shown in Table 3.1

ascgmoiuzamb not1 bhr4

It is important to note that the script demands GAMIT to download the RINEX data from SOPAC archives and to get those not available in the archive from the CDDIS archives. When the download is done for 2012, the process is repeated for 2013 and 2014, bearing in mind that 2012 was a leap year and the number of days has to change to 365 days.

3.4.6 Setting Up for GAMIT Processing

In order to set up the files and processes to be followed by the software, a series of organizing and arrangements were carried out. These involved:

i. Raw GNSS data arrangement;

ii. GAMIT Preprocessing

3.4.6.1 Raw GNSS Data Arrangement

In order to use the GNSS data obtained from the OSGOF for the GAMIT experiment, the raw data which are daily UNIX compressed Hatanaka format files(ABUZ0040.12D.Z) were uncompressed and the uncompressed files converted to RINEX format. Then the names of the RINEX files were changed from uppercase to lowercase that is understandable to the GAMIT software.

a. To uncompress the UNIX compressed Hatanaka format, the yearly directory 2012 would be slid into in the Ubuntu Terminal and the command ***uncompress*.Z***was ran. This would uncompressthe ***.Z*** file and convert it to ***.D***.

b. The Hatanaka command ***ls | awk '{print "crx2rnx",$1}' | sh*** was ran. This command converts the uncompressed ***.D*** data to ***.O*** files. These file names,

although in RINEX format already, were still in upper cases but GAMIT require the names to be in lower cases.

c. In order to conserve space in the computer, the ***.D*** files are deleted byranning the simple Ubuntu command ***rm *.12D***was ran.

d. Then, to convert the ***.O*** file names to lower cases, the command ***ls | while read upName; do loName=`echo "${upName}" | tr '[:upper:]' '[:lower:]'`; mv "$upName" "$loName"; done***was ran.

These processes prepared the raw data for the GAMIT processing. These steps was then repeated in the other yearly directories.

3.4.6.2 GAMIT Preprocessing

Before most of the set-up are ran, it is important to link up the important files (***atml.grid, map.grid, autcln.cmd, process.defaults, sestbl, sittbl, sites.defaults, station.info, and so on***) in the Table directory in the GAMIT/GLOBK Directory and create a shortcut to some of them inside the Table directory within the yearly folder, 2012, 2013 and 2014. In order to do this, the GAMIT shell script ***sh_setup -yr 2012*** would be ran. Once this is done, the files would be linked, the shortcuts created and we would be ready to adjust the different set-up files for the processing.

The following settings were done within the Table directory of the experiment.

i. ***Autcln.cmd***: According to Herring *et.al.* (2018a), this command is a set of controls for cleaning the data in program ***autcln***. It is advisable not to edit this file, unless unusual data is encountered during the processing.

ii. ***Process.defaults***: this file was edited to specify the computation environment, sources for internal and external data and orbit files, start time and sampling interval, instructions for archiving the results, and an email address to receive a

summary of the ran(Herring *et.al.* 2018a). To receive the summary locally, no email would be specified, rather ***“”***would be used. In the ***process.defaults*** file, it will be confirmed if the local directories created in section 3.4.2 are correctly specified so that ***sh_GAMIT*** can easily pick up the needed data correctly. The ***process.default***is as shown in the Appendix One.

iii. ***Station.info***: This file contains the receiver and antenna type and height of instrument (HI) values as a function of time for all occupations of the stations used. Although it can be generated during processing by ***sh_GAMIT***, the best approach is usually to construct the file prior to processing.

iv. ***Sites***.***defaults***: This file determined how each station was used in the processing. All of the stations for which data needed to be retrieved from an external archive; stations for which ***station.info***doesn’t need to be updated from RINEX headers (or use all); and stations that should be excluded from the processing even though data are available in the /rinex directory are listed here. The stations were listed in the format **“site expt keyword1 keyword2”** for example:

abuz_gps uzoh localrx

bkfp_gps uzoh localrx

cggt_gps uzoh localrx

clbr_gps uzoh localrx

The first token is the 4-character station name (as recognized by GAMIT and _gps to indicate that the station tracks GPS and not Galileo or any other GNSS); the second token is the 4-character experiment name in this case “uzoh”; the third is the read free-format, indicating ***localrx*** if GAMIT is to read the RINEX files locally, ***ftprx*** if it is to download the RINEX files from an online RINEX archives, ***ftpraw*** it is to download online from raw data archives; and the last whether to

exclude a station or not, indicating ***xstinfo*** to exclude from automatic ***station.info*** updating and ***xsite*** to exclude from processing, all days or specified days. In this case, we would not need to exclude any station.

v. ***Sestbl***: this file houses the list and setting of parameters used by GAMIT such as Satellite Constraints, Type of Analysis, Ionospheric Constraints, Ambiguity Resolution, Zenith Delay Estimation, Ocean Tidal Loading Atmospheric tidal Loading and Non-Atmospheric Tidal Loading, and many more. An Example of the ***sestbl***would be included in the Appendices. It is important to mention that the New Vienna Mapping Function (VMF1) would be selected for Dry and Wet Mapping Function. This is because the VMF1 according to Zhang *et al.(2016),* it providesa better height within ±1mm difference than the Global Mapping Function (GMF). The Global Pressure and Temperature (GPT 50) would be used for the Meteorological Observation Source because no appropriate site dependent hydrostatic delay is expected.

vi. ***Sittbl.***: According to Herring *et al*(2018a), the ***sittbl.*** contains options that can be set on a station-by-station basis. The width of the table is variable, with the entries determined by the column headers present. The apriori station constraints to be applied in GAMIT to enhance ambiguity resolution and to obtain a solution that can be inspected visually and it assumes that the final solution will come from GLOBK. An example of the listing is

```
SITE            FIX    --COORD.CONSTR.--
<< default for regional sites >>
ALL             NNN    100.  100.   100.
<< IGb08 core sites >>
ABUZ ABUZ_GPS   NNN    100.  100.   100.
BKFP BKFP_GPS   NNN    100.  100.   100.
ULAG ULAG_GPS   NNN    100.  100.   100.
UNEC UNEC_GPS   NNN    100.  100.   100.
ALIC                NNN    0.050 0.050  0.050
ARTU                NNN    0.050 0.050  0.050
```

ASC1 NNN 0.050 0.050 0.050

This means that the 4-character site name must appear in the first four columns (both local and IGS sites), the 8-character name is of arbitrary length beneath a blank header, and the coordinate constraints are free-format but must fall within the columns denoted by the header **--COORD.CONSTR.--**. The constraints are north, east, and up in meters. However, all Local Sites must bear the constraint 100. because their reliabilities are not certain yet.

Other files needed for the GAMIT processing include

i. atmdisp_cm.2012, atmdisp_cm.2013 and atmdisp_cm.2014 downloaded from ftp://everest.mit.edu/pub/GRIDS/ into the grids directory inside the tables directory of GAMIT and renamed as atml.grid.2012, atml.grid.2013 and atml.grid.2014 respectively as files for non-tidal atmospheric loading for the three years.

ii. map.grid for Time- & space dependent Zenith Hydrostatic (Dry) Delay (ZHD) and Mapping Functions (MF)

iii. otl.FES2004.grid for Oceanic Loading grid

iv. atl.grid for atmospheric tidal grid.

v. atmfilt.cm.2012, atmfilt.cm.2013 and atmfilt.cm.2014 for atmospheric filtering.

vi. vmf1grd.2012, vmf1grd.2013 and vmf1grd.2014 for the Vienna Mapping Function.

3.4.7 GAMIT Processing

3.4.7.1 GAMIT Processing (First Stage)

After setting up and arranging all the GNSS data for processing, the GAMIT shell script ***sh_GAMIT -exptuzoh -s 2012 001 366 -dopts x k c ao D >sh_GAMIT.log*** this implies

sh_GAMIT - ranGAMIT

-exptuzoh - for the Experiment named uzoh

-s 2012 001 366 - fortheyear 2012 from day 001 to day 366 (leap year)

-dopts x k c ao D - delete files with extensions x, k, c, ao and D (to save space)

>sh_GAMIT.log - save the processes in GAMIT.log.

According to Herring *et al*(2018a), the following processes were undertaken by GAMIT once the shell script isran:

1. Assign parameters for program flow, giving precedence first to the command-line arguments, then to the parameters set in ***process.defaults*** and ***sites.defaults***, and then to default assignments within ***sh_GAMIT***itself. In this case, the command-line entry for which files to delete at the end of the ran override those set in ***process.defaults***.
2. Create the day-directory and/or standard directories which do not yet exist.
3. Link into the day directory (/004) the standard tables and the RINEX files that contain data for the specified interval (00:00-24:00 as set in ***process.defaults***).
4. Download orbital sp3 files from a global data center and create GAMIT g-files using script ***sh_get_orbits***.
5. Run ***sh_upd_stnfo***, which invokes program ***mstinf***to update ***station.info*** from the RINEX headers. (It is recommended that this step be skipped by setting ***xstinfo [expt]*** all in ***sites.defaults.***)
6. Run ***makexp***to create the input files for ***makex***(scal.makex.batch) and ***fixdrv***(dscal0.004).
7. Run ***sh_check_sess***to make sure that all of the satellites included in the RINEX observation files are present in the navigation file (/brdc/brdc00400n, previously

downloaded from SOPAC archive) and in the g-file (created previously at MIT from an IGS sp3 file and downloaded from SOPAC archive).

8. Run ***sh_makej***to create a j-file of satellite clock estimates from the sp3 file (default) or navigation file.
9. Run ***makex***to create x-files (observations) and k-files (receiver clock estimates) using phase and pseudo range data from the RINEX observation files, broadcast ephemeris from the navigation file, and satellite clocks from the j-file. A record of *makex*, showing the data found and any problematic data encountered is written to ***scal.makex.infor***.
10. Run ***fixdrv***to create the batch file for GAMIT processing. Though not used directly, ***fixdrv***also reads the k-file of episodic clock values and fits a first-order polynomial to them as a crude check for jumps and rapid drifts in the receiver clock (***fixdrv.out***).
11. Execute the batch ran to generate a tabular orbital ephemeris (*arc*), model the phase observations (***model***), edit the data (***autcln***), and estimate parameters (***solve***), a sequence completed twice in order that ***autcln***may operate on flat residuals and that the final adjustments in *solve* are well within a linear range. A record of this ran is not written to sh_GAMIT.log (to save space) but is recorded in GAMIT.status, GAMIT.warning, and GAMIT.fatal in the day directory.
12. Save the cleaning summary (***autcln.post.sum***) to ***autcln.post.sum.scal***(potentially for archiving) and write key information from ***model***and ***solve***to the **HISTORY** file, which, unlike all other files in the day directory, is appended rather than overwritten in reruns so that a record of previous rans is maintained.
13. Create sky plots of phase residuals and plots of phase vs. elevation angle using the DPH files written by *autcln*; if the Image Magic program ***convert***program is available, translate the plots from postscript to ***.png*** and move them into ***/figs***.

14. Invoke ***sh_cleanup***to delete or compress files as specified by -dopt and -copt. In this case, delete files.

3.4.7.2 Inspecting the Daily GAMIT Solution Quality.

It is of utmost importance that the results obtained from the GAMIT Processing be evaluatedto help decide on the quality of the solution. The decision at the stage borders on whether to continue to the GLOBK stage or to reprocess the GAMIT stage changing either the inputs or the selected parameters in section 3.4.7.2. According to Lindsey (2019), a good way to check the quality is to open the daily summary file (***sh_GAMIT_063.summary***) and evaluate some statistics about the processing.

Herring *et al,* (2018a) indicates the following ways as means of the evaluation:

i. **All of the expected data were included**: The "***Totalxfiles***" must be equal to the number of raw or RINEX files available. If the number used is less than the total ***xfiles***, then some x-files must have been created but later discarded because they were either too small (tracking session too short or data discarded by *makex*) as measured against the ***minxf***value you set in ***process.defaults***, or because they have been excluded with the ***xsite*** option in ***sites.defaults*** or the ***sh_GAMIT***command line.

ii. **The data fit the model at the expected level**: The block of lines beginning with "RMS" are extracted from ***autcln.post.sum*** and shows the one-way root-mean-square (RMS) residuals by satellite and station. In the RMS second line, the first value is an overall rms in mm. The remaining values on that line break down the scatter by satellite and report the value in tenths of mm to allow better discernment of differences that might indicate a bad orbital model for one satellite. The last four lines report the values for the two sites with the lowest and

the highest scatter. RMS for the two best/worst sites: there is one column for each satellite, with an average in the first column. According to the Herring *et al*, (2018a), it is expected that all values would be less than 10 mm. Typically, the best sites will have values of 3-5 mm, and the worst will have 7-9 mm. Values between 10 and 15 mm indicate high but acceptable levels of noise, but when the data is reweighted using ***autcln***(default and recommended) the uncertainties in position estimates for the worst sites will be 2-3 times higher than for the better sites.

RMS values greater than 15 mm suggest

a. a poorly tracking receiver,
b. a high multipath environment, severe weather, or
c. a problem with convergence in ***autcln***, usually caused by poor coordinates or a short span of data.

For sites with high scatter, examining the sky plots and phase versus elevation plots in the /gifs directory may be helpful in understanding the source of the noise. If the two "worst" sites have high rms, it is advisable to look at other sites in ***autcln.post.sum*** that might also have high values but did not make the "top two" in the summary.

iii. **The uncertainties are acceptably small:** The third block of lines, extracted from ***solve***q-file indicate the Double Difference Statistics. It is expected that the Postfitnrms(normalized root mean square) should be approximately 0.2. Ideally, it is always about 0.18 for a good solution, and may only be 0.21 for a bad solution (Lindsey, 2019). More so, the Wide Lane (WL) and Narrow Lane (NL) Phase Ambiguity Resolutions will be expected to be within 70-85% for noisy days and greater than 90% for best days.

3.4.8 GLOBK Processing.

This phase of the processing would be in three major steps:

a. Combination of the daily h-files to get an annual H-file
b. Processing of the Time Series
c. Generation of Velocity Solution.

3.4.8.1 Combination of h-files and Outlier Editing/Removal

Herring *et al*(2018a) explained that several reasons exist, why the h-files from the daily GAMIT processing need to be combined with other h-files before generating a times series or velocity solution. Some of the reasons indicated are that it is more efficient and accurate to process the sites in GAMIT networks of 30-50 sites and combine them in GLOBK than to use a single large network. They further opined that when a regional network is being processed, and is to be tied rigorously to a larger regional or global reference frame, it can be done by combining the h-file(s) with those generated by MIT or SOPAC from IGS processing or another analysis center's processing of regional continuous networks. Furthermore, to obtain more useful long-term statistics from the time series, to strengthen the reference frame for survey-mode observations, or to reduce the computational time for velocity solutions, h-files from 5-30 days can first be combined into a single h-file to be used in subsequent solutions. To perform this task, the script ***sh_glred -cmd***will be executed to generate a daily time series from regional data combination within the yearly directory. This created***GLOBK_comb.cmd*** and ***glorg_comb.cmd*** in the ***/gsoln***directory.

By executing the ***sh_glred***, the American Standard Code for Information Interchange ASCII h-files containing the GAMIT produced loosely constrained weighted least squares estimate

of site positions and varience-covarience values were converted to Binary H-files which became the input file for the GLOBK time series and velocity solution. To achieve this, the shell script, ***sh_glred -s 2013 001 2013 365 -exptuzoh -opt H LC G T -nsigma 2 -detrend Y >sh_glred.log*** was ran. This will use the local processing in combination with global h-files previously downloaded onto the system to generate a 365-day time series for the year 2013 for the experiment ***uzoh***. The H LC G and T options provide some allowance for the independently processed regional or global networks from multiple GNSS or multiple subnets.

The –***nsigma 2*** operation allows for the removal of many outliers without weakening the solution and to automatically generate XPS commands in the *tsfit*program. –***detrend Y*** down-weighted the outliers and removed the effect of trends in the time series. Detrending was applied to remove a feature thought to distort or obscure the relationships of interest and sometimes used as a preprocessing step to prepare time series for analysis by methods that assume stationarity.

3.4.8.2 Processing of the Time Series

As explainedby Herring *et al*(2018a)***glred***or ***GLOBK***was randirectly, rather than using *sh_glred*, to generate time series or estimate velocities from several years of data. As with creating irregular combined h-files, the ***gdl*** file was created using the ***ls*** command from the ***uzoh*** directory used for the multi-year analysis. The ***gdl*** file of the multiyear (2012 – 2014) analysis in ***pwn/vsoln*** was generated using the combined Binary H-files from the individual years by running the script ***ls ../????/gsoln/H*.GLX >uzoh.gdl***.

The next step was to generate the time series so that the statistics of the data could be evaluated to determine if there are any outliers that will distort the velocity solution. ***glred***was ran directly to produce a time series from the file ***gld*** file by running***glred 6***

GLOBK_rep.prtGLOBK_rep.log uzoh.gdlGLOBK_long.cmd >glred.out. This would produce a single ***GLOBK_rep.org***file.

Next will be to examine the quality of the stabilization by running the script ***grep 'POS STAT' GLOBK_rep_06.org***. This provided a summary of the statistics and outliers or faulty data were removed or scaled down. The solution for different epochswas checked for the quality of the stabilization. The NRMS values for the stabilization were found to be near unity in all three components, and the WRMS 1-2 mm in horizontal and 3-10 mm in vertical. It was also assessed to make sure that no epoch had too few sites in the stabilization. It was discovered that three stabilization sites (MELI, ASCG and BHR4) were totally eliminated from the experiment, because they had large adjustments in the position summary.

Using the time series script ***tssum. mit.final.itrf08 -R GLOBK_rep_2019.org***, the residual pos files will be created and saved. Then the script ***sh_plot_pos -f *.pos -r -t tsfit.cmd -t1 2012_004 -t2 2014-365 –u***was used to plot the scatter diagrams using the ****.pos*** instead of ****.org*** for the input files. The histograms of nrms and wrms generated by *sh_plot_pos*was then evaluated to assess whether the distribution of scatters among the sites is approximately Gaussian with the median nrms approximately 1.0. Finally, the time series for every site to be included in the velocity solution was reviewed. Outliers were sought for at individual epochs and it was discovered that MDGR has been eliminated from the analysis due to the inconsistencies recorded, and the fact that the time series indicated that the station logged for 0.02years within the 3-year review period. Immediately theproblematic MDGR estimates were identified, ***rename***or ***sig_neu***command was created by the software to remove it, the time series was then repeated to verify that the entries accomplished the intended corrections.

3.4.8.3 Estimation of the Velocities of the Motion (Velocity Solution)

The scripts***GLOBK 6 GLOBK_vel.prtGLOBK_vel.log uzoh.gdlGLOBK_long.cmd VEL >glredvel.out***,

glred 6 GLOBK_rep.prtGLOBK_vel.log uzoh.gdlGLOBK_long.cmd VEL>GLOBK.out to were ran to generate the Velocity Solutions.

where the ***VEL*** option invoked with the template ***GLOBK.cmd*** file turned on the velocity estimates; ***glorg.cmd***, invoked from within ***GLOBK_vel.cmd*** included stabilization for velocity as well as position; and the ***.org-file***(appendix two) output contains the stabilization information and a summary table for velocities (Table 4.3) as well as positions (Table 4.4). More so, the experiment list will now contain all of the files used and the computed chi-square increments as each successive h-file is added to the solution in the manner shown in Table 3.2.

Table 3.2:Experiment List from vel.srt

#	Name	SCALE	Diag PPM	Forw Chi2	Back Chi2	Status
1	H950820_PNW.GLX	1.000	0.000	0.115	-1.000	USED
2	H970607_PNW.GLX	1.000	0.000	0.220	-1.000	USED
3	H980813_PNW.GLX	1.000	0.000	0.234	-1.000	USED
5	H990516_PNW.GLX	1.000	0.000	0.184	-1.000	USED
6	H010719_PNW.GLX	1.000	0.000	0.295	-1.000	USED

With a weighting of the coordinates estimates such that the uncertainties from each (combined) h-file are approximately 1mm for horizontal and approximately 5mm for vertical, the chi-square increments found to be less than 0.5 for the NigNet stations alone and 0.4 to 1.0 for the IGS stations. Herring *et al,* (2018a) indicates that if an h-file is based on a poor GAMIT solution or there is a model incompatibility with previous h-files, the chi-square increment will be anomalous. This would have requireda return to the time series to see which sites that show outliers that would create an incompatibility, but it didn't occur. They stated that it could be as a result of a wrong antenna height for a station, which will show up as a height anomaly in the time series. Very high chi-square values would have resulted if two sites in the solution had the same name but at different locations.

3.4.8.4 Refining the Stabilization of the Network

To generate a ***stab_site***list to include all sites with position and velocity uncertainties below a specified level program ***org2stab***, *the shell script* ***sh_exglk -f GLOBK_vel.org -apr vel_2019.apr*** was ran. This script generated an ***apr***(apriori) file that involed all the stations in the solution from the ***.org*** or ***.prt*** files. Thus, after obtaining this solution, the***glred***in section 3.4.9.3 would be rerun with the enlarged ***stab_site***list or ***apr-***file generated from the velocity solution.

The essence is that often times, the set of stations used for stabilization of the time series for editing purposes define a reference frame that is inherently weaker in the region of interest than the final velocity solution. This could be either because the editing frame encompasses a larger region and hence is more affected by spatially correlated errors, and/or because the number of well-known stations available for stabilization of individual h-files is much less than the total number of stations in the solution. The time series that best represents the final velocity solution is one that is stabilized with all of the stations in the solution. Therefore, we included all the stations in the solution for the times series after generating the apriori files.

3.4.9 Plotting the Velocities to Show the Motion

To produce the plot of the realized Velocity Solution, the shell script ***sh_plotvel -psuzoh -f GLOBK_vel.org -R2/16/4/15 -Jm30/0.5i -factor 0.4 -arrow_value 5 -page L***wasran.

Where the ***–f*** argument is the ***prt***, ***org***, or ***vel*** file from which the *SUMMARY VELOCITY*is to be plotted, and the second command-line entry gives the longitude and latitude range for the plot using standard GMT commands. To plot the stations within Nigeria, the coordinate range $2^oE - 16^oE$ and $4^oN - 15^oN$ was used. Also in order to get a holistic view of the stabilization stations, $-25^oE - 60^oE$ and $-45^oN - 40^oN$ was used.

3.5 Expected Results and Analysis

At different stages of the analysis, different results are expected. These results which will be discussed in the Result Chapter and displayed in the appendices include but are not limited to the following:

i. The daily h-files from GAMIT processing which becomes the input for GLOBK processing.

ii. The ***.gdl*** file housing the statistical report of the GAMIT Processing.

iii. The combined annual H-file to be used in GLOBK

iv. The ***.org***, ***.prt***, ***.pos*** and ***.vel*** files from the different levels of GLOBK Analysis.

CHAPTER FOUR
RESULTS AND DISCUSSIONS

Different stages of the analysis of the NigNET stations yielded different results. It would be most appropriate to discuss these results in line with the different objectives they address.

Objective No. 1: *"To acquire and analyze thedaily GPS CORs data of the NIGNET from 2012 to 2014, using GAMIT Software"*

4.1: Results from GAMIT Processing.

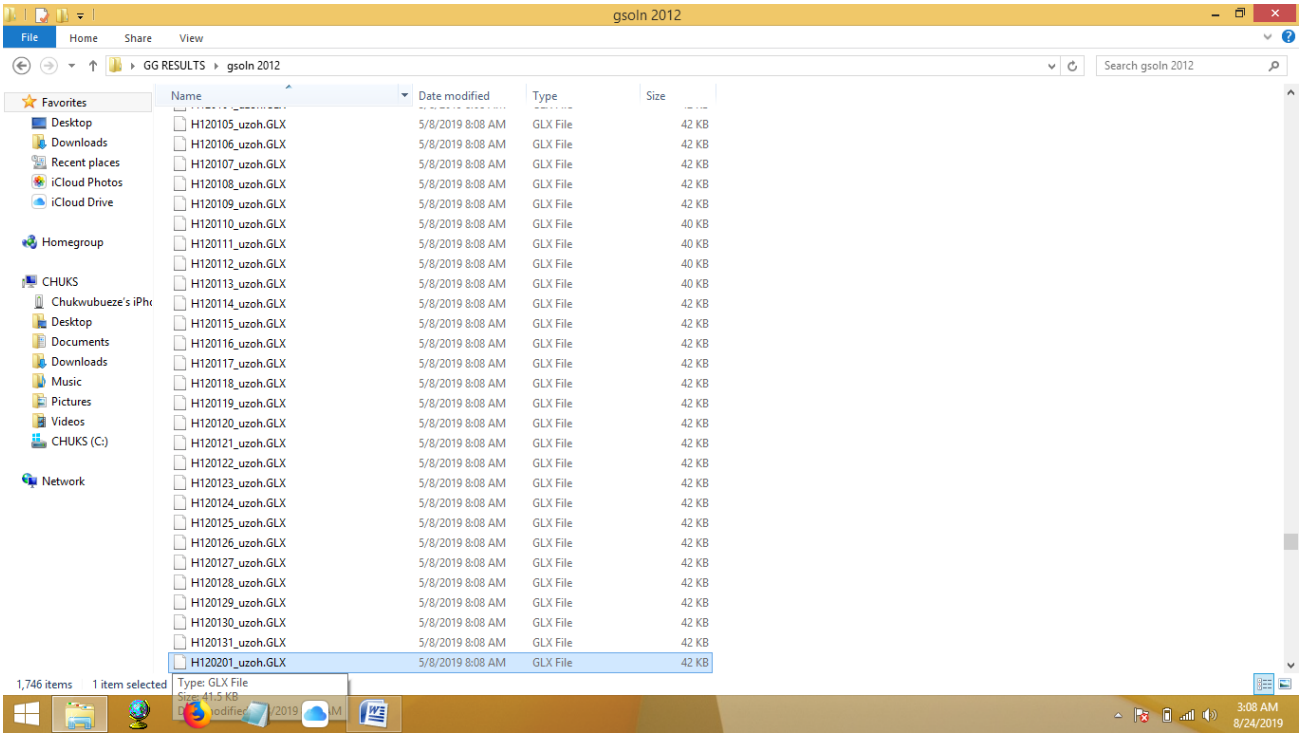

Fig 4.1: Loosely Constrained h-files

4.1.1 Assessment of the Daily Solutions

After executing the operations in section 3.4.8.1, the quality of the Daily GAMIT Solutions were investigated. The summary files (***sh_GAMIT_063.summary***) located inside the daily directories were examined. Using the Taro Yamane (1967) formula(Onwuka,Okoye and Ikekpeazu, 2015), the sample size at 95% confidence level and Precision 0.05 was determined for the assessment of the daily solutions.

$$n = \frac{N}{1 + N(e)^2} \qquad (4.1)$$

Where n = sample size

N= population size

e= the level of precision (0.05)

and 1 = Theoretical constant.

$$n = \frac{1095}{1 + 1095(0.05)^2} = 292.9766 \approx 293 \qquad (4.2)$$

This implies that eight (8) summary files must be investigated for every month. Some of the summary files randomly selected are shown in plates 4.1 – 4.8.

4.1.1.1 Included Expected Data

As discussed in section 3.4.8.2, the "***Totalxfiles***" were examined to find out if they are equal to the number of raw or RINEX files available. All 293 daily summaries examined were found to be in order. The randomly selected samples show the number of xfiles used as follows (Appendix Five):

i. Plate 1 shows the number of files used to be equal to the number of xfiles which is 14.
ii. *Plate* 2 shows the number of files used to be equal to the number of xfiles which is 10.
iii. *Plate* 3 shows the number of files used to be equal to the number of xfiles which is 14.
iv. *Plate* 4 shows the number of files used to be equal to the number of xfiles which is 13.
v. *Plate* 5 shows the number of files used to be equal to the number of xfiles which is 13.
vi. *Plate* 6 shows the number of files used to be equal to the number of xfiles which is 9.
vii. *Plate* 7 shows the number of files used to be equal to the number of xfiles which is 8.

viii *Plate* 8 shows the number of files used to be equal to the number of xfiles which is 8.

4.1.1.2 Assessment of Data-Model Fit at the Expected Level

The RMS block of lines extracted from ***autcln.post.sum***which shows the one-way root-mean-square (RMS) residuals by the 32 GPS satellites and stations were examined. The RMSs for the two best and worst sites, with the average in the first column were evaluated. On few occasions, the RMS of some of the satellites were seen to be greater than 15mm but the greater number (about 93%) of the RMS in the daily summaries were found to be less than 15mm for the worst sites which indicate high but acceptable levels of noise for such days.Figures 4.1 to 4.8 report the following sites as the best and worst sites:

Table 4.1: The Two Best and Worst Sites in some of the Selected Daily Summaries

Day of Year	Best Site I	Best Site II	Worst Site I	Worst Site II
016 of 2012	NOT1	ABUZ	ZAMB	DEAR
078 of 2012	ABUZ	NOT1	UNEC	ULAG
281 of 2012	DEAR	ZAMB	BKFP	CLBR
056 of 2013	ABUZ	BKFP	ABPO	CLBR
277 of 2013	ZAMB	DEAR	FUTY	OSGF
028 of 2014	DAKR	BKFP	ABPO	DEAR
262 of 2014	DEAR	ZAMB	DAKR	ABUZ
350 of 2014	ABUZ	RAMO	MOIU	ABPO

4.1.1.3 Small Uncertainties

The Double Difference Statistics extracted from ***solveq***-file was examined for the 293 daily summaries.From the eight above, Postfitnrms(normalized root mean square) are approximately 0.2. Some days in the 293 showed 0.21 which according to Lindsey(2019) is an indicator for bad solution. The Wide Lane (WL) and Narrow Lane (NL) Phase Ambiguity Resolutions were also inspected. The Wide Lane on the average was found to all be over 80% and the Narrow Lane around 70%. These values are within the acceptable range for noisy days. It readily gave an indication of the possible presence of outliers.

Having been satisfied that the GAMIT result were in order, it became necessary to proceed to the GLOBK stage (Objective 2). Had it not been so, the processing would have been repeated and reweighted using ***autcln***.

Objective No. 2: *"To Evaluate the Velocity of the Tectonic Motions of Nigeria within the Period using GLOBK Software".*

4.2:Results from GLOBK Processing.

4.2.1 Time Series Results

The Time Series analysis yielded the ***.pos*** file for all the stations. These files contain the following information for every day in the station recorded GNSS data within the period:

i. 4-character Identification for the station
ii. Name of the COR Station
iii. First Epoch from the station in the experiment
iv. Last Epoch from the station in the experiment
v. Release Date for the Experiment
vi. XYZ Reference position of the station with respect to ITRF 08
vii. North East and Up Reference position of the station in the WGS84 Ellipsoid
viii. YYYYMMDD Year, month, day for the given position epoch
ix. HHMMSS Hour, minute, second for the given position epoch
x. JJJJJ.JJJJJ Modified Julian day for the given position epoch
xi. X X coordinate, Specified Reference Frame in meters
xii. Y Y coordinate, Specified Reference Frame in meters
xiii. Z Z coordinate, Specified Reference Frame in meters

xiv. Sx Standard deviation of the X position in meters

xv. Sy Standard deviation of the Y position in meters

xvi. Sz Standard deviation of the Z position in meters

xvii. Rxy Correlation of the X and Y position

xviii. Rxz Correlation of the X and Z position

xix. Ryz Correlation of the Y and Z position

xx. Nlat North latitude, WGS-84 ellipsoid in decimal degrees

xxi. Elong East longitude, WGS-84 ellipsoid in decimal degrees

xxii. Height (Up) Height relative to WGS-84 ellipsoid in m

xxiii. dN Difference in North component from NEU reference position in meters

xxiv. dE Difference in East component from NEU reference position in meters

xxv. du Difference in vertical component from NEU reference position in meters

xxvi. Sn Standard deviation of dN in meters

xxvii. Se Standard deviation of dE in meters

xxviii. Su Standard deviation of dU in meters

xxix. Rne Correlation of dN and dE

xxx. Rnu Correlation of dN and dU

xxxi. Reu Correlation of dEand dU

xxxii. Soln "rapid", "final", "suppl/suppf", "campd", or "repro" corresponding to products generated with rapid or final orbit products, in supplemental processing, campaign data processing or reprocessing.

A close study of the files indicates the daily changes in the position of the active GNSS stations. It could be seen from the Longitude and Latitude columns of the Time Series report in Appendix four that the changes are consistently within the seventh decimal place of the

degree. This indicates how small the crustal motions are on a daily basis and upholds the need for software like GAMIT/GLOBK which has the capability of combining the daily files for the desired number of years. The Time Series result also shows the standard deviations of the Space Rectangular and Geographic Coordinates as well as their respective correlations.

Also the ***tsfit***file contained the Summary of the time series analysis as seen in Table 4.2

Table 4.2: Time Series Summary

* TSFIT NEU Secular trend components from command file NONE													
Stations	enu	S#	#	mean length	Sig	wrms	nrms	Slope	Sig	wrms	Nrms	dur	Mean
				(m)	(m)	(mm)		(mm/yr)	(mm/yr)	(mm)		(yrs)	(yrs)
ABPO_GPS-	N	1	828	-2117108.058	0.00003	0.75	0.69	14.33	0.03	0.75	0.69	2.99	2013.54
ABPO_GPS-	E	1	828	4970509.904	0.00003	0.81	0.69	18.93	0.03	0.81	0.69	2.99	2013.48
ABPO_GPS-	U	1	827	1552.96658	0.00027	7.72	0.62	3	0.31	7.72	0.62	2.99	2013.58
DAKR_GPS-	N	1	776	1638760.461	0.00004	0.88	0.97	17.83	0.06	0.88	0.97	2.99	2014.28
DAKR_GPS-	E	1	776	36881755.59	0.00004	0.88	1.1	19.21	0.06	0.88	1.1	2.99	2014.23
DAKR_GPS-	U	1	775	51.79942	0.00041	11.34	0.87	10.38	0.57	11.34	0.87	2.99	2013.65
DEAR_GPS-	N	1	854	-3413635.171	0.00002	0.59	0.64	18.91	0.02	0.59	0.64	2.99	2013.71
DEAR_GPS-	E	1	854	2297369.766	0.00002	0.64	0.71	16.39	0.03	0.64	0.71	2.99	2013.83
DEAR_GPS-	U	1	854	1321.71534	0.00026	7.41	0.66	1.27	0.31	7.41	0.66	2.99	2013.73
MOIU_GPS-	N	1	837	32095.72745	0.00007	2.05	0.96	18.96	0.08	2.05	0.96	2.99	2013.63
MOIU_GPS-	E	1	837	3928416.013	0.00008	2.18	0.83	25.09	0.09	2.18	0.83	2.99	2013.65
MOIU_GPS-	U	1	837	2201.51765	0.00026	7.52	0.72	-1.02	0.3	7.52	0.72	2.99	2013.7
NOT1_GPS-	N	1	940	4105000.393	0.00002	0.69	0.67	19.97	0.02	0.69	0.67	2.99	2013.73
NOT1_GPS-	E	1	940	1334829.23	0.00004	0.9	1.05	20.85	0.03	0.9	1.05	2.99	2014.05
NOT1_GPS-	U	1	938	126.34294	0.00028	8.55	0.7	2.41	0.35	8.55	0.7	2.99	2013.75
RAMO_GPS-	N	1	892	3406110.033	0.00003	0.95	0.72	19.86	0.04	0.95	0.72	2.99	2013.57
RAMO_GPS-	E	1	892	3330960.697	0.00004	0.61	0.88	22.62	0.03	0.61	0.88	2.99	2012.79
RAMO_GPS-	U	1	892	886.84472	0.00025	7.54	0.62	4.92	0.31	7.54	0.62	2.99	2013.67
ZAMB_GPS-	N	1	902	-1717163.191	0.00003	0.81	0.67	18.41	0.03	0.81	0.67	2.96	2013.65
ZAMB_GPS-	E	1	902	3038057.612	0.00002	0.32	0.72	20.07	0.02	0.32	0.72	2.96	2014.26
ZAMB_GPS-	U	1	902	1324.91919	0.00024	7.06	0.74	2.95	0.28	7.06	0.74	2.96	2013.68
ABUZ_GPS-	N	1	930	1241406.058	0.00006	1.65	0.78	20.19	0.07	1.65	0.78	2.95	2013.82
ABUZ_GPS-	E	1	930	835369.4088	0.00006	1.89	0.66	22.12	0.08	1.89	0.66	2.95	2013.78
ABUZ_GPS-	U	1	929	705.05	0.00023	6.79	0.66	1.37	0.28	6.79	0.66	2.95	2013.76
BKFP_GPS-	N	1	851	1387995.659	0.00007	1.9	0.92	19.02	0.1	1.9	0.92	2.75	2013.66

Stations	enu	S#	#	mean length	Sig	wrms	nrms	Slope	Sig	wrms	Nrms	dur	Mean
				(m)	(m)	(mm)		(mm/yr)	(mm/yr)	(mm)		(yrs)	(yrs)
BKFP_GPS-	E	1	850	459695.3557	0.00008	2.31	0.84	22.19	0.11	2.31	0.84	2.75	2013.66
BKFP_GPS-	U	1	850	249.99352	0.00025	7.22	0.68	2.05	0.33	7.22	0.68	2.75	2013.64
CLBR_GPS-	N	1	555	551065.0317	0.00009	2.04	0.78	19.72	0.17	2.04	0.78	1.99	2012.65
CLBR_GPS-	E	1	550	926224.8142	0.0001	2.28	0.63	23.31	0.19	2.28	0.63	1.99	2012.76
CLBR_GPS-	U	1	545	57.16018	0.00042	9.64	0.79	0.19	0.78	9.64	0.79	1.99	2012.74
FUTY_GPS-	N	1	655	1040808.631	0.00006	1.5	0.71	19.55	0.1	1.5	0.71	1.99	2012.9
FUTY_GPS-	E	1	655	1372763.03	0.00008	1.97	0.67	22.93	0.13	1.97	0.67	1.99	2013.05
FUTY_GPS-	U	1	655	247.38339	0.00029	7.45	0.73	-2.39	0.5	7.45	0.73	1.99	2013.01
OSGF_GPS-	N	1	662	1004955.205	0.00006	1.49	0.69	19.38	0.11	1.49	0.69	1.99	2012.96
OSGF_GPS-	E	1	662	823054.6238	0.00008	2.04	0.69	22.29	0.14	2.04	0.69	1.99	2013.06
OSGF_GPS-	U	1	662	532.62739	0.0003	7.62	0.72	-1.99	0.52	7.62	0.72	1.99	2013.09
UNEC_GPS-	N	1	698	715206.1742	0.00008	2.01	0.9	20.04	0.14	2.01	0.9	1.99	2012.93
UNEC_GPS-	E	1	698	830203.704	0.00008	2.2	0.73	22.51	0.15	2.2	0.73	1.99	2013.03
UNEC_GPS-	U	1	698	254.38567	0.00035	9.29	0.87	-3.93	0.63	9.29	0.87	1.99	2013.04
ULAG_GPS-	N	1	627	725505.5137	0.00007	1.62	0.74	18.77	0.13	1.62	0.74	1.8	2012.71
ULAG_GPS-	E	1	627	375777.6332	0.00008	2.09	0.65	22.78	0.17	2.09	0.65	1.8	2012.84
ULAG_GPS-	U	1	627	44.55113	0.00028	6.99	0.65	-2.98	0.55	6.99	0.65	1.8	2012.88
HUKP_GPS-	N	1	181	1438376.3	0.00015	1.23	0.6	19.59	0.23	1.23	0.6	1.74	2011.92
HUKP_GPS-	E	1	181	823623.5896	0.00021	1.73	0.59	20.73	0.32	1.73	0.59	1.74	2011.92
HUKP_GPS-	U	1	181	559.78704	0.00068	6.04	0.56	-1.57	1.05	6.04	0.56	1.74	2011.97
CGGT_GPS-	N	1	148	1126897.789	0.00019	2.14	0.98	14.11	0.26	2.14	0.98	1.67	2012.33
CGGT_GPS-	E	1	147	999241.3762	0.00021	2.44	0.87	28.73	0.29	2.44	0.87	1.67	2012.42
CGGT_GPS-	U	1	147	916.44445	0.00056	6.51	0.64	8.25	0.77	6.51	0.64	1.67	2012.49
FPNO_GPS-	N	1	168	604973.8702	0.00017	2.05	0.9	17.82	0.32	2.05	0.9	1.48	2013.99
FPNO_GPS-	E	1	168	779417.612	0.00017	2.03	0.65	21.21	0.32	2.03	0.65	1.48	2014.04
FPNO_GPS-	U	1	168	88.30656	0.00064	7.61	0.69	4.13	1.2	7.61	0.69	1.48	2013.99
FUTA_GPS-	N	1	171	812480.8651	0.00024	1.76	0.72	20.04	0.54	1.76	0.72	1.33	2011.29

Stations	enu	S#	#	mean length	Sig	wrms	nrms	slope	Sig	wrms	Nrms	dur	Mean
				(m)	(m)	(mm)		(mm/yr)	(mm/yr)	(mm)		(yrs)	(yrs)
FUTA_GPS-	E	1	171	567152.3559	0.0003	2.29	0.62	20.53	0.69	2.29	0.62	1.33	2011.31
FUTA_GPS-	U	1	170	410.76508	0.00094	7.09	0.59	-5.15	2.14	7.09	0.59	1.33	2011.32
RUST_GPS-	N	1	90	534537.9763	0.00066	6.19	2.46	6.55	1.58	6.19	2.46	0.99	2013.37
RUST_GPS-	E	1	90	774119.6503	0.00084	7.84	2.32	19.19	1.99	7.84	2.32	0.99	2013.37
RUST_GPS-	U	1	90	45.57211	0.00179	16.86	1.44	20.14	4.28	16.86	1.44	0.99	2013.3
GEMB_GPS-	N	1	125	770019.1559	0.00012	1.3	0.72	20.83	0.48	1.3	0.72	0.69	2014
GEMB_GPS-	E	1	125	1235925.855	0.00013	1.47	0.58	20.18	0.53	1.47	0.58	0.69	2013.83
GEMB_GPS-	U	1	125	1795.62587	0.00053	5.84	0.64	10.36	2.1	5.84	0.64	0.69	2013.77
MDGR_GPS-	N	1	9	1317810.244	0.00088	0.77	0.29	-92.6	123.7	0.77	1	0.02	2027.7
MDGR_GPS-	E	1	9	1430652.326	0.00126	3.04	0.82	35.27	170.99	3.04	1	0.02	2037.37
MDGR_GPS-	U	1	9	348.22534	0.00426	4.93	0.39	-13.91	597.02	4.93	1	0.02	2027.37

4.2.2 Velocity and Position Solutions

The Velocity and Position solutions were found in the GLOBK (GLORG) result file ***globk_vel.org***. The setup used for the analysis was as follows:

i. Stabilization with 50.0% constant, 50.0% site dependent weighting.

ii. Delete sites with 4.0-sigma condition.

iii. Height variance factor 100.00 Position, 100.00 Velocity

iv. For Position: Min dH sigma 0.0050 m; Min RMS 0.0030 m, Min dNE sigma 0.00050 m

v. For Velocity: Min dH sigma 0.0050 m/yr; Min RMS 0.0030 m/yr, Min dNE sigma 0.00010 m/yr

vi. Sigma Ratio to allow use: Position 30.00 Velocity 30.00

The position and velocity stabilizations were carried out in four (4) iterations using six (6) out of the ten (10) stabilization sites. The sites used are DAKR, ABPO, RAMO, ZAMB, DEAR, and NOT1. The geographical balance, which was the basis for the selection of the sites was verified and found to be maintained. The relative sigma levels of the sites used for the network stabilization are as shown in Table 4.3. the Velocity and Position stabilization results are contained in Appendix Two.

Table 4.3: Relative Sigma Values Used for Four Stabilization Iterations

S/N	Site	Relative Sigma Used in Stabilization							
		Position I	**Velocity I**	**Position II**	**Velocity II**	**Position III**	**Velocity III**	**Position IV**	**Velocity IV**
1	DAKR_GPS	1.000	1.000	0.970	0.960	0.950	0.950	0.950	0.940
2	ABPO_GPS	1.000	1.000	1.000	1.000	1.000	1.000	1.000	1.000
3	RAMO_3PS	1.000	1.000	0.990	0.990	0.980	0.990	0.980	0.980
4	ZAMB_GPS	1.000	1.000	0.990	0.990	0.990	0.990	0.990	0.990
5	DEAR_GPS	1.000	1.000	1.000	1.000	1.000	1.000	1.000	1.000
6	NOT1_GPS	1.000	1.000	1.050	1.050	1.070	1.070	1.080	1.070

The Summaries of the Velocity and Position Solutions are as shown in Table 4.4 and 4.5

4.2.2.1 Velocity Solutions

The Velocity Solution was extracted from ***globk_vel.org*** and shown in Table 4.4. From Table 4.4, it could be seen that:

i. The velocity of the Maiduguri site is quite problematic as its way beyond the range of the velocity of the other stations. Its Velocity was found to be 76.94 ±146.40mm/year East, -40.49 ± 102.05 mm/year North and 17.16±421.14mm/year for the Height. This is because the standard deviation of the East, North and Up components are greater than the velocities themselves. The RSUT station velocity solutionalso calls for attention as the North value appear too small compared to others.

ii. The height solution for the Center for Geodesy and Geodynamics, Toro and Rivers State University of Science and Technology were found to be anomalous. They were found to be rather too large compared to the IGS stations used for stabilization and the other NigNet stations.

iii. The Six sites (DAKR, ABPO, RAMO, ZAMB, DEAR, and NOT1) used for the stabilization were denoted with an asterisk (*), the other two IGS Stations included in the solution were MOIU and the renamed DARK data that weren't used for stabilization, but still included in the solution.

Table 4.4: Summary of Velocity Solutionsfrom GLOBK Ver 5.3

Long.	Lat.	E & N Rate		E & N Adj.		E & N ±		RHO	H Rate	H adj.	±	SITE
(deg)	(deg)	(mm/yr)		(mm/yr)		(mm/yr)			(mm/yr)			
342.56054	14.72124	19	17.91	0.1	0.7	0.05	0.05	0.084	1.01	0.31	0.71	**DAKR_GPS***
342.56054	14.72124	18.99	17.91	0.1	0.7	0.05	0.05	0.084	1.01	0.31	0.71	**DAKR_2PS**
47.22921	-19.01831	18.62	13.91	-0.07	-0.39	0.07	0.07	-0.017	4.85	4.93	0.54	**ABPO_GPS***
#35.29001	0.28832	25.07	18.27	25.07	18.27	0.11	0.09	-0.056	-0.97	-0.97	0.4	**MOIU_GPS**
34.76314	30.59761	23.44	19.59	0.18	-0.14	0.07	0.06	-0.12	2.61	1.2	0.48	**RAMO_3PS***
28.31101	-15.42554	20.33	17.86	0.14	-0.62	0.07	0.06	-0.01	4.45	3.54	0.39	**ZAMB_GPS***
23.99264	-30.66521	16.88	19.11	0.51	0.49	0.07	0.07	-0.05	4.38	2.89	0.51	**DEAR_GPS***
14.98979	36.87585	20.27	19.79	-1.14	-0.05	0.09	0.08	0.082	0.09	0.79	0.5	**NOT1_GPS***
#13.13100	11.83809	76.94	-40.49	76.94	-40.49	146.4	102.05	-0.016	17.16	17.16	421.14	**MDGR_GPS**
12.4978	9.34974	23.16	19.7	23.16	19.7	0.17	0.12	0.004	-0.32	-0.32	0.54	**FUTY_GPS**
11.18394	6.9172	20.16	20.31	20.16	20.31	0.74	0.53	0.016	2.82	2.82	2.27	**GEMB_GPS**
9.11831	10.1231	28.25	14.06	28.25	14.06	0.24	0.18	0.008	10.72	10.72	0.8	**CGGT_GPS**
8.35157	4.9503	23.1	19.91	23.1	19.91	0.26	0.19	0.011	0.91	0.91	0.82	**CLBR_GPS**
7.64869	11.15174	21.97	19.19	21.97	19.19	0.12	0.09	-0.008	0.86	0.86	0.41	**ABUZ_GPS**
7.59091	12.92115	21.6	19.23	21.6	19.23	0.34	0.24	0.016	1.11	1.11	1.11	**HUKP_GPS**
7.50499	6.42481	22.69	20.23	22.69	20.23	0.19	0.14	0.012	-1.52	-1.52	0.6	**UNEC_GPS**
7.48634	9.02767	22.31	19.47	22.31	19.47	0.18	0.13	0.008	0.44	0.44	0.58	**OSGF_GPS**
7.03324	5.43457	21.31	18.03	21.31	18.03	0.4	0.3	0.005	2.2	2.2	1.35	**FPNO_GPS**
#6.97852	4.80184	19.01	6.6	19.01	6.6	0.73	0.56	0.004	14.21	14.21	2.42	**RUST_GPS**
5.13644	7.29864	21.23	19.87	21.23	19.87	0.92	0.64	0.016	-1.72	-1.72	2.82	**FUTA_GPS**
4.22924	12.46858	21.98	18.39	21.98	18.39	0.13	0.1	-0.016	1.66	1.66	0.45	**BKFP_GPS**
3.39762	6.51733	22.99	18.77	22.99	18.77	0.22	0.15	-0.001	-0.57	-0.57	0.67	**ULAG_GPS**
VEL STATISTICS: For 6 RefSites WRMS ENU 0.40 0.50 2.92 mm/yr NRMS ENU 6.15 7.97 5.86 uzoh.gdl												
VEL MEANS: For 6 RefSites: East 0.05 ± 0.16 North 0.05 ± 0.20 Up 2.48 ± 1.19 mm/yruzoh.gdl												

iv. The velocity statistics for the six reference (stabilization) sites is also shown in the solution:

a. The Weighted Root Mean Square for the East is 0.40mm/yr, 0.50mm/yr for the North and 2.92mm/yr for the Up (Height) component. The Normalized Root Mean Square for the East is 6.15, 7.97 for the North and 5.86 for the Up components.

b. The mean velocitiesfor the six reference sites are0.05±0.16mm/yr for East, 0.05±0.20mm/yr for North and 2.48±1.19mm/yr for the Up Component.

v. Removing the outliers (MDGR and RSUT for the Horizontal and MDGR, CGGT and RSUT for the Vertical), the mean horizontal velocity of the Nigerian Region of the Nubia Plate is 22.5625±0.32583mm/yr East, 18.93±0.23417mm/yr North.

vi. Whereas some of the stations are subsiding, others are uplifting. It is however interesting to note that asides CLBR and FPNO, the other Southern stations UNEC, ULAG, and FUTA are subsiding. On the other hand, all the Northern stations: ABUZ, BKFP, OSGF, GEMB, and HUKP are all uplifting, except for FUTY.

4.2.2.2 Position Solutions

The positions of the sites used for this study were extracted from ***globk_vel.org***file as Table 4.3. In the three years, it was found that:

i. The Position Statistics for the Reference Sites records that the WRMS for the East, North and Up are 1.45mm, 1.07mm, and 5.77mm respectively. The NRMS for the East, North and Up directions are 12.27, 9.40 and 6.38 respectively.

ii. The Bearing and Distance covered by the NigNet Sites were computed from the change in eastings (dE) and Change in Northings (dN) and presented in Table 4.6

iii. Again it can be seen that the MDGR site has a problem. Whereas all the other stations are moving North East, the Bearing of the site indicates a South East.

iv. It can also be seen that the standard deviation for the MDGR site is outrageous, it was rejected from the velocity plotting of the network.

Table 4.5: Summary of Position Estimates from GLOBK Ver 5.3

Long. (deg)	Lat. (deg)	dE adj. (mm)	dN adj. (mm)	dE± (mm)	dN± (mm)	RHO	dH adj. (mm)	dH± (mm)	SITE
342.56054	14.72124	0.44	1.73	0.09	0.1	0.087	3.59	1.3	**DAKR_GPS***
342.56054	14.72124	3.9	0.58	0.44	0.37	-0.05	18.31	1.25	**DAKR_2PS**
47.22921	-19.01831	-0.4	-0.61	0.12	0.13	-0.02	12.28	0.97	**ABPO_GPS***
35.29001	0.28832	88.06	58.33	0.19	0.16	-0.05	5.71	0.75	**MOIU_GPS**
34.76314	30.59761	1.59	-0.91	0.12	0.1	-0.15	2.64	0.86	**RAMO_3PS***
28.31101	-15.42554	-0.11	-0.92	0.12	0.11	-0.01	-5.4	0.72	**ZAMB_GPS***
23.99264	-30.66521	1.56	0.67	0.13	0.12	-0.05	6.67	0.92	**DEAR_GPS***
14.98979	36.87585	-4.05	-0.14	0.17	0.15	0.075	3.46	0.91	**NOT1_GPS***
13.131	11.83809	112.5	-73.23	241.5	168.28	-0.02	51.79	694.51	**MDGR_GPS**
12.4978	9.34974	50.15	37.84	0.37	0.25	0.004	-8.43	1.12	**FUTY_GPS**
11.18394	6.9172	45.57	38.38	1.43	1.02	0.016	-7.78	4.4	**GEMB_GPS**
9.11831	10.1231	89.34	37.75	0.53	0.4	0.01	19.91	1.81	**CGGT_GPS**
8.35157	4.9503	52.36	38.52	0.52	0.37	0.009	-13.99	1.63	**CLBR_GPS**
7.64869	11.15174	100.5	97.5	0.23	0.17	-0.01	-15.34	0.77	**ABUZ_GPS**
7.59091	12.92115	161.1	150.35	0.51	0.36	0.013	-251.1	1.68	**HUKP_GPS**
7.50499	6.42481	51.69	37.28	0.38	0.28	0.009	-11.25	1.23	**UNEC_GPS**
7.48634	9.02767	50.57	36.36	0.37	0.27	0.006	-12.39	1.2	**OSGF_GPS**
7.03324	5.43457	63.82	42.17	0.82	0.61	0	17.32	2.74	**FPNO_GPS**
6.97852	4.80184	32.69	3.86	1.54	1.19	-0	83.52	5.1	**RUST_GPS**
5.13644	7.29864	54.7	49.85	1.38	0.94	0.016	159.28	4.2	**FUTA_GPS**
4.22924	12.46858	47.6	34.46	0.25	0.19	-0.02	-4.7	0.84	**BKFP_GPS**
3.39762	6.51733	51.16	34.52	0.48	0.32	-0.01	-12.34	1.41	**ULAG_GPS**
POS STATISTICS: For 6 RefSites WRMS ENU 1.45 1.07 5.77 mm NRMS ENU 12.27 9.40 6.38 uzoh.gdl									
POS MEANS: For 6 RefSites: East 0.21 ± 0.59 North 0.03 ± 0.43 Up 2.78 ±2.36 mm uzoh.gdl									

Table 4.6, is an attempt to make the result of this experiment more appreciable to the layman. This was achieved using the dE Adj and dN Adj from Table 4.5, which are the Eastern and Northern change in positions. The mathematical models (4.1) and (4.2) were used to generate the Bearings and Distances of the positions of the stations between 2012 and 2014.

$$\theta = \tan^{-1}\left(\frac{\Delta E}{\Delta N}\right) \qquad (4.1)$$

$$l = \sqrt{\left(\Delta E^2 + \Delta N^2\right)} \qquad (4.2)$$

The Table 4.6 shows that all the stations with the exception of Maiduguri are moving in the North East direction in agreement with Altamimi*et al* (2011) and Bawa*et al* (2018). The Maiduguri station showed a south east direction motion which influenced the decision to exclude the station as an outlier.

Table 4.6: Bearing and Distances of the Motions

S/N	Site	Bearing	Distances
1	MDGR_GPS	123°04'23.1276"	8.8566m
2	FUTY_GPS	52°57'50.8248"	13.26575m
3	GEMB_GPS	49°53'42.7956"	12.95762m
4	CGGT_GPS	67°5'37.8492"	15.94302m
5	CLBR_GPS	53°39'32.2956"	13.48184m
6	ABUZ_GPS	45°51'23.9472"	19.89774m
7	HUKP_GPS	46°58'17.4432"	24.95676m
8	UNEC_GPS	54°12'0.0108"	13.33942m
9	OSGF_GPS	54°17'1.4568"	13.1856m
10	FPNO_GPS	56°32'40.8552"	14.55953m
11	RUST_GPS	83°15'56.7288"	8.549854m
12	FUTA_GPS	47°39'21.6216"	14.46029m
13	BKFP_GPS	54°5'50.4852"	12.81093m
14	ULAG_GPS	55°59'26.3508"	13.09045m

4.3: Velocity Model

Figure 4.2 and 4.3 show the Velocity Plot for the experiment from 2012 to 2014. It is evident from the plots, and as seen in Table 4.6 that although the direction of all the stations used for the Velocity plot are in the North East direction, the bearings of the motions are not the same.

The stations with the most deviating bearings from the majority are the CGGT and the RUST stations at 67^{o}5'37.8492" and 83^{o}15'56.7288" respectively. However, it is interesting to note that the ten degrees (10^{o}) range of change in bearing of the different displacements is wide enough to suggest possible presence of fault lines.

It can be deduced that most of the closely located stations have the same direction of motion. UNEC (Enugu), FPNO (Owerri), CLBR (Calabar) and OSGF (Abuja) have bearings of 54^{o}12'0.0108", 56^{o}32'40.8552",53^{o}39'32.2956" and 54^{o}17'1.4568" respectively. ABUZ (Kaduna) and HUKP (Katsina) have the bearings 45^{o}51'23.9472" and 46^{o}58'17.4432" respectively. FUTY (Yola) and GEMB (Gembu) have 52^{o}57'50.8248" and 49^{o}53'42.7956" respectively. Most interestingly, whereas ULAG (Lagos) and BKFP (Birin-Kebbi) are identical with 54^{o}5'50.4852" and 55^{o}59'26.3508" respectively, FUTA (Akure) is 47^{o}39'21.6216" this is indicative of an existing (possibly active) fault between lagos – Birin-Kebbi and Akure – ABUZ sections (the Ifewara – Zungeru Fault).

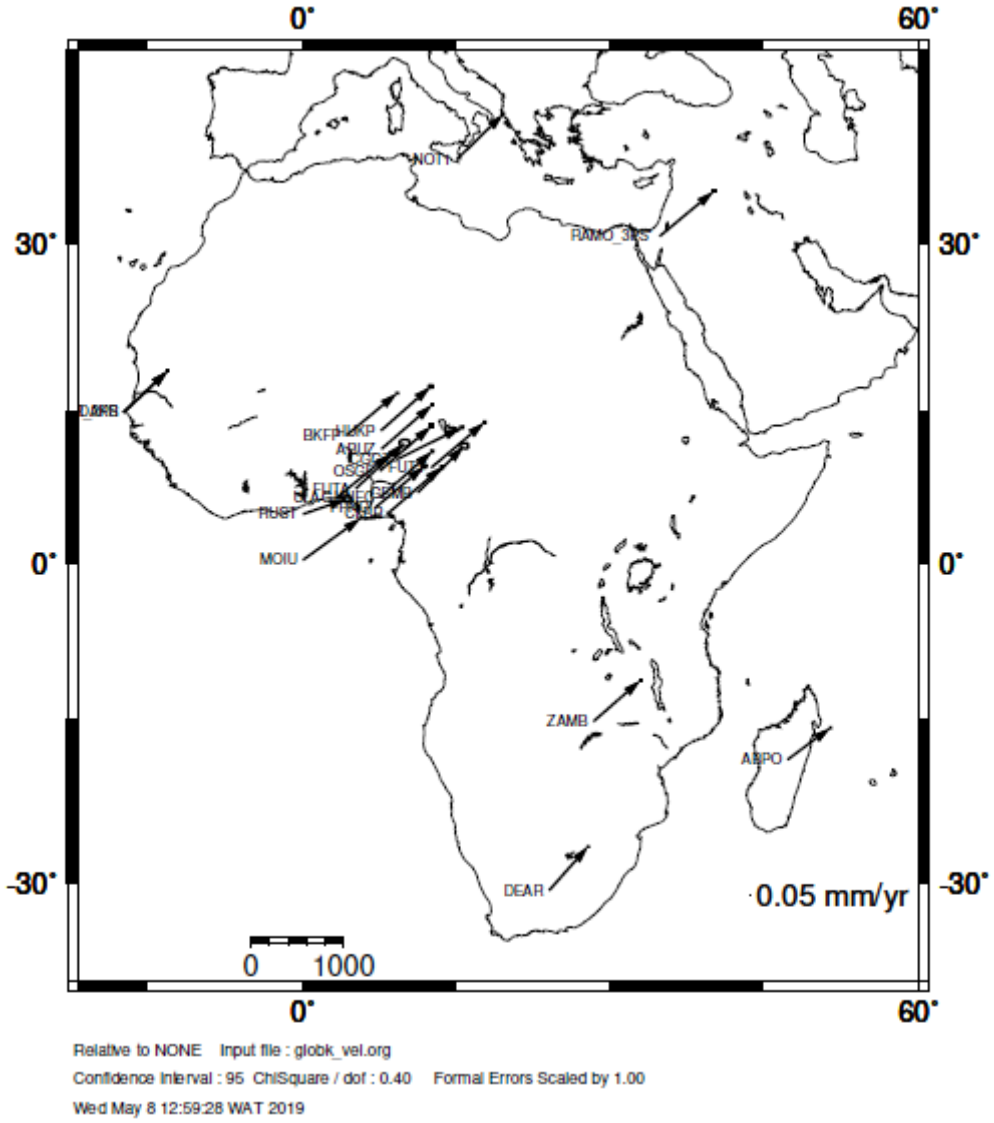

Fig 4.2: *NigNet Velocity Model for 2012 – 2014 with respect to the Stabilization Points*

That notwithstanding, the Nigerian CORs Network, NIGNET, is too sparse to actually indicate or define fault lines. Although the sharp difference in bearing between points that are either close or lie on the same sides of a suspected fault line, the number and locations of the NIGNET Stations make it impossible to actually detect the physical position of the fault lines.

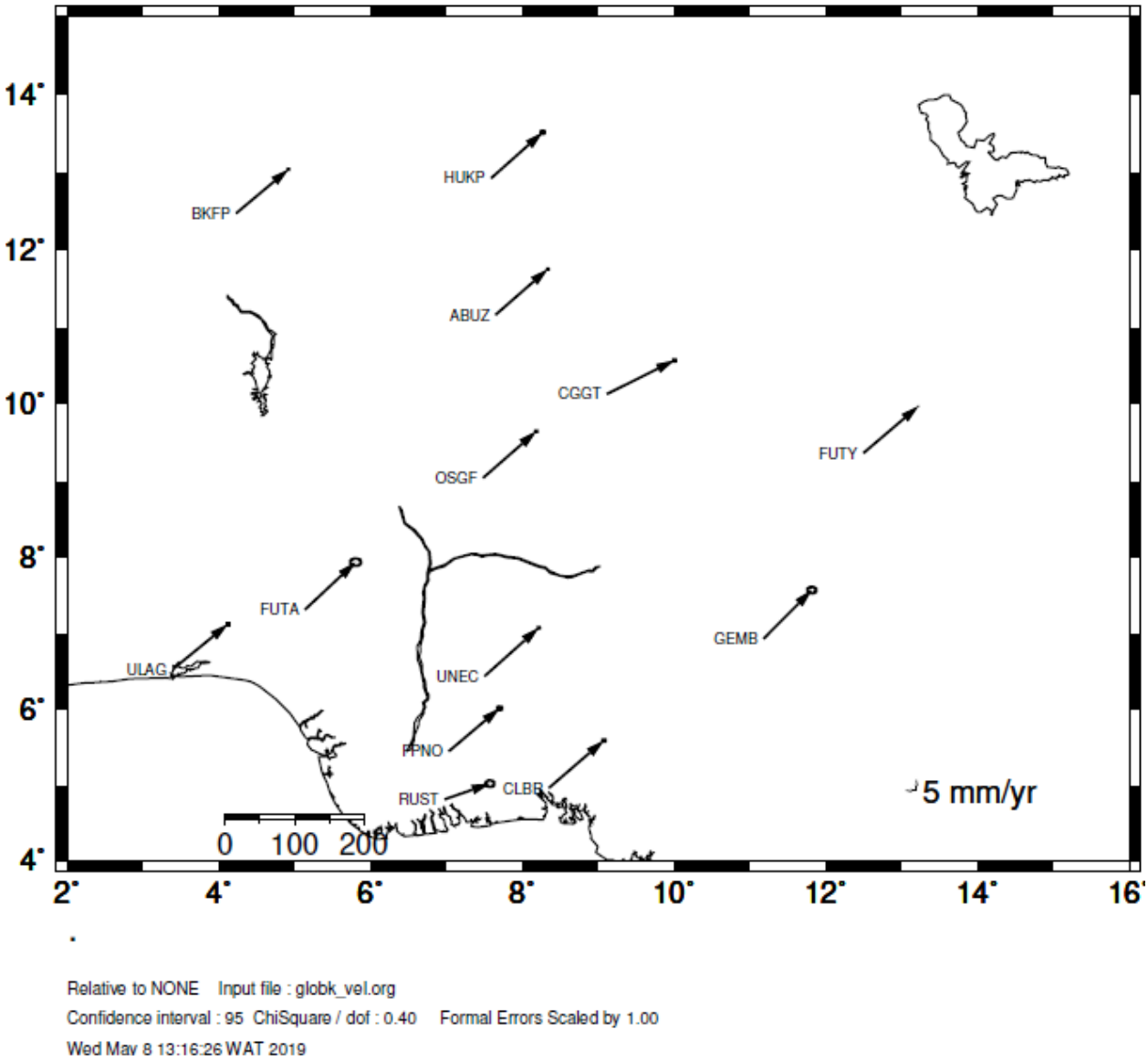

Fig 4.3: NigNet Velocity Model for 2012 – 2014

Interestingly, Figure 4.2 indicates the reason for the eventual exclusion of the MOIU site from the stabilization (no asterisk on the site in Tables 4.4 and 4.5). Whereas the site is located in Kenya, with the correct coordinates reflected in Tables 4.4 and 4.5, the plot in Figure 4.2 shows that something went wrong with the Easting coordinate of the site moving from 35^{o} to 3^{o}.

Objective No. 3: *To evaluate the quality of data from the different stations as an assessment of the health of the Network*

4.4: Performance of the Sites

Fig. 4.4, extracted from Table 4.2, shows the number of days each of the station used was able to log data successfully. This can be used as a measure of the health of the stations, because the whole essence of a COR station is to be able to log daily GNSS data that can be used for a wide range of surveys and studies. Therefore inability of a COR station or active GPS station to log files or record the logged files in the central depository is an abnormality.

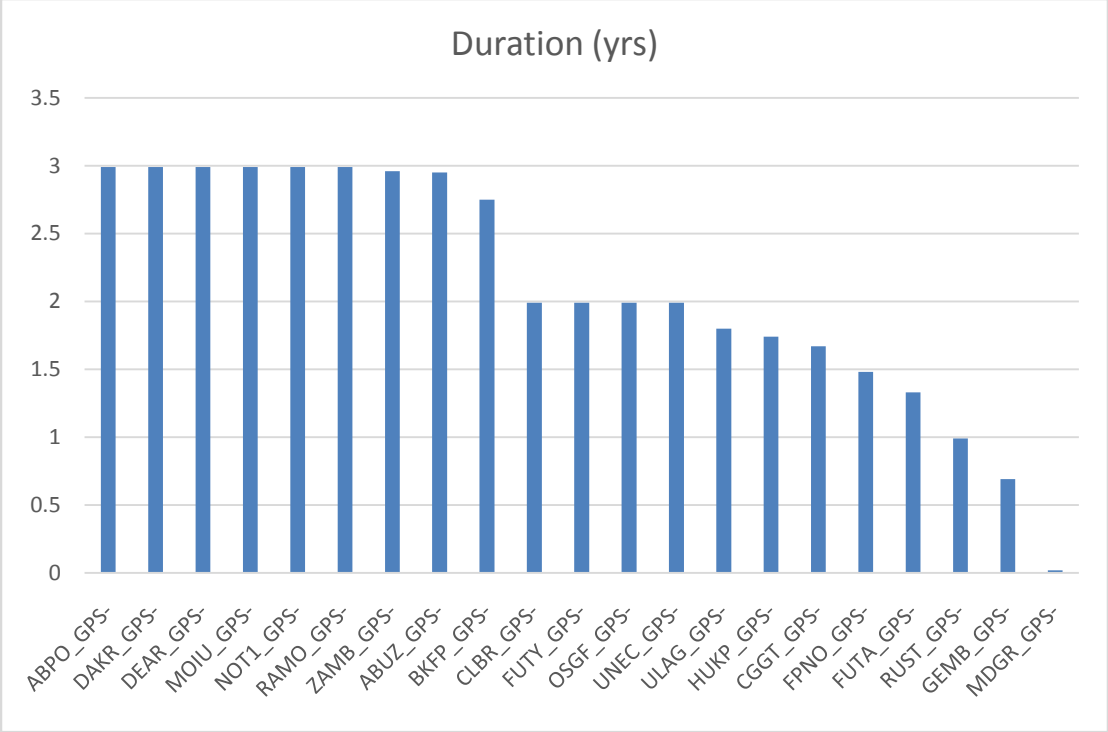

Fig 4.4: Performance of the Stations Used.

From Fig. 4.4, it can be seen that all the IGS stations used eventually for the stabilization performed creditably well, logging for 1092.35 days out of the expected 1096 days studied.It can be seen that the best performing NigNET station between 2012 and 2014 is ABUZ at 98.33%, this is closely by BKFP at 91.67%. Other stations such as CLBR, FUTY, OSGF,

UNEC, ULAG, HUKP, CGGT all performed above average. Stations like FPNO, FUTA, RUST and GEMB performed below average, while MDGR's performance was abysmally poor.

Although the reason for the performance or health status of the stations is beyond the scope of this research, one can conclude that the Nigerian Network needs serious attention if nothing has been done between 2014 and now. The Time Series plotting is as shown in appendix three.

4.5 Test of Hypotheses

4.5.1 Hypothesis One

H_o The Nigerian Region of the Nubia Plate did not experience any movement between 2012 and 2014.

From the experiment, the mean horizontal velocity of the Nigerian Region of the Nubia Plate is 22.5625±0.32583mm/yr East, 18.93±0.23417mm/yr North. The H_o was rejected because of sufficient evidence from the velocities that there was a motion within the period.

4.5.2 Hypothesis Two

H_o **Hypothesis Two**

H_o The Nigerian CORs Network is not healthywithin the period under review.

As shown in Fig. 4.4, nine of the Nigerian sites performed above 50% and only five of the stations were seen to perform below 50%, which makes it insufficient to accept the H_o. H_o

was therefore rejected because a greater number of stations were found to be healthy or close to being healthy.

4.6 Contribution to Knowledge

This study has successfully brought forward different information that is needed to have an insight in the nature of tectonic displacement in the region. Some of the contributions are as follows:

1. The velocity result of this study validates the velocity result of Bawa, Ojigi and Dodo (2018).
2. The direction of the Nigerian Crustal motion is generally the North East direction.
3. The bearings of all the stations' displacement are not uniform which is suggestive of the presence of faults, since there is a regional uniformity of some sort, however, the stations are too sparsely located to readily define the Nigerian fault lines.
4. The best performing NigNET stations within the period under review are ABUZ and BKFP, while the worst performing station is MDGR.

CHAPTER FIVE
SUMMARY,CONCLUSION AND RECOMMENDATIONS

5.1 Summary

It has been seen from a wide range of literature, that the mechanism that drives the continents apart, a controversial discourse till date, is the convectional activities of the constituents of the mantle layer of the earth crust, a widely accepted theory. The most painful thing about the continental drift theory, irrespective of its acceptability or rejection, is not that the resultant effect of the natural disasters (earthquakes, tremors, volcanoes, landslides andtsunamis) it causesare very devastating and that the economic loss involved is tremendous, it is the fact that it is not mostly causedby human activities and most regrettably, cannot be stopped by any human activity. However, the wide range of opportunities the GNSS technology offers affords humans the capability of studying the activities of the tectonic plate, earthquake build up and processes. This opportunity gives the Geodesist and Geodynamist the ability to predict and create an early warning system in order to reduce the general loss of lives and property in events of these disasters.

Nigeria has been seen to have had a lot of seismic activities and the frequency of the earth tremors in recent times call for a serious concern and makes this study very apt. It is only unfortunate that due to the fact that the GNSS COR stations in Nigeria are too few, and that a handful of them are not very functional or performing optimally, the study could not successfully define the actual geographic location of the Nigerian Fault lines.

5.2 Conclusion

This study has clearly demonstrated the monitoring of the tectonic motions of the Nigerian Region of the Nubia Plate between 2012 and 2014 using GNSS technology and GAMIT/GLOBK software. It showed clearly, in line with the results of Bawa*et al* (2018) and Altamimi*et al* (2011),that the region is moving in the North-East direction. It also showed, in close agreement with Bawa*et al* (2018), that the average velocity of the NIGNET Stations (after removing the outlying stations) for the period under the review is 22.5625 ±0.32583mm/yr in the East direction and 18.93±0.23417mm/yr in the North direction.

It is also evident from the study, that the wide range of difference in the bearings of the motions is suggestive of the presence of fault lines within the country, giving empirical support the hypotheses of several studies (Afegbua in Orakpo (2017); Eze *et al*. (2012); Tsalha*et al*. (2015);Afegbua*et al*. (2011) and Akpan and Yakubu (2010)). However, the study failed to define the position of the Nigerian fault lines because the NIGNet Stations are very sparsely located and needs to be densified in order to make such refined definition.

The time seriesresult of this study succeeded in showing that the a number of the NIGNet stations performed poorly within the period under review, and indicated the need for a close station-based forensic study of the stations in order to understand why they logged very poorly. The health of the stations can generally be monitored using this methodology and technical attention paid to the stations found to be unhealthy like the MDGR, GEMB and RUST.

5.3 Recommendations

The need for a continuous monitoring and evaluation of the tectonic motions of a country like Nigeria cannot be over emphasized, especially with the increase in the occurrence of earth tremors in the country. It is therefore recommended that:

1. All stakeholders, both governmental, non-governmental and private, including the Federal Government of Nigeria (FGN), the Office of the Surveyor General of the Federation (OSGOF), Surveyors Council of Nigeria (SURCON), Nigerian Institution of Surveyors (NIS), National Space Research and Development Agency (NASRDA), Geodesists, Geologists, Geophysisists, Geologists and Surveyors should intensify efforts to densify the Continuously Observing Reference Stations (CORs) in the Country.
2. The use of GAMIT/GLOBK software for the analysis of GNSS data for both crustal and structural deformation monitoring should be encouraged by all geophysical and geodynamical research agencies and association.
3. By way of creating an early warning system, in the establishment of new CORs stations recommended above, attention should be given to the areas along the Ifewara-Zungeru fault line, and the eastern fault line suspected to run through Bayelsa, Rivers, Abia, Enugu, Nassarawa, and Bauchi states, connecting Adamawa and Taraba States.
4. Further researches should channel technical attention to the ailing COR Stations such as MDGR, RUST, GEMB, CGGT, FPNO, and FUTA, to bring them all to speed and make them perform optimally like the very healthy stations (ABUZ and BKFP).

5. The Velocities of the other countries in West Africa and indeed Africa should be evaluated with the hope of getting a holistic view of what is happening on the interiors of the Nubia plate.
6. IGS should evaluate ABUZ and BKFP with respect to other criteria needed to be met for inclusion or upgrade to an IGS Station cadre.

5.4 Future Research Topics

In the course of this study, a number of research interests were developed which could not be covered by this research work. The following topics, therefore, are posited for future research involvements and contributions:

1. Monitoring of the Mid Atlantic Ridge System: A Study of the Divergent Boundary System.
2. Evaluation of the Effect of Atmospheric Delays on the NIGNet GNSS Data using GAMIT/GLOBK Software.
3. Tectonic Plate Monitoring of the West African Region of the Nubia Plate using GNSS Technology and GAMIT/GLOBK Software.
4. Definition of the Nigerian Fault System using GNSS Technology and GAMIT/GLOBK Software.
5. Comprehensive Study of the Internal Motions of the Nubia Plate.
6. Study of Earthquake build up and release Mechanism and an Attempt at its Prediction.

References

Adedeji O. O. (2011): Climatic Zones for Architectural Design with Climate in Nigeria. *ARC/03/1485 Lecture Notes Department of Architecture,* Federal University of Technology, Akure, Nigeria www.sdngnet.com/Files/Lectures/FUTA-ARC-810 Applied Climatology/Assignments/2012-2011 Assignments PDF/ARC-03-1485-Adedeji-Climatic Zones for Architectural Design.pdf

Afegbua in Orakpo E. (2017): Earthquake in Nigeria: Measures to Avert Devastating Impacts-Experts., *Vanguard* January 4, 2017. Online Version, https://www.vanguardngr.com/2017/01/earthquake-nigeria-measures-avert-devastating-impacts-experts/ Accessed 26th Nov. 2017.

Akpan O. U. and Yakubu T. A. (2010): A Review of Earthquake Occurrences and Observations in Nigeria. *Earthquake Science* June 2010, 23 (3), 289−294. https://doi.org/10.1007/s11589-010-0725-7 Accessed 26th Nov. 2017.

Alden (2018): Why the Earth's Crust Is So Important. *ThoughtCo*. February 05, 2018.

AltamimiZ., Collilieux X., and Metivier L.(2011): ITRF 2008: An Improved Solution of the International Reference Frame. *Journal of Geodesy 85, 457 – 573.*https://doi:10.1007/s00190-011-0444-4

American Geophysical Union (2014): Sahara's Abrupt Desertification Started By Changes In Earth's Orbit, Accelerated By Atmospheric And Vegetation Feedbacks. *Science Daily* Retrieved 13 January 2017.

Argus and Gordon, (1991) No-Net-Rotation model of current plate velocities incorporating plate motion model NUVEL-1. *Geophysical Research Letters* 18(11) December 1991

Aung P. S., Satirapod C. and Andrei C. O. (2016): Sagaing Fault slip and Deformation in Myanmar observed by continuous GPS measurements. *Geodesy and Geodynamics* 2016 7 (1), 56-63

Baire Q., Pottiaux E., Bruyninx C., Defraigne P., Legrand J., Bergeot N., (2011): Comparison of receiver antenna calibration models used in the EPN, *EUREF2011 symposium*, Chisinau, Moldova, May 23-27, 2011

Barzaghi R., Betti B. and De Gaetani C. I.(2018): Estimating Crustal Deformations by GNSS Time Series Data Analysis. New Advanced GNSS and 3D Soatial Techniques. *Lecture Notes in Geoinformation and Cartography* 35-48. Springer International Publishers AG 2018

Barzaghi R., Borghi A., Crespi M., Pietrantonio G., and Riguzzi F. (2004) *GPS Permanent Network Solution: the Impact of Temporal Correlations*. International Association of Geodesy Symposia vol. 127: V Hotine-Marussi Symposium on Mathematical Geodesy Springer-Verlag.

Bastos L, Bos M and Fernandes R. M. (2010): *Deformation and Tectonics: Contribution of GPS Measurements to Plate Tectonics – Overview and Recent Developments*. Sciences of Geodesy, 155-184, Springer-Verlag Berlin Heidelberg 2010

Bawa, Ojigi and Dodo (2018), GPS Velocity Time Series of NigNet CORS. *Nigerian Journal of Geodesy, 2* (2), 163 - 180

Behr J. A., Hudnut K. W. and King N. E. (1999) Monitoring Structural Deformation at Pacoima Dam, California Using Continuous GPS https://pdfs.semanticscholar.org/6311/7d9d2614cacefcd65f2a7d593f553d7a5853.pdf

Bellahsen, N., FaccennaC., FunicielloF., DanielJ. M., and Jolivet L. (2003), Why did Arabia Separate from Africa? Insights from 3-D Laboratory Experiments, *Earth Planet Science Lett*ers., 216(3), 365–381,

Bird, P., 2003. An updated digital model of plate boundaries. [Los Angeles, California, USA].*Geochemistry, Geophysics, Geosystems* AGU and the Geochemical Society. Vol 4, 1-52.

Brown D. (2016): *Plate Tectonics: S279_1 Our Dynamic Planet: Earth and Life. Open Learn*, The Open University, Walton Hall, Milton Keynes, 2016 http://www.open.edu/openlearn/science-maths-technology/science/geology/plate-tectonics/contentsection-0

Buforn, E., UdiasA., and Colombas M. A. (1988):Seismicity, Source Mechanisms and Tectonics of the Azores Gibraltar Plate Boundary. *Tectonophysics*, 152, 89–118.

Çelik, C. T. (1998): *Crustal Deformation Monitoring by the Kalman Filter Method*. PhD thesis, University of Nottingham. October 1998.

Collins R. O. and Burns J. M. (2007):.A History of Sub-Saharan Africa. Cambridge University Press.ISBN 9780521867467.

Corti G. (2009). Continental rift evolution: From rift initiation to incipient break-up in the Main Ethiopian Rift, East Africa. [Firenze, Italy]. *Elsevier, Earth-Science Reviews*. 96 (1-2), 1-53.

Corti G. Van Wijk J. P. H.,Cloetingh S. and Morley C. K. (2007): *Tectonic inheritance and continental rift architecture: Numerical and analogue models of the East African Rift system*. Tectonics, 26

Davies, P. B. H. (1997): *Assembling the IGS Polyhedron A identified Weekly GPS Terrestrial Reference Frame*, Ph. D Thesis, University of New Castle-Upon-Tyne.

Degnan, J.J(1993): Millimeter Accuracy Satellite Laser Ranging: a Review. *AGU Monograph Geodynamics Series* 25, *Contributions of Space Geodesy to Geodynamics Technology*,Smith, D.E. and Turcotte, D.L. (eds.) Washington, 133–162 in Bastos L, Bos M and Fernandes R. M. (2010): Deformation and Tectonics: Contribution of GPS Measurements to Plate Tectonics – Overview and Recent Developments. *Sciences of Geodesy*, 155-184, Springer-Verlag Berlin Heidelberg 2010

Delescluse M., Chamot-Rooke N., Cattin R., Fleitout L., Trubienko O., and Vigny C,(2012) April 2012 intra-oceanic seismicity off Sumatra boosted by the Banda-Aceh Megathrust. *Nature*490,240–244 (11 October 2012)

Devoti R., Zuliani D., Braitenberg C., Fabris P. and Grillo B. (2015) Hydrological indduced slope deformations detected by GPS and clinometric surveys in the Consiglio Plateau, Southern Alps. *Earth Planet Science Letters* 419 (2015): 134-142 (Elsivier)

Du Toit A. L. (1937): *Our Wandering Continents: An Hypothesis of Continental Drifting* Edinburgh: Oliver and Boyd, 1937

Duarte J. C. and Schellart W. P. (2016): Introduction to Plate Boundaries and Natural Hazards. *Geophysical Monograph* (219), First Edition. American Geophysical Union. John Wiley & Sons, Inc. 1-10

Eagles G., Gloaguen R., and Ebinger C. (2002). Kinematics of the Danakil microplate. [Egham, England].*Earth and Planetary Science Letters*. Vol 203, Pages 607-620.

Earthquake Track (2018): Earthquake Track, https://www.earthquaketrack.com/search?utf8=%E2%9C%93&q=west+africa&commit=Go Accessed 14th July, 2018.

Eberhard, D. M., Simons G. F., and Fennig C. D. (2019): *Ethnologue: Languages of the World*. Twenty-Second Edition. Dallas, Texas: SIL International. Online version: http://www.ethnologue.com.

Ehret C. (2002): The Civilizations of Africa. University Press of Virginia 2002.

El-Rabbany (2002) *Introduction to GPS: The Global Positioning System.* Artech House, Boston London 2002.

Encyclopedia Britannica, (2019) *Nigeria* Online Version https://www.britannica.com/place/Nigeria/Climate Accessed 12th June, 2019.

FreeBSD, 2019 chmod, https://www.freebsd.org/cgi/man.cgi?query=chmod&sektion=1 Accessed 23 December, 2018.

Floyd M. (2018): GAMIT/GLOBK http://geoweb.mit.edu/gg/ Accessed 18th January, 2019.

Gatt M. (2016): Finding Hotspots in the Theory of Plate Tectonics. *Ingenium Channel*, 28th February, 2016..https://ingeniumcanada.org/channel/innovation/finding-hotspots-theory-plate-tectonicsAccessed: 14 June 2018.

Gentoo, 2018 Multilib Gentoo Foundation, Inc https://wiki.gentoo.org/wiki/Multilib accessed 6/2/19

Geological Society of America (2015). pp. 599–620. In Duarte J. C. and Schellart W. P. (2016): Introduction to Plate Boundaries and Natural Hazards, Geophysical Monograph (219), First Edition. American Geophysical Union. John Wiley & Sons, Inc. 1-10

Gordon, R. G., and Stein S. (1992), Global tectonics and Space Geodesy. *Science*, 256, 333–342.

Hackl M., Malservisi R. and Wdowinski S. (2009): Strain Rate Patterns from Dense GPS Networks.*Natural Harzards and Earth System Sciences.* Copernicus Publications on behalf of the European Geosciences Union. 17 July 2009. (1177 - 1187)

Henton J. A., Craymer M. C.,Ferland R., Dragert H., Mazzotti S. and Forbes D. L. (2006): *Crustal motion and deformation monitoring of the Canadian landmass*. *Geomatica* 60(2) 173-191 · *January 2006.*

Hess, H. H. (1962), History of Ocean Basins.*Petrologic Studies: a Volume to Honor A. F. Buddington* 599-820 November 1962

Holmes A. (1944), *Principles of Physical Geology* (1 ed.), Edinburgh: Thomas Nelson & Sons, ISBN 0-17-448020-2

Holmes P. (1987): *Nigeria: Giant of Africa*. National Oil and Chemical Marketing Co. of Nigeria; Revised edition (January 1, 1987)

Hu Y., Zhang K. and Liu G., (2005) Deformation Monitoring and Analysis Using Regional GPS Permanent Tracking Station Networks.*TS 43 – Deformation Measurement and Analysis*. From Pharaohs to Geoinformatics, FIG Working Week 2005 and GSDI-8 Cairo, Egypt April 16-21, 2005

Ibezim I. G. (2014): The Challenges of Religion andEthnic Identity in Nigeria. *Journal of Religion and Human Relations*, 1 (6), 90-100, 2014. Available athttps://www.ajol.info/index.php/jrhr/article/view/111518/101302Accessed: 01.05.2019.

Iliffe J. (2007). *Africans: The History of a Continent. African Studies*. (2nd ed.). Cambridge University Press.ISBN 9781139464246.

Incorporated Research Institutions for Seismology (IRIS) (2007): Tectonic Plate Boundaries https://www.iris.edu/hq/inclass/animations

Ingolfsson O., (2008): *Plate Tectonics and Continental Drift*. Online Version. https://docplayer.net/24150854-Plate-tectonics-and-continental-drift-jardsaga-1-saga-lifs-og-lands-olafur-ingolfsson.html Accessed 6th February 2018

Isacks B. and Oliver J. (1968): Seismologyand the New Global Tectonics. *Journal of Geophysical Research*. 75 (18), September 15, 1968

Jadhav S. S. (Undated): *Presentation on Continental Drift Theory*. Online Version https://www.google.com/url?sa=t&rct=j&q=&esrc=s&source=web&cd=12&ved=2ahUKEwiBtL_Ej7fjAhURTsAKHdOLAmcQFjALegQIABAC&url=https%3A%2F%2Fwww.kcesmjcollege.in%2FICT%2FGeography%2FContinental%2520Drift%2520Theory.pdf&usg=AOvVaw03bLFMdjxoqHf3vroIQEQH Accessed 14th February, 2017

Jiang Z., Zhang X., Zhu Y, Zhang X. and Wang S. (2003): Regional tectonic deformation background before the Ms8. 1 earthquake in the west of the Kunlun Mountains Pass. *Sci China (Series D)* 2003: 33(Supp.):163e72.

Joffe, S., and Garfunkel, Z., (1987): Plate Kinamatics of the Circum Red Seaa Re-evaluation.*Tectonophys.* 141, 5–22.

Kalkan Y., Alkan R. M. and Bilgi S. (2010): *Deformation Monitoring Studies at Atatürk Dam.* FIG Congress 2010 Facing the Challenges – Building the Capacity Sydney, Australia, 11-16 April 2010

Kreemer, C., Blewitt G., and E. C. Klein (2014), A Geodetic Plate Motion and Global Strain Rate Model Geochemistry. *Geophysics, Geosystems*, 15, 3849–3889. DOI: 10.1002/2014 GC005407

Kreemer, C., W. E. Holt, and A. J. Haines (2003), *An Integrated Global Model of PresentDay Plate Motions and Plate Boundary Deformation.* Geophysical Journal International, 154, 8–34. DOI: 10.1046/j.1365-246X.2003.01917.x.

Krishnamurti T. N., (2019): Monsoon *Encyclopædia Britannica* https://www.britannica.com/science/monsoon

Kudela (2016): *Global Plate Tectonics*. University of California, Sanya Cruz, 2016

Le Pichon X. and Kreemer C., (2010) The Miocene-to-Present Kinematic Evolution of the Eastern Mediterranean and Middle East and Its Implications for Dynamics. *Annual Review of Earth and Planetary Sciences* 38:323-351 30 May 2010

Legrand J., Bruyninx C., Griffiths J., Craymer M., Dawson J., Kenyeres A., Sanchez L., Saria E., Santamaria-Gomez A. and Altamimi Z. (2015): The IAG Working Group 1.3.1: Inegration of Dense Velocity Fields in the ITRF. Final Results and Conclusion. IUGG General Assembly.

Levtzion, N. (1973). Ancient Ghana and Mali. New York: Methuen & Co Ltd.(3). ISBN 0841904316.

Liangqian G., Wanju B., Guohua Y., Juzhong C. and He G. (2011) Recent Crustal Movement and Great Earthquakes in Qinghai-Tibet Sub-Plate. *Geodesy and Geodynamics* 2(3), August 2011, 50-55

Lindsey E., (2019): *GPS tutorial: Basics of GAMIT/GLOBK*. Online Version https://www.planetmechanic.net/GAMIT-globk-tutorial Accessed 28 May, 2019.

Malservisi, R., Ugentobler U., Wonnacott R., and Hackl M. (2013): How rigid is a rigid plate? Geodetic constraint from the TrigNet CGPS network, South Africa, *Geophys. J. Int*., 192, 918–928, doi:10.1093/gji/ggs081. Assessed 14th June

McClusky, S., Reilinger, R., Mahmoud, S., Ben Sari, D. and Tealeb, A., (2003). GPS Constraints on Africa (Nubia) and Arabia plate motions. *Geophysics Journal* International 155, 126-138.

McGregor K. (2018): *Alfred Wegener's Theory of Continental Drift Became Modern Plate Tectonics*. University of North Texas, Plate Tectonics Revise. https://geography.unt.edu/~mcgregor/Earth_Science/plate.tectonics.revise.pdf Accessed 14th July, 2018.

McGuire J. J., and Beroza C. G., (2012): A Rogue Earthquake Off Sumatra *Science* 336 (6085):1 –18 9 May 2012

McKenzie, D. P., and R. L. Parker (1967):The North Pacific: an Example of Tectonics on a Sphere, *Nature*, 216, 1276–1280.

Muller, R. D., RoyerJY., and. Lawver L. A (1993), Revised Plate Motion Relative to the Hotspots from Combined Atlantic and Indian Ocean Hotspot Tracks. *Geology*, 21, 275–278. DOI:10.1130/00917613(1993).

Nace T., (2016): Layers of the Earth: What Lies Beneath Earth's Crust. Forbes, 16 January, 2016. https://www.forbes.com/sites/trevornace/2016/01/16/layers-of-the-earth-lies-beneath-earths-crust/#48c4ea22441d Accessed 14th July, 2018.

Ono, M. N., Agbo, J. A., Ijioma, D. I. and Chubado, M. (2014): Establishment of Baseline Data for Monitoring of Deformation of Murtala Mohammed Bridge (MMB) LokojaKogi State, Using GPS.*International Journal of Science and Technology*, 4 (5) 86-92.

Onwuka, S.U., Okoye, C.O and Ikekpeazu, F.O (2015): Effect of rural household income on biodiversity conservation, A Study of Awka South Local Government Area of Anambra State, Nigeria. Proceedings of 1st National Conference of the Faculty of Environmental Sciences, Nnamdi Azikiwe University, Awka, Anambra State, Nigeria.

Opara V. E.(2015): *Plate Tectonic Monitoring for Nigeria*, B.Sc. Project, NnamdiAzikiwe University, Awka, Nigeria, 2015.

Oregon State University (OSU) (2018): The Earth's Layers Lesson #1, http://volcano.oregonstate.edu/earths-layers-lesson-1 Accessed 29th November, 2018.

Rebischung P., Griffiths J., Ray J., Schmid R., Collilieux X. and Garayt B. (2011) IGS08: The IGS realization of ITRF2008, *GPS Solutions*, 16(4):483-494, doi:10.1007/s10291-011-0248-2.

Reilinger R. and McClusky S. (2011): Nubia–Arabia–Eurasia plate motions and the dynamics of Mediterranean and Middle East Tectonics.*Geophysical Journal International*186, 971–979. doi: 10.1111/j.1365-246X.2011.05133.x Accessed 30th January, 2019.

Reilinger R., McClusky S., Vernant P., Lawrence S., Ergintav S., Cakmak R., Ozener H., Kadirov F., Guliev I., Stepanyan R., Nadariya M., Hahubia G., Mahmoud S., Sakr K., ArRajehi A., Paradissis D., Al-Aydrus A., Prilepin M., Guseva T., Evren E., Dmitrotsa A., Filikov S. V., Gomez F., Al-Ghazzi R. and Karam G. (2006). *GPS constraints on continental deformation in the Africa–Arabia Eurasia continental collision zone and implications for the dynamics of plate interactions.* Journal of Geophysical Resources, **111,** B05411, doi:10.1029/2005JB004051.

SagiyaT. (2013): *Crustal Deformation.* Presentation made to the International Institute of Seismology and Earthquake Engineering. 17 February, 2013.

Sawitsky A. (2010): *Somali Plate*https://africa-arabia-plate.weebly.com/somali-plate.html Accessed 12 June, 2019.

Serpelloni, E., Vannucci, G., Pondrelli, S., Argnani, A., Casula, G., Anzidei, M., Baldi, P., Gasperini, P., (2007). Kinematics of the Western Africa-Eurasia Plate Boundary From Focal Mechanisms and GPS Data. *Geophysics Journal International* 169, 1180-1200.

Shirzaei M. (2010): *Crustal Deformation Source Monitoring using Advanced InSAR Time Series and Time Dependent Inverse Modeling*. PhD Dissertation, University of Postdam. Germany. December, 2010.

Smart C. L. (2012): Plate Tectonics.*In*: *Observing the Earth*, https://www.google.com/url?sa=t&rct=j&q=&esrc=s&source=web&cd=11&cad=rja&uact=8&ved=2ahUKEwjL24_jiazlAhXRQ0EAHaS0ANUQFjAKegQIAhAC&url=

https%3A%2F%2Fwww.kean.edu%2F~csmart%2FObserving%2F05.%2520Plate%2520tectonics.pdf&usg=AOvVaw3ljzG1t7xFVU4aQU4k3xkj Accessed 27th December, 2018.

Soudarin, L. and Grétaux, J.F. (2006): A Model of Present-Day Tectonic Plate Motions From 12 Years of Doris Measurements. *J. Geodesy*., 80, 609–624, doi: 10.1007/s00190-006-0090-4 Accessed 2ndJauary, 2018

Stamps D. S., Saria E and Kreemer C (2016), *A Geodetic Strain Rate Model for the East African Rift System.* Scientific Reports 2018 8(732) 1-8

Stein, S., and Sella G. F. (2002), Plate Boundary Zones' Concept and Approaches. *Plate Boundary Zones*, Stein S., and Freymueller J. T. (eds). American Geophysical Union Geodynamic Series 30, 1–26. https://doi.org/10.1029/GD030p0001Accessed 19th April 2018.

United States Embassy in Nigeria (2012): Nigeria Fact Sheet Online PDF version http://library.fes.de/pdf-files/bueros/nigeria/09372.pdf

University of Chicago News (2018) Stone Age Graveyard reveals Lifestyles of a 'Green Sahara': Two Successive Cultures Thrived Lakeside. UChicago News. University of Chicago News.Retrieved 2 August 2018.

Uzodinma N.V. &Ezenwere O.C., (1993). *Map Projections*. El'Demak Book Co., Enugu. Nigeria.

Vermaat, E., Degnan, J.J., Dunn, P., Noomen, R. and Sinclair, A. (1998): *Satellite laser ranging, status and impact for Wegener*. J. Geodynamics, 25, 195–212

Vernant, P., Fadil, A., Mourabit, T., Ouazar, D., Koulali, A., Martin Davila, J., Garate, J., McClusky, S., Reilinger, R., 2010. Geodetic constraints on active tectonics of the Western Mediterranean: Implications for the kinematics and dynamics of the Nubia-Eurasia plate boundary zone.*Journal of Geophysics* 49, 123-129.

Wang, T., Lin, J., Tucholke, B. and Chen, Y.J. (2011). Crustal thickness anomalies in the the North Atlantic Ocean basin from gravity analysis. *Geochem. Geophys. Geosyst.* 12, 1-25.

Wei W., Jiang Z., and Wu Y. (2015): Cognitions and Questions Regarding Crustal Deformation and Location Forecasts of Strong Earthquakes. *Geodesy and Geodynamics* 2015, x(x), 1-10 http://www.jgg09.com/jweb_ddcl_en/EN/volumn/home.shtml Accessed 8th May, 2017

Wessel P. and MullerR. D. (2007): Plate Tectonics: Manuscript 101, *Treatise on Geophysics* 6 2007.

Wilson J. T. (1965): A New Class of Faults and their Bearing on Continental Drift, *Nature* (4995) 343-347, July, 1965

Zhang L., Lia J., Liaob W., and Wang Q. (2016): Source Rupture Process of the 2015 Gorkha, Nepal Mw7.9 Earthquake and Its Tectonic Implications.*Geodesy and Geodynamics* 2016, X(X) ,1-8.

Zilenas Andrius (2012) Installing Compilers https://help.ubuntu.com/community/InstallingCompilers 6/2/19 Accessed 23 December, 2018.